THE DELAMINATION THEORY OF WEAR

PAGES _____

ARE

MISSING

IN

ORIGINAL

DOCUMENT

(12)

THE DELAMINATION THEORY OF WEAR

by
Nam. P. Suh and coworkers

Department of Mechanical Engineering,
Massachusetts Institute of Technology,
Cambridge, Mass. 02139, U.S.A.

These papers were also published in Volume 44 no. 1 of the journal *Wear*, edited by D. Scott.

ELSEVIER SEQUOIA S.A., LAUSANNE, 1977

Printed in the Netherlands

PREFACE

In 1972 the basic concept of the delamination theory of wear was presented to my colleagues in a private memorandum. The mixed reaction it received made it apparent that experimental evidence in support of the theory was essential before it could be accepted widely. Thus, a series of experimental and analytical investigations was initiated to examine the theory from three different points of view: mechanics, materials and applications. Twelve papers on the delamination theory of wear resulting from these investigations were prepared for publication in the special issue of *Wear*, August 1977. These papers on the delamination theory are reproduced here in hard cover by Elsevier.

The delamination theory of wear represents an attempt to understand the nature of sliding wear. It departs completely from the more classical adhesion theory of wear. Like many endeavours of mankind, it is easy to accept a widely recognized view and develop our thoughts along a fixed path, even in scientific fields. This tendency persists even when the view (or theory) may occasionally deviate from simple observations and known laws of nature. The deviations are often treated as exceptions rather than as causes for alarm, questioning and inquiry. However, advances in science emerge only through our willingness to question what is generally accepted, when logical deductions based on a theory do not coincide with reality. These papers on the delamination theory of wear are presented to foster this questioning spirit.

I have been fortunate to have had many students and colleagues who have provided intellectual stimulus to our inquiry. Many of them are coauthors of the papers presented here. In particular, Dr. Said Jahanmir performed many critical experiments from the very early days of our research; Dr. Nannaji Saka and Dr. Ernest P. Abrahamson, II, made valuable contributions to the materials aspect of the project; and Mr. Jonathan R. Fleming reviewed ten of the 12 manuscripts. During the early stages of this research the encouragement and criticisms of my colleagues Professors Nathan H. Cook and Frank A. McClintock were invaluable. The presentation of our work in a special issue of *Wear* would not have been possible without the enthusiasm and support of Messrs. Douglas Scott and Vernon C. Westcott.

This kind of research cannot readily be undertaken at a private university without the understanding of forward looking supporters in funding agencies. In this regard, the authors are greatly indebted to Dr. Edward C. Van Reuth of the Defense Advanced Research Projects Agency. The authors are also indebted to Dr. Richard S. Miller, Dr. Arden L. Bement, Jr, and Lt. Commander Kirk Petrovic for their continuing support of and confidence in this work. I am, however, responsible for any shortcomings of the work presented in this volume.

My wife and our four daughters deserve special thanks for their love, understanding and patience.

Cambridge, Massachusetts
June 1977

Nam Pyo Suh

CONTENTS

Wear, 44 (1977) 1 - 16

AN OVERVIEW OF THE DELAMINATION THEORY OF WEAR

NAM P. SUH

Department of Mechanical Engineering, Massachusetts Institute of Technology, Cambridge, Mass. 02139 (U.S.A.)

(Received January 2, 1977)

Summary

The fundamental mechanisms of sliding wear postulated by the delamination theory of wear are reviewed in terms of the experimental and analytical work done to date at MIT. Each of the rate determining processes involved in delamination wear, *i.e.* plastic deformation of the surface layer, crack nucleation and crack propagation, is discussed for various metals with different microstructures. The effects of sliding speed, lubricants and complex loading on wear are also discussed. A hypothesis (without experimental verification) is advanced for the formation of the Beilby layer. Various dislocation mechanisms that might be responsible for the "dislocation depleted layer" are considered.

Introduction

The delamination theory of wear was introduced in 1973 in order to explain the wear of metals and other solid materials [1]. In that paper many of the postulated mechanisms involved in delamination wear were qualitatively shown to occur but only a limited amount of experimental data and analytical evidence in support of the theory was presented. Since then, extensive analytical and experimental work has been done by the author and his associates at MIT [2 - 10] and also by others [11 - 14], which has confirmed the validity of the theory. The purpose of this paper is to give an overall review of the current state of understanding of sliding wear in terms of the delamination theory of wear and to outline the relative significance of each of the subjects discussed in the companion papers presented in this issue of *Wear*.

The significance and implications of the mechanisms postulated by the delamination theory of wear can best be understood by considering the following questions.

(1) Where does all the energy supplied by the external agent go?

(2) Why and how does the coefficient of friction affect the wear rate?

(3) Why do some hard metals wear faster than softer metals?

(4) Why do most wear particles have an aspect ratio greatly different from unity?

(5) Why does seizure occur?

(6) How does the microstructure of metals affect the wear rate?

(7) How do initial surface roughness and waviness influence the wear phenomenon?

An attempt is made to answer these questions in this and the companion papers based on the delamination theory of wear.

The primary purpose of this paper is to give a perspective on our current state of understanding of sliding wear. It discusses well-established aspects of sliding wear mechanisms and also those areas which still require further research.

Mechanisms of delamination wear

General description

The delamination theory of wear describes the following sequential (or independent, if there are pre-existing subsurface cracks) events which lead to wear particle formation.

(1) When two sliding surfaces come into contact, normal and tangential loads are transmitted through the contact points by adhesive and plowing actions. Asperities of the softer surface are easily deformed and some are fractured by the repeated loading action. A relatively smooth surface is generated, either when these asperities are deformed or when they are removed. Once the surface becomes smooth, the contact is not just an asperity-to-asperity contact, but rather an asperity–plane contact; each point along the softer surface experiences cyclic loading as the asperities of the harder surface plow it.

(2) The surface traction exerted by the harder asperities on the softer surface induces plastic shear deformation which accumulates with repeated loading*.

(3) As the subsurface deformation continues, cracks are nucleated below the surface. Crack nucleation very near the surface is not favored because of a triaxial state of highly compressive stress which exists just below the contact regions.

(4) Once cracks are present (owing either to the crack nucleation process or to pre-existing voids), further loading and deformation causes cracks to extend and to propagate, joining neighboring ones. The cracks tend to propagate parallel to the surface at a depth governed by material properties and the coefficient of friction. When cracks cannot propagate because

*The increment of permanent deformation per asperity passage is small compared with the total plastic deformation per passage (which is almost completely reversed). This accounts for the dissipation of energy [5, 15].

of either limited deformation or an extremely small tangential traction at the asperity contact, crack nucleation is the rate controlling mechanism.

(5) When these cracks finally shear to the surface (at certain weak positions) long and thin wear sheets "delaminate". The thickness of a wear sheet is controlled by the location of subsurface crack growth, which is controlled by the normal and the tangential loads at the surface.

The remainder of this section elaborates on each one of the mechanisms described above in order to establish our current state of knowledge.

Effect of topography on wear and the formation of the Beilby layer

All machined surfaces, and to some extent the surface created by the delamination wear process, have asperities. When the harder surface slides over the softer surface, the softer asperities either fracture immediately or deform. The rate at which these asperities are removed by the sliding process and the mechanism of removal depend on the initial surface roughness, the applied load and the mechanical properties of the asperities. For example, the wear rate of AISI 1020 steel was shown to be higher for rougher surfaces than for smoother surfaces when the applied normal load was high but the opposite was found to be true under a lighter normal load [10].

The wear particles generated by the fracture of deforming asperities will be smaller than delaminated wear particles produced by the subsurface crack propagation process but their aspect ratio may be larger than unity.

Figure 1 shows asperities of AISI 1018 steel (generated by a machining process) which were deformed under the sliding action of an AISI 52100 steel slider. High asperities were deformed first and these covered the lower ones. Upon further deformation the lower asperities also deformed, eventually forming a layered structure of deformed asperities. The deformation process is illustrated in Fig. 2 which shows the deformation of the gold–steel

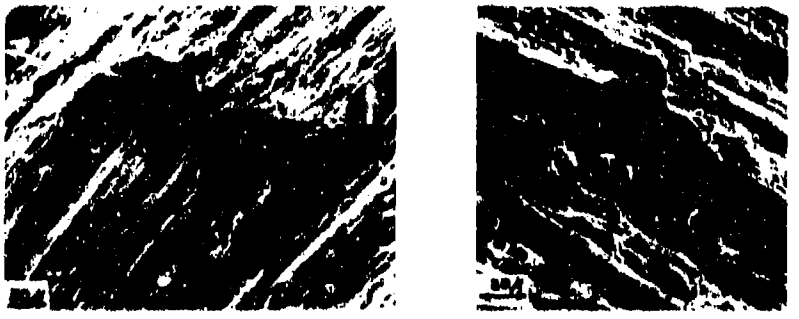

(a) (b)

Fig. 1. Plastic deformation of the original asperities on machined AISI 1018 steel during cylinder-on-cylinder wear tests: (a) sliding perpendicular to the machining marks, 2.0 μm (c.l.a.) surface finish, under a normal load of 0.91 kg after 0.2 m of sliding; (b) sliding parallel to the machining marks, 3.3 μm (c.l.a.) surface finish, under a normal load of 0.35 kg after 0.25 m of sliding.

Fig. 2. The deformation of substrate asperities due to the sliding action on a thick plate of Au on an AISI 1020 steel substrate.

interface of gold plated AISI 1020 steel due to the surface traction exerted on the gold surface by an AISI 52100 steel slider. The micrograph shows one deforming asperity overlying another asperity. If the gold plating had not been present, the fresh surface of a highly elongated asperity would have overlaid another highly deformed asperity, possibly forming a chemical bond (*i.e.* cohesive bonding).

If these layers are removed by fracture or by bond failure before the subsurface delamination process finally creates a wear particle, then the number of layers of these deformed asperities stacking on top of each other will depend only on the ductility of the layers and on the quality of the cohesive bonding. In contrast, if the surface is removed only through the subsurface crack propagation process (*i.e.* the delamination process), the deformed asperities will undergo severe elongation. In this case the thickness of each layer can be very small, being of the order of 10 Å. Since each layer has a different crystallographic orientation, the resulting lamellar structure at the surface will not exhibit a unique crystallographic structure when viewed by X-ray diffraction or by electron diffraction. This may explain the formation of the so-called Beilby layer or shear-mixed layer discussed in the literature [16]. Experimental evidence for this hypothesis about the formation of the Beilby layer is yet to be secured.

In certain less ductile metals, *e.g.* those with inclusions, the asperities may simply fracture rather than form the lamellar structure when they are deformed. The degree of deformation before fracture will depend both on the microstructure and on the environmental conditions. For example, asperities are likely to undergo less deformation when metal-to-metal adhesion between deformed asperities is prevented by the presence of lubricants. Another equally plausible explanation for the Beilby layer is the formation of very small grains or dislocation cells which cannot be resolved by an optical metallograph. Van Dijck's transmission electron microscopy showed that small elongated grains of the order of 250 - 600 Å were formed at the surface of worn copper specimens [17].

One aspect of surface topography that has not been investigated to any extent is surface waviness. Surface waviness differs from surface rough-

ness in that the former refers to the long range deviation of the surface profile from the nominal shape, while the latter refers to a short range deviation. In a stiff sliding system (*i.e.* a geometrically confined sliding system) waviness can increase the tangential component of the surface traction; this affects the wear rate significantly, as discussed in greater detail in following sections.

Deformation of the surface layer

The plastic deformation of an elastoplastic surface layer under the influence of normal and tangential loads exerted by a hard asperity has been analyzed in the companion paper by Jahanmir and Suh [15]. Qualitatively the plastic deformation occurs in such a manner that the shear strain component in planes perpendicular to the surface accumulates incrementally each time a hard asperity passes over the surface. The depth of the plastic deformation zone and the plastic strain depend on the actual surface traction. In an elastic perfectly plastic solid the magnitude of plastic strain accumulated at a given depth per cycle remains constant when the magnitude of the surface traction does not change. This implies that the plastic deformation can accumulate indefinitely when two surfaces slide over each other until the surface layer is delaminated. Therefore the resistance to delamination wear can be increased either by suppressing the crack nucleation and propagation process or by reducing the plastic deformation by increasing the flow strength.

One of the major difficulties encountered in predicting analytically the deformation of the surface layer is the inability to measure or to derive the exact magnitude of the normal and tangential loads exerted by the hard asperities and the actual area of asperity contact. Therefore it is often necessary to make arbitrary assumptions; the common assumption is that the normal stress is equal to the hardness of the metal. This is a reasonable assumption when the tangential load is absent, but it is a poor assumption under a typical sliding situation. For this latter case, Green [18] showed that the normal load depends on the coefficient of friction and may be smaller than the hardness when both normal and tangential loads are applied to a perfectly plastic solid. Even this analysis is of limited value since it cannot accurately predict the coefficient of friction unless an arbitrary assumption is made that some of the junctions support significant tensile loading. This is a result of neglecting the plowing action at the surface. Further evidence that the normal stress at the asperity–surface contact is not equal to the hardness is provided by experimental results. The experimentally observed plastic zone depth is a strong function of the flow stress, *i.e.* the higher the flow stress, the shallower is the depth of plastic deformation. If the contact stress at the surface increases in proportion to the hardness, the depth of the plastic zone should be approximately constant.

It has been experimentally observed that the depth of the plastically deformed zone in copper increases with the distance slid or with the number of loading cycles when freshly annealed copper is slid against a hard surface [3]. This increase may be due to experimental difficulty in measuring small

strains or it may be due to the changes in material behavior under cyclic loading conditions. When metals are loaded cyclically, some undergo cyclic softening (leading to cyclic creep) or cyclic hardening. However, even metals which initially undergo cyclic hardening may eventually soften under continued cyclic deformation. The role of cyclic creep in wear is not yet fully understood.

When plowing is considered, the mechanics of deformation very near the asperity contact point can only be analyzed to a first approximation using a numerical technique for an assumed plowing model. Otherwise, it is difficult to satisfy the equilibrium condition. The MIT work to date has relied on St. Venant's principle and has ignored the actual deformation of the region very close to the loading points for three reasons: the high computation cost associated with elastic–plastic numerical methods such as finite elements; the high probability that crack nucleation and propagation do not occur very near the asperity–surface contact point; and the fact that other more gross assumptions were made in the analyses.

Another approximation made in the analysis of deformation is the assumption of isotropy. It is well known that worn surfaces have texture and are thus not isotropic. Buckley [19] and Scott and Wilman [20] have shown that the slip planes of worn surfaces become oriented parallel to the surface. When such texture develops the metal is no longer isotropic, especially if the metal has a limited number of slip systems (as in h.c.p. metals). The effect of anisotropy on friction and wear needs further understanding.

There is also ample evidence that the flow properties of a worn material vary as a function of the depth from the surface, which is ignored in the analyses done to date. Although the microscopic mechanisms responsible for the heterogeneity are discussed in a later section, very little basic understanding on the role of heterogeneity in wear is yet available. This subject is of interest since the introduction of heterogeneity through heat treatment and plating is a major tool in combatting wear.

Crack nucleation

In the original paper on the delamination theory of wear it was reasoned that crack nucleation is likely to occur away from the surface rather than very near the surface owing to the high hydrostatic compressive pressure acting near the asperity contact. The analysis presented in the companion paper [15] shows that this is indeed the case. The analysis assumed that crack nucleation occurs when the radial stress acting at the interface between a rigid cylindrical inclusion and the matrix reaches a critical value. The radial stress was computed by considering both the stress accumulated due to the residual stress associated with strain concentration around the inclusion and the stress due to the applied load. It is significant to note that when the normal load is higher than four times the critical shear stress of the metal, the rate of crack propagation per loading cycle vis-à-vis the crack nucleation rate in an elastoplastic solid appears to be the wear rate determining process in the range of friction coefficients investigated (*i.e.* $\mu > 0.125$).

It is also interesting to note that cracks are nucleated at a greater depth as the normal and tangential applied loads increase. Furthermore, the size of the region over which cracks nucleate also increases with increased applied loads.

The crack nucleation analysis was done for an individual cylindrical inclusion; the stress and strain fields were not influenced by the presence of other inclusions. The analysis should be extended to the case of two neighboring inclusions where crack nucleation occurs much more readily owing to the interaction of neighboring stress fields and stress or strain concentrations. Non-cylindrical inclusions should also be considered, *e.g.* when the microstructure is pearlitic, crack nucleation is likely to occur by cohesive fracture of the carbide lamella owing to the shear stress exerted on the carbide–ferrite interface.

There is no definitive evidence that the crack nucleation condition used in the analysis is valid under all conditions. For example, when there is shear stress acting at the inclusion–matrix interface, crack nucleation may occur at a lower magnitude of the radial stress. The analysis of these details of crack nucleation is still one of the remaining tasks in tribology and the fracture of metals.

Metallurgical and microstructural evidence for the crack nucleation predicted by the delamination theory is overwhelming. As the paper by Teixeira *et al.* [21] on wear of single-phase metals shows, the wear rate of solid solutions decreases with solute content*. This decrease in the wear rate is due to the increased hardness and the consequential decrease in the coefficient of friction. The increase in hardness of single-phase metals decreases the rate of plastic deformation and the decrease in the frictional coefficient results in crack propagation at a shallower depth and a lower crack propagation rate. The relative importance of hardness and of the number of crack nucleation sites is more dramatically illustrated by studies of precipitation hardened two-phase metals. The maximum wear resistance is exhibited by a metal that still has coherent precipitates rather than by a specimen which has a higher hardness but which has incoherent precipitates [22]. This shows that the hardness alone is not a good measure of wear resistance. The importance of crack nucleation is further illustrated by considering the wear of internally oxidized copper [23]. In these metals the particle–matrix interface is equivalent to pre-existing cracks, since the bonding between the particles and the matrix is extremely poor. Therefore, although the hardness increases with the volume fraction of internally oxidized particles in the copper matrix, the wear rate also increases owing to the increase in the number of pre-existing cracks and to the decrease in the distance that a crack must propagate to link up with other cracks. Therefore the crack propagation rate controls the wear rate in these metals.

It should be noticed that, if the mechanism of crack propagation

---

*This is true only if the solute does not segregate at grain boundaries and does not thus lower the ductility.

parallel to the surface is not operative, wear particles will still form when a sufficient number of adjacent cracks are nucleated and make the substrate weak. This will be the case when the coefficient of friction is very low and/or when limited plastic deformation occurs. Then the wear particles formed by this process of crack nucleation will not necessarily be flat. The wear rate for this case will be smaller than when cracks can propagate.

Crack propagation

There are three important questions related to crack propagation in delamination wear.

(1) Why is the wear rate (equivalent to the crack propagation rate) in steady state wear proportional to the distance slid when the total length of each crack is actually changing with the distance slid?

(2) What determines the depth at which crack propagation occurs?

(3) When do cracks propagate parallel to the surface rather than perpendicular to the surface?

These questions are answered by the linear fracture mechanics analysis of crack propagation given by Fleming and Suh [24] in one of the companion papers.

The stress analysis given by Jahanmir and Suh [15] shows that the subsurface in front of the moving asperity is in a plastic state, while the region behind it is in an elastic state. Furthermore, the crack tip is in compression in most of the plastic region and is in tension in the elastic region behind the slider. Therefore, ignoring the compressive region, a linear elastic fracture mechanics analysis can be applied to the crack tip. The crack propagation rate is always constant regardless of the total crack length, because only that portion of the crack which is in the tensile region contributes to the stress concentration and to crack tip opening and it thus controls the crack propagation rate. The analysis shows that the stress intensity factors reach maximum values at a finite distance below the surface, indicating that the cracks located at this depth will propagate faster than those at other locations. It is also significant to note that the depth increases as the frictional force increases. Therefore, it may be concluded that the increased wear rate observed at a higher frictional coefficient is due to the thicker wear particles and is also due to the faster crack propagation rate.

The phenomenon of seizure which occurs when a sliding interface is deprived of a lubricant can be explained in terms of the delamination theory of wear. In a geometrically confined (*i.e.* stiff) system the tangential component of the surface traction increases suddenly when lubricants are depleted. Consequently, large thick wear particles will be generated, which may be wedged in the confined space available at the interface and may mechanically lock the interface.

Cracks propagate parallel to the surface even though both an isotropic homogeneous elastic solid and an elastoplastic solid experience the maximum normal stress behind the asperity contact parallel, rather than perpendicular, to the surface (Fig. 3). One reason for this is that the imperfections at the

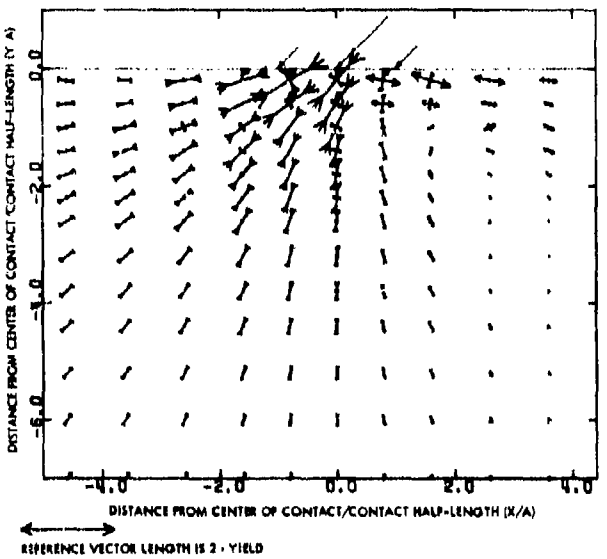

(a)

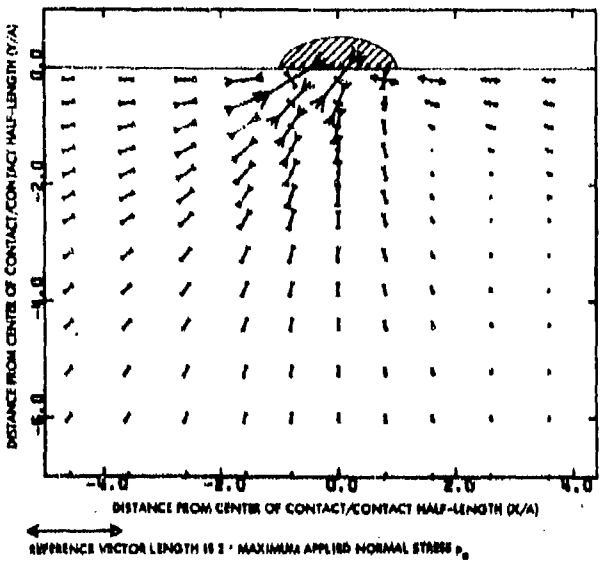

(b)

Fig. 8. The stress field under an asperity contact (coefficient of friction = 1). (Lines show the directions and magnitudes of principal stresses, arrowheads indicate signs and "p" indicates plasticity.) (a) An elastoplastic solid (finite element solution, applied load vectors not to scale); (b) an elastic solid (solutions for an elliptically distributed load [25], load vectors not to scale).

surface close very easily under the shearing action in front of and under the sliding asperity. Furthermore, the state of the normal stress component parallel to the surface changes from tension to compression a short distance away from the surface, which prevents "surface cracks" from growing very deep. In contrast, a subsurface crack parallel to the surface experiences a compression–tension cyclic loading each time an asperity passes over the surface, which causes the crack to propagate a short distance. The stress concentration at these crack tips can be large owing to the finite length of the crack in the tensile region. For these reasons, in elastoplastic solids cracks can propagate parallel to the surface. Even in extremely brittle solids cracks may propagate parallel to the surface if subsurface defects exist in the form of microcracks. However, in the absence of significant subsurface defects cracks in a brittle solid grow preferentially from the surface because defects are more prevalent at the surface and the normal stress parallel to the surface is maximum at the trailing edge of the asperity–surface contact.

The analysis given by Fleming and Suh [24] is deficient in that it does not take into account the variation in flow stress and that the values for the surface traction must be assumed *a priori*. An explicit determination of the latter cannot yet be made from first principles for reasons cited in an earlier section. The analysis is valuable, however, since it explains a number of experimentally observed phenomena in addition to the crack propagation mechanics discussed, *e.g.* it is clear why the waviness of a sliding surface used in a geometrically confined system can accelerate the wear rate. It was shown by Suh and Nagao [9] that the increase in surface traction, especially the tangential component, can create thicker wear particles and can cause a change in the wear rate.

Wear particle generation and the rate limiting process

Wear particles are generated when a subsurface crack breaks through to the surface. Since the propagating end of the crack (*i.e.* the crack tip at which the stress is maximum) is always situated behind the moving asperity, the crack reaches the surface after the asperity moves over the crack. Consequently, the wear particle always lifts up from the surface so that the underside is facing the direction opposite to the slider motion (Fig. 4). This direction is opposite to that of similar flat particles formed by the deformed asperities and thus enables an easy separation of particles formed by subsurface crack propagation from those formed by deformed asperities.

In research on wear, a knowledge of the rate determining process is the key to the understanding, prediction and minimizing of wear. In such metals as internally oxidized copper which have pre-existing cracks, the rate determining process is clearly the crack propagation rate once the surface traction is fixed by experimental conditions and by the materials. However, the wear rates of pure elements and of solid solutions are initially controlled by the deformation rates which are controlled by hardness and the friction force. The frictional force is in turn controlled by adhesion and by a flow stress parameter that is probably related to hardness. There can be deviations

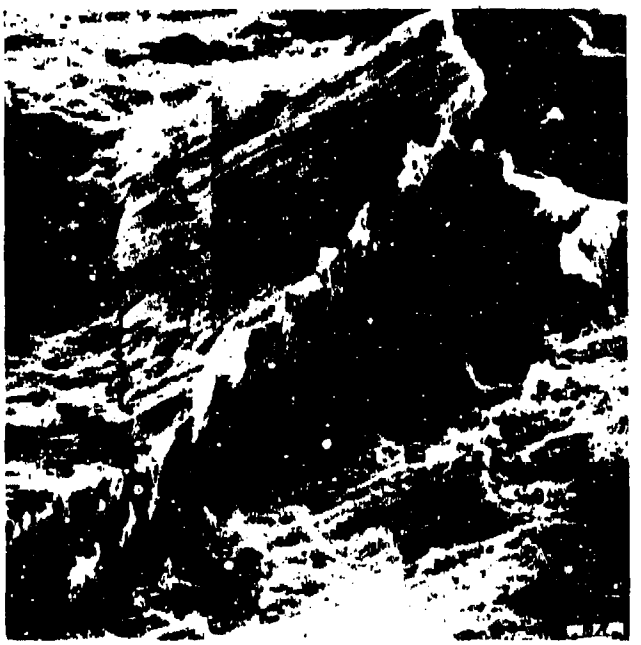

Fig. 4. Wear sheet formation in an iron solid solution. Note that the sheet is lifting up opposite to the sliding direction. (The sliding direction is from right to left.)

from this if impurities segregate to the grain boundaries and if the stacking fault energy is significantly affected by the alloying elements. Once cracks nucleate in these metals, the surface traction will determine those cracks that will propagate the fastest. Therefore, in the case of solid solutions and pure elements, the rate of any of the steps involved in delamination wear can strongly affect the wear rate. However, the relative importance of each step in this process cannot be specified quantitatively *a priori*. In between these extreme wear behaviors of single-phase metals and of internally oxidized metals lie the behaviors of precipitation hardened alloys. In the materials tested by Jahanmir *et al.* [26] and by Saka *et al.* [22], the crack propagation rate again seems to be the phenomenon that controls the wear rate, since the number of cycles required for crack nucleation is much smaller than that required for crack propagation. When the metals are so hard that gross plastic deformation does not occur under the applied load, the crack nucleation rate may become the rate determining process.

Dislocation dynamics and sliding wear

In the original paper on the delamination theory of wear [1] one postulate concerned the possibility that there might be a "dislocation

depleted zone" near the worn surface. This aspect has been a source of controversy, as evidenced by the papers of Hirth and Rigney [14] and of Ruff [27]. An attempt will be made here to clarify what is known about this problem and to determine where further clarification is required.

Suh speculated that, since fresh surfaces free from a coherent oxide layer may be generated when asperities move over a soft surface under a heavy load, generated dislocations may experience sufficient image forces to be pulled out of the surface. Consequently, there may be a finite layer (less than 1 μm in typical commercial grade metals) in which the dislocation density is lower than that in the layer below it. Such a layer may undergo large plastic deformation without fracturing, since normal fracture mechanisms which depend on dislocation interactions may not be operative. There is evidence that dislocations do indeed experience such a force (*e.g.* see ref. 28) and that there can be a flow stress gradient near a deformed surface, as shown by Fourie and Dent [29], who found the surface to be softer than the bulk. In contrast, Kramer [30] claims that the surface is harder.

Hirth and Rigney [14] advanced the argumont that the surface can be either softer or harder than the substrate, depending on the stacking fault energies involved. Ruff [27, 31] conducted electron channeling experiments with copper and with high purity iron and concluded that the residual strain is highest at the surface rather than at the subsurface. The channeling experiment may not be a conclusive measure of the flow stress of metals near the surface for two reasons. First, the dislocation density reaches a "saturation" value at relatively low strain vis-à-vis the strains encountered in sliding wear. The dislocation dynamics responsible for the flow of metals after the dislocation density has reached a saturation value is not yet known. Therefore, there is no way of extrapolating these residual strain measurements to the actual flow stress existing under sliding situations. Second, there is a question of how effective an electron channeling experiment is when a surface is made up of a composite layer, as discussed earlier.

Van Dijck's experiments, which showed that the worn surface of metals consists of fine grains of 250 - 600 Å, indicate that such metals should have a high yield stress at the onset of plastic deformation [17]. However, these fine grained metals also show plastic instability at small strains under normal tensile loading conditions, with subsequent plastic deformation at low stress [32]. Whether the fact that the frictional force of metal specimens plated with a very thin layer of a softer metal decreases from a high value during the early stage of wear to a lower value at steady state is related to this behavior of small grained metals is not known. However, it offers an interesting possibility.

The behavior of dislocations near a surface still requires further understanding and clarification. It is unlikely that the controversies involved can be resolved in the near future in view of the difficulties involved in performing definitive experiments. Even the hardness tests performed in the past may be unreliable in that the flow of metals under sliding conditions occurs parallel to the sliding direction, whereas this is not the case for the flow

under an indenter. This is an important issue when the metal near the surface is highly oriented, with its slip planes nearly parallel to the surface.

The effect of sliding speed

As the sliding speed increases, the interface temperature increases [33]. The consequences of this temperature rise are: the decrease in the flow stress of metals; the formation of different oxide layers on the surface, which change the surface traction; phase transformations; and/or increased diffusion across the contact interface. The experimental results presented by Saka *et al.* [33] indicate that the effect of these changes, except perhaps the effect of the increased diffusion rate, may only be changes in the details of delamination wear (*e.g.* where the cracks nucleate etc.) rather than deviations from the fundamental mechanisms postulated by the delamination theory of wear. This is in contrast to the notion advanced by Quinn [34] that the wear rate is equal to the oxidation rate in high speed sliding.

Sliding wear of non-metals

The delamination theory of wear is applicable to all materials in which subsurface crack nucleation and propagation mechanisms are operative. Swain [11] showed that alumina can wear by delamination. It is very likely that thermoplastics with inclusions also wear by the mechanisms postulated by the delamination theory, whereas glassy thermosetting plastics fail through crack nucleation at the surface and pure thermoplastics fail either by surface melting or by continuous deformation. When the material is highly anisotropic and when plastics are reinforced by large diameter fibers, the stress field and the mechanisms of crack nucleation and propagation may be significantly different [35].

The effects of lubricants on sliding wear

Lubricants are applied either to eliminate or to minimize metal-to-metal contacts. This reduces the tangential component of the surface traction and distributes the normal load over a larger surface area (in the case of hydrodynamic lubrication) and thus reduces the wear rate significantly. When the applied normal load is very small, gross plastic deformation may be entirely eliminated. In this case, wear may be due to microplastic deformation, to crack nucleation through dislocation pile-up in hard metals, and to the formation of adhesive junctions.

Chemical reaction between the additives in lubricants and the metal surface is also possible. The formation of hard layers (*e.g.* sulfide and oxide)

on the metal surface has been discussed [36] and the glassy behavior of lubricants in elastohydrodynamic lubrication has been considered [37]. However, the effects of these on wear have not been established. One of the interesting possibilities investigated at MIT is preferential chemical reaction between constituents of the lubricant and the heterogeneously deformed metal surface (with high strain energy). In multi-phase metals it is reasonable to expect heterogeneous deformation owing to the difference in basic nature of each phase and their differing crystallographic orientations. On unloading, the residual stress distribution will be highly heterogeneous. Therefore, any chemical reaction that can occur between the lubricant and the deformed metal surface will occur fastest at the regions of highest strain energy. When the reaction product is not mechanically compatible with the original matrix, cracks may form.

Wear under combined loading

The possibility that the initial phase of fretting wear may be caused by the delamination process was discussed by Suh [1], Waterhouse and Taylor [12] and van Leeuwen [38]. One of the basic questions often asked in this area is: "where do the cracks form — at the surface or at the subsurface ? " The answer to this question depends on the state of stress and on the relative displacement between the surfaces in contact. When a bending type of fatigue loading is applied to a shaft and the stress exerted by the inner race of a bearing reinforces the maximum bending stress, cracks can nucleate perpendicular to the surface near the ends of the inner race–shaft contact area. However, if there is a large relative displacement between the two surfaces, cracks may form at the subsurface parallel to the surface.

When the bending stress and the stress applied by the contact do not reinforce each other in any substantial way and if the crack propagation rate determines the fatigue life, then the fatigue life under such a combined loading is essentially independent of wear. This latter case is reported in the companion paper by Nagao *et al.* [39].

Conclusions

(1) The experimental and analytical work done to date supports the postulates of the delamination theory of wear for the sliding wear of metals and other plastically deforming solids.

(2) The wear rate of metals may be predicted in the near future, based on first principles and fundamental material properties.

(3) Further work needs to be done to provide a more complete description of the behavior of metals near the surface and of the exact mechanisms of load transmission at asperity–surface contact points.

Acknowledgment:

The work presented in this and companion papers would not have been possible without the support of the Defense Advanced Research Projects Agency, under contract No. N00014-67-A-0204-0080, through the Office of Naval Research. The author is particularly grateful to Dr. Edward C. van Reuth and Dr. Richard S. Miller for their personal support of the work. The MIT staff is also grateful to Dr. Arden Bement and Lt. Commander Kirk Petrovic for their continuing support. The author is also grateful to Mr. Douglas Scott, who has been more than generous in his spiritual support of our research over the past several years. This research in wear has benefited a great deal through the author's association with Mr. Vernon Westcott of Foxboro/Trans-Sonics, Inc.

References

1 N. P. Suh, Wear, 25 (1973) 111 - 124.
2 S. Jahanmir, N. P. Suh and E. P. Abrahamson, II, Wear, 28 (1974) 235 - 249.
3 N. P. Suh, S. Jahanmir, E. P. Abrahamson, II, and A. P. L. Turner, J. Lubr. Technol., 96 (1974) 631 - 637.
4 S. Jahanmir, N. P. Suh and E. P. Abrahamson, II, Wear, 32 (1975) 33 - 49.
5 N. P. Suh and P. Sridharan, Wear, 34 (1975) 291 - 299.
6 N. P. Suh, Microstructural effects in wear of metals. In R. J. Jaffrey (ed.), Fundamental Aspects of Structural Alloy Design, Plenum Press, New York, 1976.
7 E. P. Abrahamson, II, S. Jahanmir, N. P. Suh and D. A. Colling, Application of the delamination theory of wear to a composite metal surface, Proc. Int. Conf. on Production, Tokyo, Japan, 1974, pp. 408 - 413.
8 S. Jahanmir, E. P. Abrahamson, II, and N. P. Suh, Wear, 40 (1976) 75 - 84.
9 N. P. Suh and T. Nagao, CIRP Ann. Int. Inst. Prod. Eng. Res., 25 (2) (1976) 513 - 519.
10 E. P. Abrahamson, II, S. Jahanmir and N. P. Suh, CIRP Ann. Int. Inst. Prod. Eng. Res., 24 (1975) 513 - 514.
11 M. V. Swain, Wear, 35 (1975) 185 - 189.
12 R. B. Waterhouse and D. E. Taylor, Wear, 29 (1974) 337 - 344.
13 J. A. Kirk and T. D. Swanson, Wear, 35 (1975) 63 - 67.
14 J. P. Hirth and D. A. Rigney, Wear, 39 (1976) 133 - 141.
15 S. Jahanmir and N. P. Suh, Mechanics of subsurface void nucleation in delamination wear, Wear, 44 (1977) 17 - 38.
16 L. E. Samuels, Metallographic Polishing by Mechanical Methods, 2nd edn., Pitman, London, and Elsevier, New York, 1971.
D. Scott, W. W. Seifert and V. C. Westcott, The particles of wear, Sci. Am., 230 (1974) 88 - 89.
17 J. A. B. Van Dijk, Wear, 42 (1977) 109 - 117.
18 A. P. Green, J. Mech. Phys. Solids, 2 (1954) 197 - 211.
19 D. R. Wheeler and D. H. Buckley, Wear, 33 (1975) 65.
20 V. C. Scott and H. Wilman, Proc. R. Soc. London, Ser. A, 247 (1958) 353.
21 J. J. Pamies-Teixeira, N. Saka and N. P. Suh, Wear of copper-based solid solutions, Wear, 44 (1977) 65 - 75.
22 N. Saka, J. J. Pamies-Teixeira and N. P. Suh, Wear of two-phase metals, Wear, 44 (1977) 77 - 86.
23 N. Saka and N. P. Suh, Delamination wear of dispersion hardened alloys, J. Eng. Ind., in the press.

24 J. R. Fleming and N. P. Suh, Mechanics of crack propagation in delamination wear, Wear, 44 (1977) 39 - 56.
25 J. O. Smith and C. K. Liu, Stresses due to tangential and normal loads on an elastic solid with applications to some contact problems, J. Appl. Mech., 20 (1953) 157 - 166.
26 S. Jahanmir, E. P. Abrahamson, II, and N. P. Suh, The effect of second phase particles on wear, Proc. 3rd North American Metal Working Research Conf., Carnegie Press, 1975, pp. 854 - 864.
27 A. W. Ruff, Wear, 40 (1976) 59 - 74.
28 R. M. Latanision, Surface effects in crystal plasticity: general overview, Proc. NATO Advanced Study Institute on Surface Effects in Crystal Plasticity, in the press.
29 J. T. Fourie and N. C. G. Dent, Acta Metall., 20 (1972) 1291.
30 I. R. Kramer and L. J. Demer, Prog. Mater. Sci., 9 (1961) 133.
31 A. W. Ruff, Study of initial stages of wear by electron channeling, NBS Rep. NBSIR76-1141, Washington, D.C., 1976.
32 V. Ramachandran and E. P. Abrahamson, II, Scr. Metall., 6 (1972) 187.
33 N. Saka, A. M. Eleiche and N. P. Suh, Wear of metals at high sliding speeds, Wear, 44 (1977) 109 - 125.
34 T. F. J. Quinn, ASLE Trans., 10 (1967) 158.
35 N.-H. Sung and N. P. Suh, Friction and wear of fiber reinforced polymeric composites: effect of fiber orientation on wear, to be presented at ANTEC of Soc. Plast. Engrs., 1977.
36 F. G. Rounds, ASLE Trans., 9 (1966) 88 - 100.
37 J. F. Dill, P. W. Drake and T. A. Litovitz, The applicability of light scattering spectroscopy to the measurement of the viscoelastic parameters of lubricants, Technical Rep. no. 2 to ONR, Catholic University of America, March, 1974.
38 H. P. Van Leeuwen, Discussion on Suh's delamination theory of fretting wear and possible role of hydrogen, Proc. 39th Meeting of the Structures and Materials Panel, NATO Rep., AGARD-CP-161, 1974.
39 T. Nagao, J. J. Pamies-Teixeira and N. P. Suh, Behavior of medium carbon steel under combined fatigue and wear, Wear, 44 (1977) 101 - 108.

Wear, 44 (1977) 17 - 38

MECHANICS OF SUBSURFACE VOID NUCLEATION IN DELAMINATION WEAR

S. JAHANMIR* and N. P. SUH

Department of Mechanical Engineering, Massachusetts Institute of Technology, Cambridge, Mass. 02139 (U.S.A.)

(Received February 1, 1977)

Summary

An analysis of the mechanics of void nucleation around subsurface hard particles during delamination wear is presented. The analysis is based on the state of subsurface stress and the accumulation of plastic deformation after each passage of a slider asperity. It is shown that voids can only nucleate in a small region below the sliding contact and that the depth of this region increases with increases of both the normal load and the friction coefficient. Under a given situation, voids first nucleate in a small region below the surface after 1 - 10 asperity passes. During subsequent passes void nucleation becomes possible deeper below the surface. The number of passes required for void nucleation at a given depth is found to decrease with increasing friction coefficient. The analysis indicates that either void nucleation or crack propagation can control the wear rate depending on the materials and the sliding conditions.

Introduction

In previous publications by the authors [1 - 3] sliding wear of metals was shown to occur by the process of delamination. The delamination wear process consists of plastic deformation of a surface layer of finite thickness, of void nucleation and of crack propagation below the surface. It was reasoned that voids around either inclusions or hard second-phase particles could nucleate only below a certain depth from the surface owing to the large hydrostatic pressure near the asperity contact and only above some other depth owing to the decrease in stress and deformation with distance from the contact.

*Present address: Department of Mechanical Engineering, University of California, Berkeley, Calif. 94720, U.S.A.

The purpose of this paper is to analyze the mechanics of crack nucleation around hard cylindrical inclusions as a first step in understanding the crack nucleation process. The analysis is based on the assumption that voids nucleate by separation of the matrix from the particle when the radial stress component exceeds a critical tensile stress. Such an assumption is reasonable when the inclusions are large enough to satisfy the energy criterion for crack nucleation.

The results of the analysis support the original predictions of the delamination theory of wear. They show that cracks should indeed nucleate a finite distance below the surface and that the location of possible crack nucleation sites is affected by the magnitudes of the normal and tangential forces at the asperity–surface contact. The analysis is also used to determine the number of asperity passes required for void nucleation and to determine whether void nucleation or crack propagation is the controlling mechanism. (The mechanics of crack propagation are analyzed in the companion paper [4].)

The results obtained in this paper cannot be extended to the case of single-phase metals with no inclusions. However, the results are relevant to many commercially pure metals since inclusions are often present in these metals. Even if the crack nucleation occurs owing to dislocation interactions, the basic argument regarding the effect of hydrostatic pressure on crack nucleation may still be valid.

Review of the literature on void nucleation

The mechanics of void nucleation from inclusions or hard particles during sliding wear have not been studied previously. However, the void nucleation process in uniaxial tension or in pure shear testing has been the subject of extensive investigations, both theoretical and experimental. Although the state of stress and strain in wear is different from that found in uniaxial testing, some similarities in void nucleation have been observed [5]. Therefore a review of the literature on void nucleation in simple testing is instructive in understanding and analyzing the void nucleation process in delamination.

Some recent reviews of the subject are given by Mogford [6], Rosenfield [7], Rogers [8] and Argon *et al.* [9]. Although the process is not yet completely understood, some facts are clear. The experimental results indicate that voids nucleate from hard particles by either particle–matrix separation or by particle fracture. Generally, matrix–particle separation is the mode if the particles are equiaxed and particle fracture is the mode for elongated particles. Here only equiaxed particles are considered.

Previous investigations on void formation around an equiaxed particle can be grouped into three categories according to the criterion used for void formation, namely the energy criterion, the local stress criterion and the local strain criterion. Gurland and Plateau [10] proposed that voids at the

interface can form when the locally concentrated elastic strain energy, which could be released upon decohesion, becomes comparable with the energy of the surfaces to be generated. A more recent and complete analysis of Tanaka *et al.* [11] shows that in a purely elastic situation the energy criterion is always satisfied for particles larger than 25 nm (250 Å) when the stress almost reeches the yield stress. However, in many instances much larger particles have been observed to remain attached to the matrix even at strains much larger than the yield strain. Thus the energy criterion is a necessary but not sufficient condition. It follows that for very small particles (smaller than 25 nm) void nucleation becomes very difficult since the energy criterion is not satisfied.

Since the energy requirement is not a sufficient condition, some local stress or local strain criterion must be satisfied before void nucleation is possible. Stroh [12 - 13] analyzed void nucleation by considering local stress concentrations due to dislocation pile-ups at inclusions (this idea was proposed by Zener [14]). However, this mechanism cannot be responsible for void formation in metals with moderate flow stress at moderate temperatures, since the ease of secondary slip makes the development of high stresses very difficult. Ashby [15] introduced a stress criterion based on a dislocation model for void nucleation in which it is considered that the dislocations generated by primary slip interact with the dislocations generated by secondary slip at particles. These interactions form reverse pile-ups and can build up to cause a large tensile interfacial stress at the particle–matrix interface. Ashby's dislocation model was later modified by Brown and Stobbs [16] to include an energy argument for void nucleation.

McClintock [17], in considering an elastic–plastic continuum analysis of stress distribution around cylindrical inclusions in anti-plane shear, found that large strain concentrations can develop around rigid inclusions in a non-hardening matrix. He therefore suggested a local strain criterion or a criterion which is a mixture of a local interfacial shear strain and a local interfacial tensile stress.

The above review on the criteria for void nucleation indicates that, for void nucleation from hard particles in a deforming matrix, the energy criterion must be satisfied and a tensile stress larger than the interfacial strength must be developed. Since the energy criterion is always satisfied for large particles, the stress criterion becomes the necessary and sufficient condition for such particles. (Since the strain criterion has not been developed to a point that can be implemented, it is assumed that the stress criterion is a sufficient condition.)

In the analysis of interfacial tensile stress development, two methods can be used. Which one is preferable depends on the size of the particles. For particles smaller than 1 μm, the dislocation analysis of Ashby is suitable, whereas for larger particles continuum mechanics is simpler and more appropriate since the slip plane spacings are much smaller than 1 μm. Several continuum mechanics analyses of void nucleation have been published.

Huang [18] analyzed the stresses around a rigid cylindrical inclusion embedded in an elastic power law hardening matrix subjected to pure shear.

He found a maximum interfacial tensile stress which was independent of boundary shear strains. However, physically this stress must depend on the boundary shear strain. Orr and Brown [19] found an interfacial tensile stress which depended on the boundary shear strains. Their solution, which was obtained for a rigid inclusion in an elastic–plastic non-hardening and in a linearly hardening matrix, did not reach a steady state value and the interfacial tensile stress increased continuously with the boundary shear strain. The difficulties involved with these two solutions, *i.e.* boundary shear strain independent stress in Huang's solution and the lack of a steady state in Orr and Brown's solution, indicate that these solutions are not accurate and cannot be useful.

Argon *et al.* [9, 20, 21] analyzed the process of void nucleation around rigid inclusions of circular cross section embedded in an elastic–plastic matrix in plane strain subjected to pure shear and superposed hydrostatic tension. They demonstrated that the interfacial tensile stress must be limited by two solutions. Following Rhee and McClintock [22], an upper bound solution was found by assuming the matrix to be incompressible and linearly hardening (with zero yield stress), and a lower bound solution was found for an elastic perfectly plastic matrix. The two limiting solutions yielded very close results and they concluded that the maximum interfacial tensile stress due to pure shear at the boundary is equal to the yield strength of the material. They also suggested that the hydrostatic tension component of the stress may be superposed on the interfacial tensile stress or

$$\sigma_{rr} = y(\bar{\epsilon}^{p}) + \sigma_{h} \tag{1}$$

where σ_{rr} is the maximum interfacial stress, $y(\bar{\epsilon}^{p})$ is the yield strength of the material and σ_{h} is the hydrostatic stress. Void nucleation is then possible if σ_{rr} reaches the particle–matrix bond strength.

From the above criterion it follows that void nucleation can be retarded if the particle–matrix bond strength is increased. It has been shown that the particle–matrix adhesion can be increased by a small addition of an alloy to the matrix, which increases the ductility [23, 24]. (Ductility is controlled by void nucleation around particles and by void coalescence.)

Equation (1) indicates that voids can nucleate more easily if a hydrostatic tensile stress is present and that void nucleation can be suppressed in the presence of a hydrostatic compressive stress. Sufficient experimental results have been published to show that in fact void nucleation is suppressed in the presence of a large hydrostatic pressure [25 - 27] and that ductility under uniaxial testing [28] or under shear deformation [29] can be increased by superimposing a large hydrostatic pressure.

State of stress under a sliding contact

The investigations on void nucleation from hard particles reviewed in the last section were all for uniaxial tension or pure shear loading. The state

of stress under a sliding contact, however, is very complex. Before the process of void nucleation in delamination can be analyzed, the state of stress below the surface must be determined.

No exact solution exists for an elastic–plastic solid subjected to sliding at the surface. However, an approximate solution for an elastic perfectly plastic half-space is given by Merwin and Johnson [30] and Johnson and Jeffries [31]. This method of solution, which is described in the Appendix, gives the state of stress, the residual stresses and the residual strains during steady state sliding of an elastic perfectly plastic half-space against a rigid stationary plane contact, as sketched in Fig. 1. The cartesian coordinate axes in Fig. 1 are fixed in the stationary body and the maximum applied normal and tangential stresses at the contact are designated p_0 and q_0, respectively. In order to find the state of stress in the moving plane, p_0 and q_0 must be first specified.

It is well established that in the sliding of two surfaces with applied normal and tangential loads N and T, the contact is made at asperities of the two surfaces (Fig. 2(a)). In order to simplify the problem, it can be assumed that the lower surface is smooth and that the upper surface is rough*

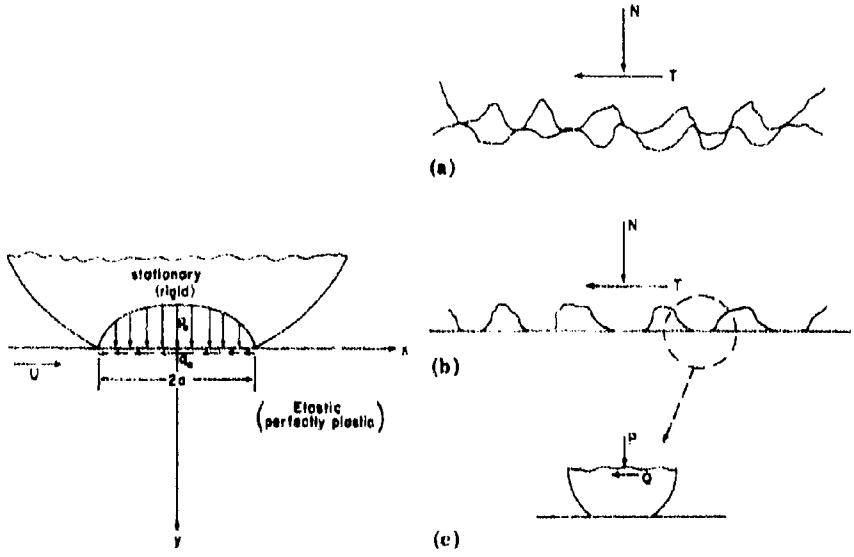

Fig. 1. A model of a contact between a stationary rigid asperity and a moving elastic perfectly plastic half-space.

Fig. 2. Contact of two sliding surfaces: (a) a physical model; (b) an idealized model; (c) a model of a single contact.

*This is a reasonable assumption since the surface becomes very smooth during the early stages of sliding.

(Fig. 2(b)). Therefore, in order to analyze the state of stress in the lower plane, one asperity contact is considered, as in Fig. 2(c). The main problem is to find the stresses P and Q at the contacts. If it is assumed that the stresses are the same at all contacts, that all contacts have the same area A and that there are n such contacts, it is found that

$$N = nAP \tag{2}$$

$$T = nAQ \tag{3}$$

The friction coefficient μ is then found:

$$\mu = T/N = Q/P \tag{4}$$

If adhesion occurs at the contact, the contact stresses P and Q may be found by a slip-line method proposed by Green [32, 33] (Fig. 3(a)). In satisfying the yield condition at the contact, a relation between P and Q can be obtained (Fig. 3(b)). Green's analysis applies to a rigid perfectly plastic material and Q is limited to k, the yield strength in shear. The problem with this solution is that the slip-lines degenerate to a single slip-line along the contact for friction coefficients larger than 0.38. This means that for large friction coefficients the lower body remains rigid, which is physically unrealistic. If the adhesion is "weak" (the contact shear strength is less than k), the maximum Q is lowered further.

If plowing occurs at the contact, Q can be larger than k and the slip-lines would not degenerate for larger friction coefficients. Therefore, in the contact model of Fig. 2(c) it is assumed that plowing occurs and that the tangential stress Q can be larger than k. It should be noted that under this assumption the yield condition is violated very near the surface by the simple contact configuration assumed, since the actual surface configuration caused by plowing is not properly accounted for in the analysis. Nevertheless the St. Venant's principle and the Merwin and Johnson solution guarantee that the yield condition is satisfied everywhere below the surface (*i.e.* away from the surface).

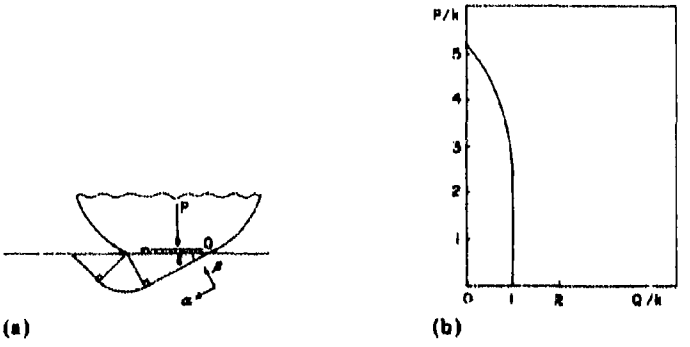

(a) (b)

Fig. 3. A slip line analysis of adhesive contact: (a) Green's slip line field; (b) the yield locus relating normal and tangential applied stresses.

The Merwin and Johnson method was used to find the size of the plastically deforming zone under a contact, the state of stress, the residual stresses and the residual strains during steady state sliding. The results for cases in which the local applied normal stress $p_0 = 4k$ and local applied tangential stresses q_0 ranged from 0 to $4k$ are given in Figs. 4 - 9. The plastically deformed region under steady state sliding is shown in Fig. 4. It should be noted that for zero friction a state of shakedown is reached and the steady state deformation is purely elastic. The size of the plastic region increases with increasing friction coefficient. For friction coefficients smaller than 0.5 the plastic region is below the surface, whereas at larger friction coefficients the plastic region exterds to the surface. The large size of the plastic zone in front of the asperity for large friction coefficient is surprising. Perhaps this is due to the fact that plowing was assumed for the stress boundary condition but the displacements for plowing (*i.e.* raised material in

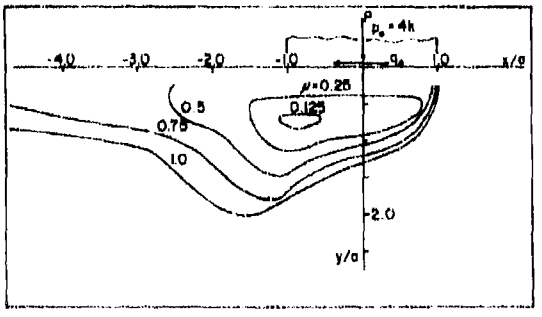

Fig. 4. Steady state plastic deformation regions for different friction coefficients.

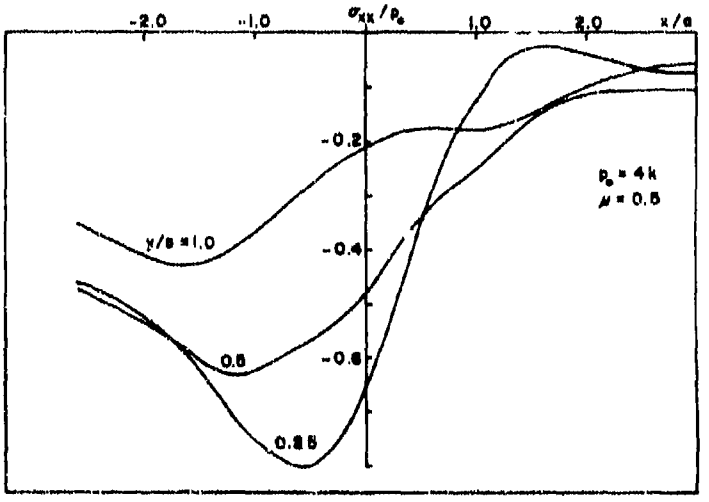

Fig. 5. The steady state xx component of the stress as a function of depth and of x.

front of the asperity) were not considered. If the solution were to allow a raised surface in front of the contact, stresses would be relieved below the surface in front of the contact and the size of the plastic zone would decrease.

The steady state components of stress σ_{xx}, σ_{yy} and σ_{xy} at various depths are given in Figs. 5 - 7. (The coordinates are described in Fig. 1.) σ_{xx} is always compressive, whereas σ_{yy} becomes tensile behind the contact and close to the surface. This tensile zone has also been found in obtaining a similar solution by a finite element method [34]. The distribution of steady state residual stress $(\sigma_{xx})_r$ is given in Fig. 8 for different friction coefficients. (As shown by Merwin and Johnson the only possible residual stresses are σ_{xx} and σ_{zz}.) Figure 8 shows that the residual stress is compressive and that its magnitude for large friction coefficients is largest near the surface.

The steady state increment $(\delta_{xy})_r$ of shear strain for each passage of a slider asperity is given in Fig. 9. If the friction coefficient is large the increment of shear strain is largest at the surface. It should be noted that

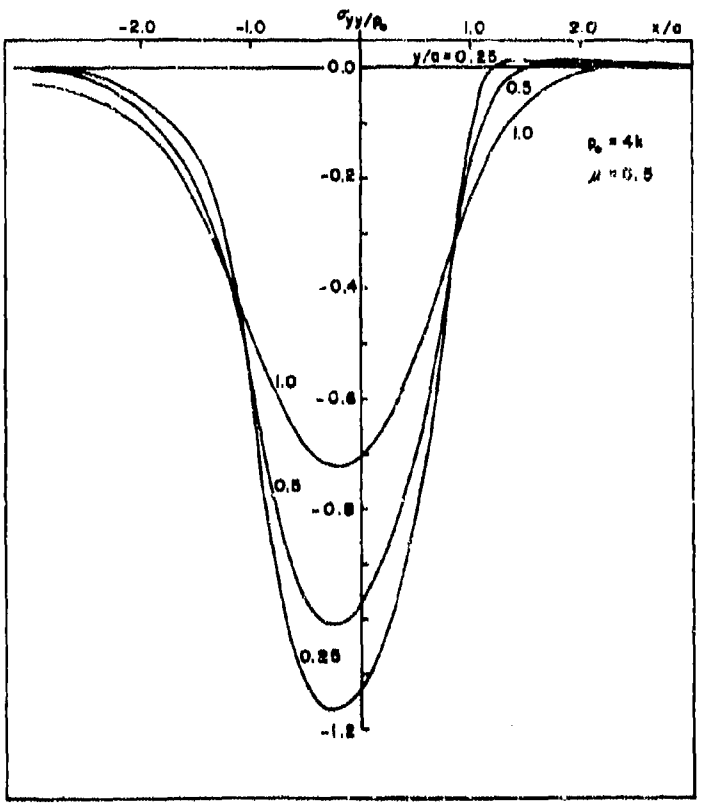

Fig. 6. The steady state yy component of stress as a function of depth and of x.

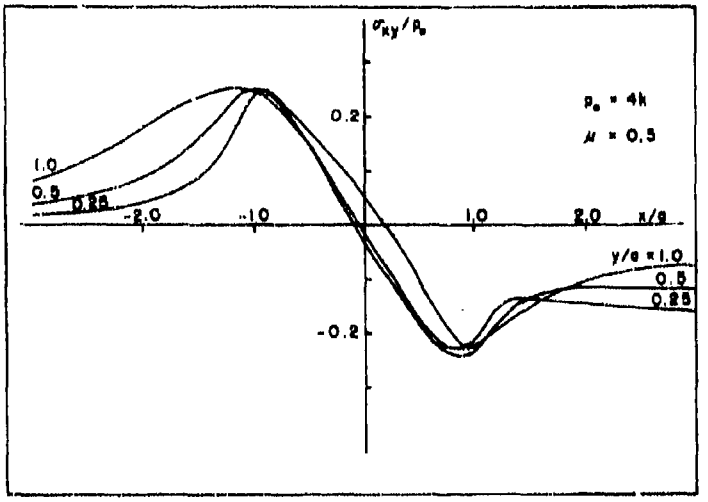

Fig. 7. The steady state xy (shear) component of stress as a function of depth and of x.

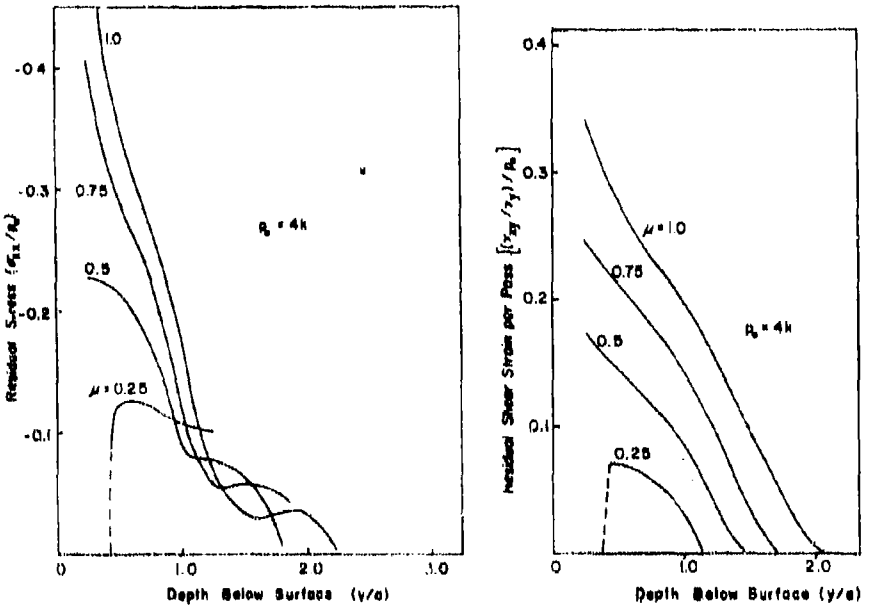

Fig. 8. The steady state residual stress σ_{xx} as a function of depth and of the coefficient of friction.

Fig. 9. The total plastic shear strain increment per asperity passage as a function of the depth and of the coefficient of friction.

during steady state sliding the only non-zero plastic strain increment is the shear strain which accumulates with an amount $(\delta_{xy})_r$ after each passage of a slider asperity.

Analysis of void nucleation below the surface

Since the state of stress and the residual stresses and strains can be obtained for the case of steady state cyclic loading, the process of void nucleation from hard particles can be analyzed for steady state delamination wear. It is assumed that the inclusions are larger than 1 μm, that therefore the energy criterion for nucleation is satisfied and that the problem can be treated by continuum mechanics. It is also assumed that a stress criterion can be used for this case, *i.e.* that void nucleation from hard particles occurs when the interfacial tensile stress becomes equal to or greater than the particle–matrix bond strength. Therefore, the problem is to find the interfacial normal stress at subsurface hard particles*.

It is assumed that the particles are cylindrical and rigid and are embedded in an elastic perfectly plastic matrix. The normal stress at the particle–matrix interface depends both on the state of stress and on the accumulated plastic strain. It is assumed that the interfacial normal stress σ_{rr} can be found from a superposition of independently calculated stresses due to applied load at the contact and due to accumulated strain. It is also assumed that the stress fields around inclusions do not interact, *i.e.* that only one inclusion need be considered.

In order to find the stress due to the accumulation of plastic shear strain, the solution of Argon *et al.* [9] for pure shear is used, namely eqn. (1). A point (x, y) is considered that is below the surface and is subjected to a shear strain δ_{xy}. The point is then considered as a small element with the shear strain δ_{xy} applied at the boundaries. It is assumed that a rigid cylindrical particle is inserted at the center of the element as shown in Fig. 10. The shear strain δ_{xy} develops an interfacial normal stress σ_{rr} around the particle, where σ_{rr} is a function of δ_{xy}:

$$\sigma_{rr} = f(\delta_{xy}) \tag{5}$$

It is assumed that during cyclic sliding σ_{rr} depends on δ_{xy} as shown in Fig. 11 (an elastic perfectly plastic relationship). The shear strain δ_{xy} is the total accumulated strain and it is increased by increments of $(\delta_{xy})_r$ after each asperity pass. According to Fig. 11, the maximum σ_{rr} is developed when

$$\delta_{xy} = \delta_y = k/G \tag{6}$$

where δ_y is the yield strain in pure shear and G is the elastic shear modulus.

---

*An attempt was made to find the interfacial normal stress around particles by using a finite element program. However, the finite element method was found to be very expensive for this problem and it was discontinued.

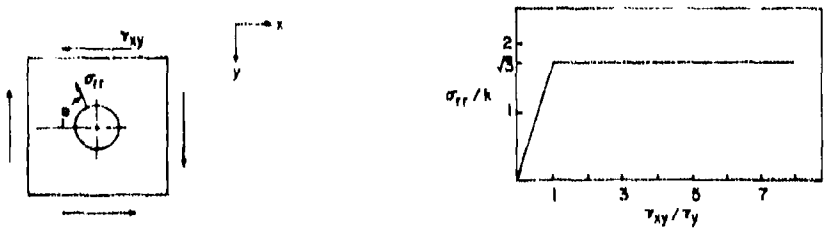

Fig. 10. A rigid cylindrical inclusion subjected to pure shear strain.

Fig. 11. Elastic perfectly plastic normal stress–shear strain curve for the model of Fig. 10.

The number of slider asperity passes before the maximum σ_{rr} is developed can be found since the shear strain increment per pass $(\delta_{xy})_r$ at a given depth is known from the overall analysis. From the assumed relation between σ_{rr} and δ_{xy} given in Fig. 11 the maximum σ_{rr} due to accumulated plastic strain is equal to $\sqrt{3}k$. However, σ_{rr} depends on the angular position θ around the particle or

$$(\sigma_{rr})_1 = \sqrt{3}k \sin 2\theta \tag{7}$$

where $(\sigma_{rr})_1$ is the normal interfacial stress due to the cumulative plastic deformation around a particle located at a depth y below the surface.

In order to find the maximum interfacial normal stress σ_{rr} due to the state of stress under the contact, Argon *et al.*'s criteria (eqn. (1)) may be used. However, the stresses at each point must first be transformed to a state of maximum shear stress and hydrostatic stress by using Mohr's circle. Following the procedure of the last paragraph, it is assumed that the stresses act on an element and that a particle is inserted at the center of the element (Fig. 12). Therefore, using eqn. (1)

$$(\sigma_{rr})_2 = \sqrt{3}\,\tau_{max} \sin 2(\theta - \phi) + \sigma_h \tag{8}$$

where τ_{max} is the maximum shear stress at the point (x, y), ϕ is the angle from the x axis to the axis of the maximum positive shear stress and σ_h is the hydrostatic stress at (x, y); $\sqrt{3}$ appears in the equation since the von Mises yield criterion was used.

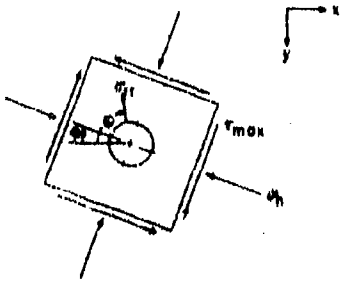

Fig. 12. A rigid cylindrical inclusion subjected to a general state of stress.

The total σ_{rr} due to both the applied stress and the accumulation of plastic shear strain is found by adding eqns. (7) and (8). The maximum σ_{rr} which occurs at some angle $\theta = \theta_0$ can be obtained for each point (x, y):

$$(\sigma_{rr})_{max} = \sqrt{3}k \sin 2\theta_0 + \sqrt{3}\tau_{max} \sin 2(\theta_0 - \phi) + \sigma_h \qquad (9)$$

As was shown above, the number of slider passages before $(\sigma_{rr})_{max}$ can be developed at a given depth is also determined since the shear strain increment per pass is known at that depth.

Equation (9) was programmed in DGC FORTRAN IV language using Merwin and Johnson's method to calculate the state of stress and the residual stresses and strains.

The "nominal" stress solution used in the Merwin and Johnson method was the elastic solution for elliptically distributed loads at the contact, from Smith and Liu [35]. The contours of constant $(\sigma_{rr})_{max}$ found from eqn. (9) are plotted in Fig. 13 for an applied normal stress at each asperity contact of $4k$ and friction coefficients of 1.0, 0.5 and 0.25. It should be noted that $(\sigma_{rr})_{max}$ is compressive immediately below the contact and attains its largest values in front of the slider, well below the surface.

If the particle–matrix bond strength is equal to $2k$, Fig. 13 shows that the size of the region in which void nucleation is possible decreases with decreasing friction coefficient. The size of the void nucleation region is smaller for a stronger particle–matrix bond. The figures show that voids can only nucleate well below the surface ($\sigma_{rr} \geq 2k$), which is consistent with the subsurface observations of wear samples in previous publications [1 - 3].

The minimum and the maximum depth of the void nucleation region is plotted in Fig. 14 as a function of the friction coefficient for applied normal contact stresses p_0 of $4k$ and $6k$. The range of depths for void nucleation increases with increasing friction coefficient for both applied normal stresses but the voids can nucleate deeper below the surface for a larger applied normal stress. It is interesting to observe that, at $p_0 = 6k$ and for a zero friction coefficient (which applies to a case of pure rolling), void nucleation is possible in a small region. However, at $p_0 = 4k$ and for a zero friction coefficient, voids do not nucleate since the stresses shake down to an elastic state during steady sliding.

The depth of the void nucleation region ($\sigma_{rr} \geq 2k$) is plotted in Fig. 15 against the number of passes required to reach the maximum σ_{rr} at each depth, for different friction coefficients and p_0 of $6k$ and $4k$. At a given depth as the friction coefficient increases a smaller number of passes is required for void nucleation. It should be noted that voids first nucleate at the minimum depths only after 1 - 10 asperity passes (depending on the friction coefficient and the normal load); as the number of passes increases, the void nucleation region moves deeper below the surface.

It should be pointed out here that calculation of the interfacial normal stress at inclusions by superposing that due to the cumulative plastic deformation and that due to the applied stress violates the yield criterion. This violation occurs because for an elastic perfectly plastic material σ_{rr}

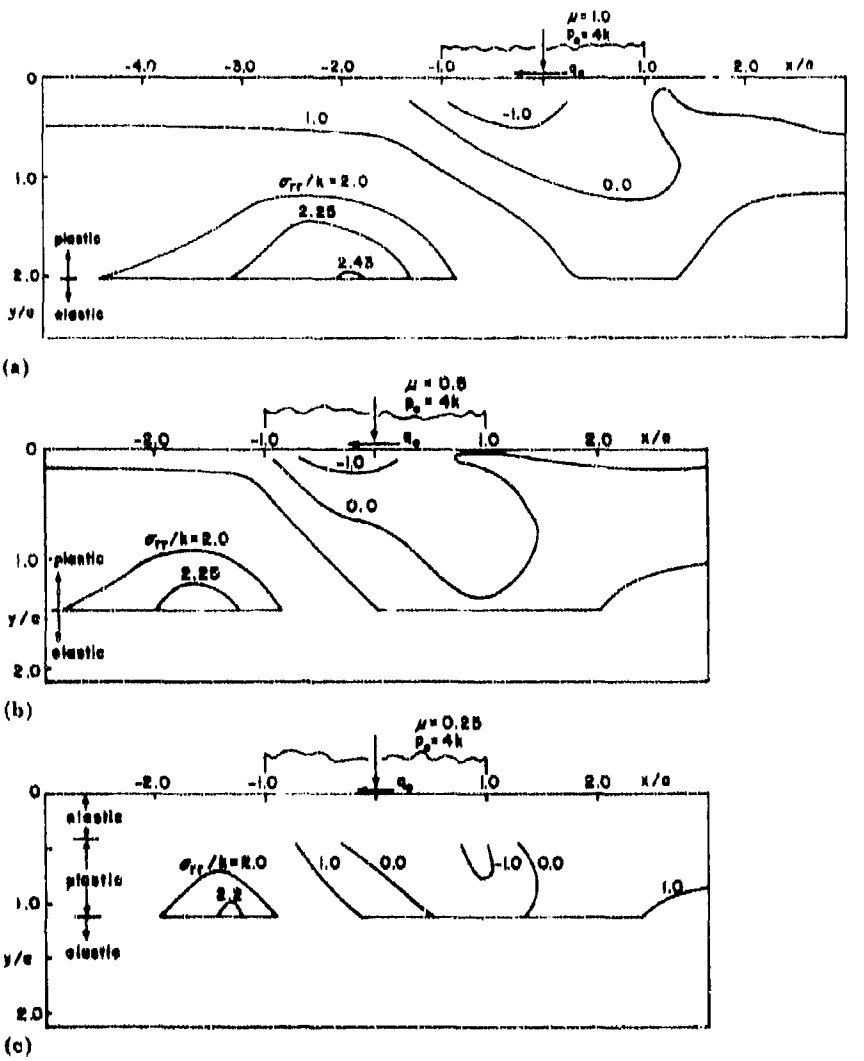

Fig. 13. Contours of constant $(\sigma_{rr})_{max}$ around an inclusion for coefficients of friction of (a) 1.0, (b) 0.5 and (c) 0.25.

cannot exceed the yield stress, *i.e.* $\sqrt{3}k$, and the solution may not be correct for $\sigma_{rr} > \sqrt{3}k$. However, if the voids nucleate when $\sigma_{rr} = \sqrt{3}k$, the stresses can relax and the yield criterion can be satisfied. The solution, however, does indicate that voids nucleate below the surface and that the depth and the number of zones depend on the friction coefficient and on the applied normal load.

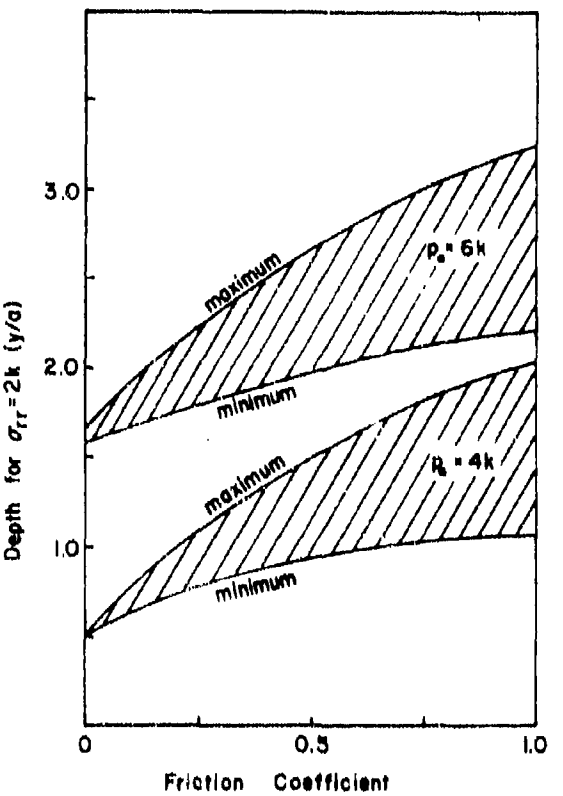

Fig. 14. Depth of void nucleation region as a function of the friction coefficient for two applied local normal stresses.

In the analysis of void nucleation it was assumed that the hard particles were rigid. However, in real materials the particles have some elasticity, which would result in values of σ_{rr} smaller than the ones calculated by the above procedure.

As was pointed out by McClintock [17], the criterion for void nucleation from large particles may be a combination of a local shear strain criterion and a local interfacial tensile stress criterion. In the above analysis it was assumed that the local stress criterion was sufficient. This assumption may be a good approximation for equiaxed particles but not for elongated particles. In the analysis of elongated particles the local strain concentrations are large and void nucleation generally occurs by particle fracture. Therefore, as the particles become more elongated, the local shear strain criterion for void nucleation may become the dominant criterion.

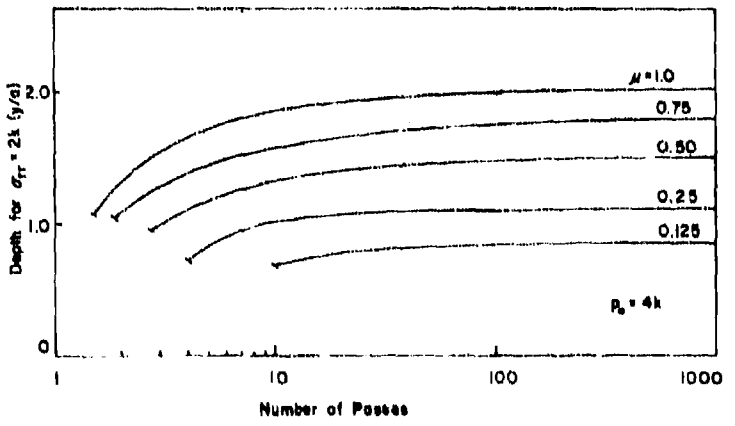

(a)

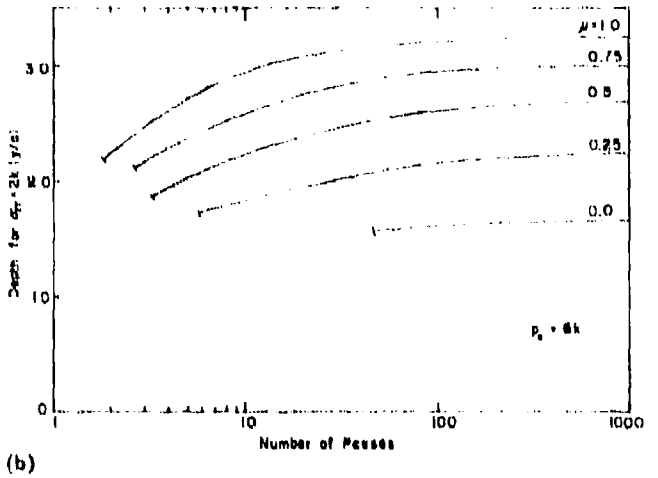

(b)

Fig. 15. Depth of the void nucleation region as a function of the friction coefficient and the number of asperity passes: (a) $p_0 = 4k$. (b) $p_0 = 6k$.

Discussion on crack propagation

Once the voids are nucleated from hard particles they will become enlarged with repeated passes of the slider asperities. Furthermore, cracks can develop from these cavities either by void coalescence or by crack propagation between the voids. The process of void growth has been analyzed for pure shear [36]. Void coalescence for hydrostatic tension has also been analyzed [37 - 39]. However, the analysis of this process during delamination wear seems complex and has not been done.

When the subsurface cracks reach a certain length (by void coalescence or crack propagation between the voids), the stress intensity factor at the crack tip can become sufficiently large to propagate the cracks by some increment after each pass (similar to fatigue crack propagation). Fleming and Suh [4] analyzed this process. A maximum stress intensity factor exists behind the contact and at a certain depth below the surface. This may cause crack propagation parallel to and below the surface, which has been observed experimentally [1 - 3].

Comparison between void nucleation and crack propagation

In materials which contain hard second-phase particles or inclusions, void nucleation and crack propagation must occur to generate the wear sheets. Therefore it is of primary importance to determine which one of these processes is the rate controlling mechanism. A qualitative comparison based on experimental results can be made between void nucleation and crack propagation.

Subsurface observations [1 - 3] have indicated that, in general, the number of subsurface voids is far larger than the number of cracks. This observation together with the result of the void nucleation analysis which showed that voids can nucleate even after one asperity pass, indicates that crack propagation may be slower than void nucleation in a material such as spheroidized AISI 1020 steel. In order to check this conclusion the crack propagation rate is calculated below for two examples. Although the calculation is very approximate it can provide some insight into the process.

The model in Fig. 16 is used to determine approximately the number of asperity passes required for wear sheet generation by crack propagation. The lower cylinder of diameter d (the specimen) is rotated at an angular speed ω. The upper block is stationary and makes a contact with a length L and a width L. It is assumed that the specimen wears in layers with thickness h and width L, where h corresponds to the thickness of the wear sheets. If after R revolutions n layers wear off, the worn volume V per revolution is given by

$$V = n\pi dLh/R \tag{10}$$

If the asperity contact spacing is assumed to be λ, the number of asperities per length of contact is L/λ. This corresponds to the number of asperity passes per revolution. Therefore the total number of asperity passes required for removal of one layer of material is given by

$$N = \frac{R}{n}\frac{L}{\lambda} \tag{11}$$

Since the worn volume V per revolution can be determined experimentally, the number of layers removed per revolution can be calculated from eqn. (10) if the thickness of the sheets and the size L of the contact is known.

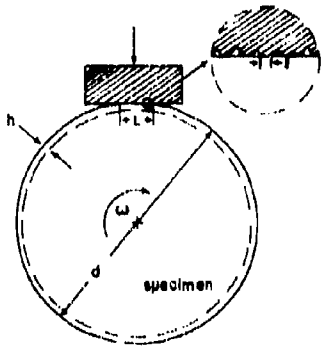

Fig. 16. A model of a wearing specimen.

Then the number of asperity passes for removal of one layer can be calculated from eqn. (11) by assuming an asperity contact spacing.

Example 1

For an AISI 1020 steel specimen of diameter 6.3 mm rotating against a 52100 steel slider under a load of 2.25 kg in air, the wear rate is 2×10^{-13} m^3 rev^{-1} and the friction coefficient is 0.5. If the apparent contact length $L = 2$ mm and the asperity contact spacing λ is assumed to be 100 μm and the wear sheet thickness h is 2 μm, then

$$\frac{R}{n} = \frac{\pi(6.3 \times 10^{-3})(2 \times 10^{-3})(2 \times 10^{-6})}{2 \times 10^{-13}} = 400 \text{ revolutions per layer}$$

$$N = 400 \frac{2 \times 10^{3}}{100 \times 10^{-6}} = 8 \times 10^{3} \text{ asperity passes}$$

Example 2

For the same material as in example 1 but tested in argon, the wear rate is 7.5×10^{-13} m^3 rev^{-1} and the friction coefficient is 0.85. If $L = 400$ mm, $h = 10$ μm and $\lambda = 100$ μm, then

$$\frac{R}{n} = \frac{\pi(6.3 \times 10^{-3})(4 \times 10^{-3})(10^{-5})}{7.5 \times 10^{-13}} = 1.1 \times 10^{3} \text{ revolutions per layer}$$

$$N = 1.1 \times 10^{3} \frac{4 \times 10^{-3}}{100 \times 10^{-6}} = 4 \times 10^{4} \text{ asperity passes}$$

The above examples indicate that approximately between 10^3 and 10^4 asperity passes are required for wear sheet generation. If only ten of these passes are needed for void nucleation, the rest, *i.e.* $(10^3 - 10^4) - 10$ or approximately $10^3 - 10^4$ passes, are necessary for crack propagation. In example 1, if the length of the wear sheets is 100 μm, the crack growth rate

per cycle dC/dN becomes approximately 10^{-2} μm pass^{-1} which is very small. For the second example dC/dN is about 2.5×10^{-3} μm pass^{-1}. Therefore, the subsurface crack propagation process is the rate controlling mechanism for metals in which void nucleation can occur readily.

Discussion and summary

The delamination theory of wear postulated that voids can nucleate below the surface but not at the surface [1]. This is because the large hydrostatic pressure which exists directly under a contact will oppose void formation. However, incremental plastic deformation which is largest at the surface will favor void nucleation. Therefore, voids can nucleate below a depth where the hydrostatic pressure is not large enough to suppress void formation and above a depth where the plastic deformation is insufficient to nucleate voids around the hard particles. Even though the analysis presented here is approximate, it shows excellent agreement with the above postulate and with experimental observations of wear.

It was shown that void nucleation is possible in a region below the sliding contact and that the size and depth of this region increases with increasing friction coefficient and normal load. Under a given situation voids first nucleate in a small region below the surface only after 1 - 10 asperity passes. During subsequent passes void nucleation becomes possible at larger depths below the surface. The number of passes required for void nucleation at a given depth was found to decrease with increasing friction coefficient, *i.e.* a larger number of asperity passes is required for void nucleation under situations where the friction coefficient is low.

The analysis indicated that void formation occurs very readily around subsurface hard particles but that crack propagation occurs very slowly. Therefore, for materials under wear situations where void nucleation can occur easily crack propagation may be the rate controlling mechanism. This is the case for metals of medium tensile strength and a large fracture toughness (such as 1020 steel) under high friction situations. However, if void nucleation is extremely difficult but crack propagation can occur easily for a given material under a given situation, void nucleation can become the controlling mechanism. This case could arise for metals of high tensile strength and low fracture toughness under conditions of low friction coefficients.

Acknowledgments

The work reported in this report was sponsored by the Defense Advanced Research Projects Agency through the Office of Naval Research under contract N00014-67-A-0204-0080. We are grateful to Dr. Edward van Reuth, Lt. Richard S. Miller, Dr. Arden Bement and Lt. Cdr. Kirk Petrovic for their personal support and guidance of our work.

References

1 N. P. Suh, The delamination theory of wear, Wear, 25 (1973) 111 - 124.
2 N. P. Suh, S. Jahanmir, E. P. Abrahamson, II and A. P. L. Turner, Further investigation of the delamination theory of wear, J. Lubr. Technol., 96 (1974) 631 - 637.
3 S. Jahanmir, N. P. Suh and E. P. Abrahamson, II, Microscopic observations of the wear sheet formation by delamination, Wear, 28 (1974) 235 - 249.
4 J. R. Fleming and N. P. Suh, Mechanics of crack propagation in delamination wear, 44 (1977) 39 - 56.
5 S. Jahanmir, E. P. Abrahamson, II, and N. P. Suh, The effect of second phase particles on wear, Proc. 3rd North American Metalworking Research Conf., Carnegie Press, Pittsburgh, Pa., 1975, pp. 854 - 864.
6 I. L. Mogford, The deformation and fracture of two-phase materials, Metall. Rev., 12 (1967) 49 - 68.
7 A. R. Rosenfield, Criteria for ductile fracture of two-phase alloys, Metall. Rev., 13 (1968) 29 - 40.
8 H. C. Rogers, The effect of material variables on ductility. In Ductility, Am. Soc. Metals, Metals Park, Ohio, 1968, pp. 31 - 61.
9 A. S. Argon, J. Im and R. Safoglu, Cavity formation from inclusion in ductile fracture, Metall. Trans., 6A (1975) 825 - 837.
10 J. Gurland and J. Plateau, The mechanism of ductile rupture of metals containing inclusions, Trans. Am. Soc. Met., 56 (1963) 442 - 454.
11 K. Tanaka, T. Mori and T. Nakamura, Cavity formation at the interface of a spherical inclusion in a plastically deformed matrix, Philos. Mag., 21 (1970) 267 - 279.
12 A. N. Stroh, The formation of cracks as a result of plastic flow, Proc. R. Soc. London, Ser. A, 223 (1954) 404 - 414.
13 A. N. Stroh, The formation of cracks as a result of plastic flow, II, Proc. R. Soc. London, Ser. A, 232 (1955) 548 - 560.
14 C. Zener, Fracturing of Metals, Am. Soc. Metals, Novelty, Ohio, 1949, pp. 3 - 31.
15 M. F. Ashby, Work hardening of dispersion-hardened crystals, Philos. Mag., 14 (1966) 1157 - 1178.
16 L. M. Brown and W. M. Stobbs, The work-hardening of copper - silica, Philos. Mag., 23 (1971) 1185 - 1233.
17 F. A. McClintock, On the mechanics of fracture from inclusions. In Ductility, Am. Soc. Metals, Metals Park, Ohio, 1968, pp. 255 - 277.
18 W. C. Huang, Theoretical study of stress concentrations at circular inclusions in strain hardening materials, Int. J. Solids Struct., 8 (1972) 149 - 192.
19 J. Orr and D. K. Brown, Elasto-plastic solution for a cylindrical inclusion in plane strain, Eng. Fract. Mech., 6 (1974) 261 - 274.
20 A. S. Argon and J. Im, Separation of second phase particles in spheroidized 1045 steel, Cu 0.6% Cr alloy, and maraging steel in plastic straining, Metall. Trans., 6A (1975) 839 - 851.
21 A. S. Argon, formation of cavities from non-deformable second phase particles in low temperature ductile fracture, J. Eng. Mater. Technol., 98 (1976) 60 - 68.
22 S. S. Rhee and F. A. McClintock, On the effects of strain hardening on strain concentrations, Proc. 4th U.S. Natl. Congress on Applied Mechanics, Vol. 2, 1962, pp. 1007 - 1013.
23 H. F. Fischmeister, E. Navara and K. E. Easterling, Effects of alloying on structural stability and cohesion between phases of oxide/metal composites, Met. Sci. J., 6 (1972) 211 - 215.
24 K. E. Easterling, H. F. Fischmeister and E. Navara, The particle to matrix bond in dispersion-hardened austenitic and ferritic iron alloys, Powder Metall., 16 (1973) 128 - 145.
25 E. Rozovsky, W. C. Hahn, Jr., and B. Avitzur, The behavior of particles during plastic deformation of metals, Metall. Trans., 4 (1973) 927 - 930.

26 A. R. Austen and B. Avitzur, Influence of hydrostatic pressure on void formation of hard particles, J. Eng. Ind., 97 (1974) 1192 - 1197.
27 K. J. Kahlow and B. Avitzur, Void behavior as influenced by pressure and plastic deformation, J. Eng. Ind., 96 (1974) 901 - 911.
28 P. W. Bridgman, Studies in Large Plastic Flow and Fracture, Harvard Univ. Press, Cambridge, Mass., 1964.
29 T. J. Walker and M. C. Shaw, On deformation at large strains. In S. A. Tobias and F. Koenigsberger (eds.), Proc. 10th Int. Machine Tool Design and Research Conf., Adv. Mach. Tool Des. Res., Pergamon Press, Oxford, 1970, pp. 241 - 252.
30 J. E. Merwin and K. L. Johnson, An analysis of plastic deformation in rolling contact, Proc. Inst. Mech. Eng., London, 177 (1963) 676 - 690.
31 K. L. Johnson and J. A. Jefferies, Plastic flow and residual stresses in rolling and sliding contact, Proc. Symp. on Fatigue in Rolling Contact, Inst. Mech. Eng., London, 177 (1963) 54 - 65.
32 A. P. Green, The plastic yielding of metal junctions due to combined shear and pressure, J. Mech. Phys. Solids, 2 (1954) 197 - 211.
33 A. P. Green, Friction between unlubricated metals: a theoretical model of the junction model, Proc. R. Soc. London, Ser. A, 228 (1955) 191 - 204.
34 N. P. Suh, An overview of the delamination theory of wear, Wear, 44 (1977) 1 - 15.
35 J. O. Smith and C. K. Liu, Stresses due to tangential and normal loads on an elastic solid with application to some contact problems, J. Appl. Mech., 20 (1953) 157 - 166.
36 F. A. McClintock, S. M. Kaplan and C. A. Berg, Ductile fracture by hole growth in shear bands, Int. J. Fract. Mech., 2 (1966) 614 - 627.
37 F. A. McClintock, A criterion for ductile fracture by the growth of holes, J. Appl. Mech., 30 (1963) 363 - 371.
38 F. F. Thompson, A theory for ductile fracture by internal necking of cavities, J. Inst. Met., 96 (1968) 360 - 365.
39 J. R. Rice and D. M. Tracey, On the ductile enlargement of voids in triaxial stress fields, J. Mech. Phys. Solids, 17 (1969) 201 - 217.

Appendix: Calculation of elastic–plastic subsurface stresses in sliding contacts

This appendix describes the method which was used to calculate the state of stress and the residual stresses and strains during cyclic sliding. The procedure was first developed by Merwin and Johnson [30] for rolling contacts and was later modified [31] to be used for sliding contacts.

The general problem is simplified by assuming that an elastic perfectly plastic plane slides with a speed U past a rigid stationary surface which makes a contact of length $2a$. The analysis is carried out for the plane strain condition. Therefore, in terms of the coordinate axes shown in Fig. 1 of the main text and associated with the stationary surface, e_{zz} is zero and all stresses and strains are independent of z.

A brief description of the procedure

The analysis is performed by the following steps.

(1) The steady state residual stresses and strains in the plane x–y are assumed to be zero.

(2) A fixed point in the plane is considered (initially at $x = -\infty$ and $y = y_0$). Since the contact is far away from the point, the state of stress is

calculated by superimposing the elastic and residual stresses. The stresses are recalculated at this point as it moves towards the contact with a speed U and by increments of dx.

(3) When the state of stress at the point satisfies the von Mises yield criterion, the Prandtl–Ruess equations are used to calculate the state of stress for successive movements of the point, assuming that the total strains are the same as that given by elastic relations.

(4) The Prandtl–Ruess equations are integrated using Gill's modification of the Runge–Kutta method to fourth order.

(5) When the von Mises yield criterion is not satisfied any more or when the rate of plastic work becomes negative, plastic deformation terminates. For successive movements of the point, the state of stress is found from elastic equations.

(6) Since no attempt is made to satisfy equilibrium during the cycle, the final state of stress violates the equilibrium condition. Therefore, at the end of the cycle, the stresses are relaxed elastically to satisfy equilibrium. This procedure may give non-zero residual stresses and strains.

(7) Steps 2 - 6 are repeated for the same point using the residual stresses from the previous cycle. The procedure is repeated until a steady state condition in the state of stress, the residual stresses and the residual strains is reached. (This is when the residual stresses and strains found in step (6) are

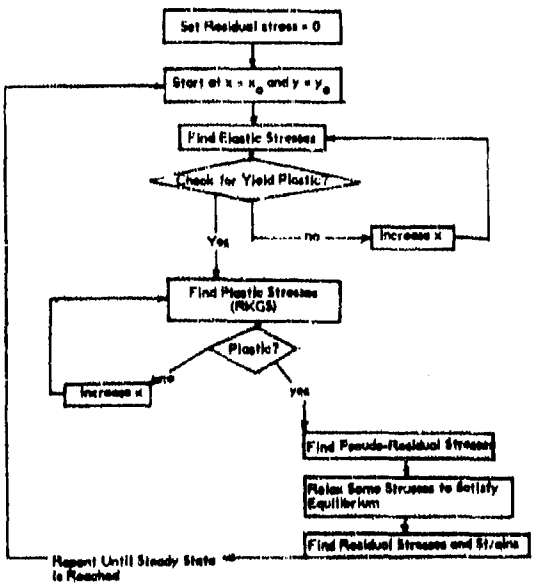

Fig. A1. A flow chart for the numerical calculation of stress and strain under a sliding contact.

not significantly different from the residual stresses and strains at the beginning of the cycle.) The final result is an approximate solution of the steady state stresses in a sliding contact at a given depth.

(8) The same procedure is followed for points at different depths to approximate the total state of stress.

The preceding method was programmed in DGC FORTRAN IV language and a Nova 2 mini-computer (which uses 32 bits for real numbers) was used to perform the computations. The procedure is shown by a flow chart in Fig. A1. It should be noted that the DGC FORTRAN IV language used differs from ANSI FORTRAN IV (especially in its handling of DATA statements) so that the program may require modification to run on another computer.

Discussion of the solution

The final state of stress and the residual stresses and strains calculated by the above procedure is an approximate solution for the case of steady state sliding (*i.e.* when the residual stresses become constant and the pseudo-residual stress in the y direction becomes zero). Merwin and Johnson considered the integration cycles before a steady state is reached to be the actual transient solution but this is not necessarily correct since it is only after the last integration cycle that the pseudo-residual stress in the y direction approaches zero.

The assumption of allowing the total strains during plastic deformation to be identical with the elastic strains is reasonable for low friction coefficients (*i.e.* less than 0.5) since the region which continuously deforms plastically is contained by an elastic region around it. Therefore the total strains cannot be much different than the elastic strains. For larger friction coefficients one boundary of the plastic region is the free surface, which may allow larger strains near the surface. Therefore the solution becomes less exact at larger friction coefficients and near the free surface. However, it should still be reasonable deep below the surface near the elastic–plastic boundary.

The approximate solution found from the preceding method has two types of instabilities. The plastic stresses at the surface cannot be obtained owing to the singularity of the elastic strain gradients at $x = \pm a$. The solution also becomes unstable in that the residual stresses do not converge to steady state values very near the steady state elastic–plastic boundaries for low friction coefficients (lower than 0.5). However, there is no problem at a small distance from the elastic–plastic boundary inside the plastic region.

Wear, 44 (1977) 39 - 56

MECHANICS OF CRACK PROPAGATION IN DELAMINATION WEAR

J. R. FLEMING and N. P. SUH

Department of Mechanical Engineering, Massachusetts Institute of Technology, Cambridge, Mass. 02139 (U.S.A.)

(Received February 1, 1977)

Summary

A mathematical model of subsurface crack propagation in sliding contact is developed. It is shown that linear elastic fracture mechanics may be applied to such problems, even for elastoplastic solids. An equation to predict wear rates is derived, which should apply in delamination wear to materials in which crack nucleation is easy. Results of calculations of stress intensity factors for various subsurface cracks and coefficients of friction are presented. The numerical calculations were done only for coefficients of friction greater than 0.5.

The calculations show that there is a characteristic crack propagation depth below the surface, which increases with increasing coefficient of friction. In addition, the change in stress intensity factor, and hence the crack propagation rate, increases with increasing coefficient of friction. A comparison between these calculations and approximate crack growth rates in sliding wear shows that the results agree reasonably well.

The model is used to explain the phenomenon that increased hardness sometimes increases wear. A possible explanation for seizure in geometrically constrained systems is advanced. The model may be used to predict wear rates from first principles in the near future.

Introduction

The first paper [1] in this issue of *Wear* and its list of references presented an overview of the current state of the delamination theory of wear and the evidence supporting it. Sufficient experimental evidence is now available to justify the acceptance of delamination as a wear mechanism in sliding wear. In addition, physical reasoning and a qualitative understanding of the delamination theory has been used to reduce wear by several orders of magnitude under experimental conditions. The next step in the development of the theory must be mathematical modeling of delamination wear.

The study of wear has two major purposes: to predict wear and to reduce wear. Mathematical models are necessary in order to predict wear

qualitatively. They are also useful in the process of planning experiments and in gaining further physical understanding, since they are often more easily manipulated than experimental situations.

Five processes are involved in delamination wear: transmission of forces, deformation, crack nucleation, crack propagation, and wear sheet separation. The first and the last processes are not currently amenable to analysis; transmission of forces involves adhesion and plowing which requires an understanding of chemical interactions and a three-dimensional large strain elastic–plastic analysis, and wear sheet separation probably depends strongly on material defects and random factors. The deformation and crack nucleation processes were analyzed approximately in the preceding paper [2]; although some insight has been gained, the analysis has not yet been used to formulate an equation to predict wear. This paper is dedicated to modeling crack propagation in delamination wear, and to developing an equation to predict wear rates.

In developing such an equation, it must be assumed that crack propagation controls the wear rate. This is not necessarily true for all materials, since at a given point in the material deformation generally precedes crack nucleation which must precede crack propagation; it is conceivable that the deformation rate or nucleation rate can control the wear rate. However, Jahanmir and Suh [2] have shown that deformation and crack nucleation around hard particles take a short time if the hard particles are common in the material and sufficient deformation takes place. Since most engineering materials (*e.g.* steels) contain many hard particles and the matrix of such materials can be greatly deformed during sliding [3], we feel that crack propagation will control the wear rate in many common metals.

A model of crack propagation

In developing the model, several aspects of the sliding process must be considered. First, a wearing surface generally becomes very smooth [1]. Second, the distance between asperity contacts is generally large compared with the asperity contact size (since the real area of contact is so much smaller than the apparent area of contact for realistic loads) and the stress falls off with distance r from the contact approximately as a $1/r$ proportionality (see eqn. (1)); therefore, the stress beneath and near an asperity contact is not significantly affected by other contacts. Third, in most sliding situations there is unaffected material on either side of the wear track and the deformation is uniform across most of the wear track, so that most of the wearing material is in plane strain. Fourth, experimental evidence has shown that all wear cracks appearing in reasonably ductile materials are essentially parallel to the surface and are very long compared with their distance below the surface [1]. Fifth, the wearing body is essentially infinite in dimension compared with the size of an asperity contact.

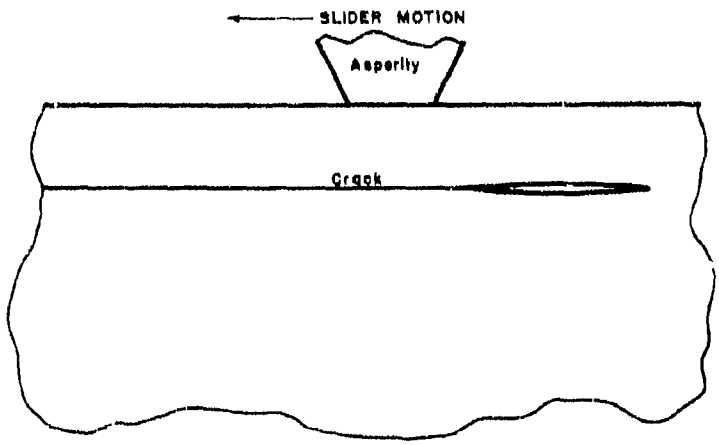

Fig. 1. A model of a subsurface crack in sliding contact.

The physical model chosen on the basis of these observations is illustrated in Fig. 1. It consists of a half-space in plane strain contacted by a single asperity and containing a straight crack parallel to the surface. The crack is drawn as being closed over most of its length for reasons discussed below.

It is known that some of the material in the region of an asperity contact is plastic. Thus, the first question arising in regard to this model is whether it can be analyzed by linear elastic fracture mechanics (*i.e.* can the plasticity be ignored?). The answer to this question lies in the nature of the stress field below the surface.

Approximate subsurface stresses on a crack in sliding contact

A quick approximation to the subsurface stresses may be found from the elastic solution for a point load (in plane strain, a line load along a line into the paper in Fig. 2) [4]. In the notation of Fig. 2

$$\sigma_{rr} = \frac{-2F}{\pi r}\cos(\alpha + \theta) \qquad \sigma_{r\theta} = 0 \qquad \sigma_{\theta\theta} = 0 \tag{1}$$

For this stress field, lines of constant maximum shear stress form circular arcs, as shown in Fig. 2. Using the Tresca yield criterion for such a contact, the plastic zone will lie inside such a line. Also, the stress to the left of the broken line in Fig. 2 is all compressive, while the stress to the right of the broken line is tensile. (The broken line is a line of zero stress and is perpendicular to the line of action of the applied force.)

Finite element analyses of a half-space subjected to a distributed load [5] indicate that this approximation is quite good farther than a quarter

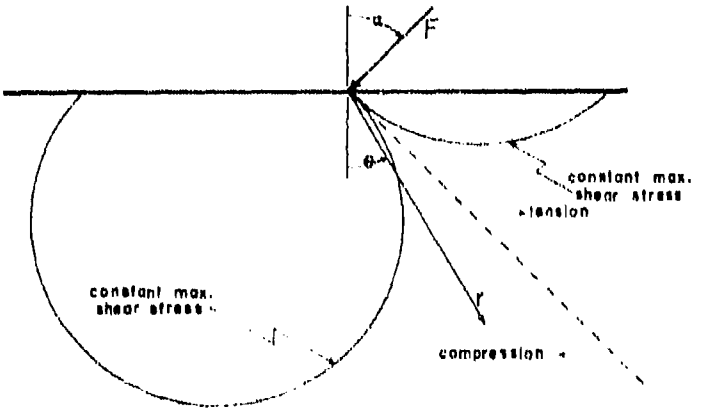

Fig. 2. A point load (line load into the paper, in plane strain) on a half-space.

contact length or so from the contact. In addition, Jahanmir and Suh [2] showed that the residual stresses formed after many asperity passages tend to suppress the tensile plastic zone. Thus, the material to the right of the broken line in Fig. 2 is elastic and is subjected to tensile stress. The material to the left of the broken line is elastic or plastic and the stress is compressive.

Physics of the model

Now consider the introduction of a crack into the half-space, as in Fig. 1. In the compressive region, the crack will tend to close and normal stresses will be transmitted across the crack. In view of the large compressive stresses near the surface, it is not unreasonable to assume that the faces of a crack near the surface will mechanically look together and transmit shear stresses. Under this assumption, the portion of the crack which experiences compressive loading essentially does not exist! The crack can only propagate when the crack and the asperity contact are so situated that part of the crack is in the tensile region. Furthermore, only the portion of the crack in the tensile region will affect propagation.

Linear elastic fracture mechanics may be applied to a crack propagation problem if the nominal stresses are elastic, if the area around the crack tip is in plane strain and if the plastic zone around the crack tip is small compared with the smallest dimension of the problem. Since the material around the important (open) portion of the crack is all elastic and a condition of overall plane strain exists, two of these conditions are met. The third condition cannot be checked until stress intensity factors are calculated. Before covering this calculation, the mathematical implications of the physical model will be explored in order to define the quantities necessary in the analysis.

Mathematical description of the model

As asperities pass over the surface (from right to left in Fig. 1) the crack will pass from compressive to tensile to compressive stresses continuously. Thus the crack extension dC per asperity passage dN (or cycle) should be a function of the change in the stress intensity factor Δk and of two material constants β and n (n is typically 2 - 5), as in fatigue crack growth:

$$\frac{dC}{dN} = \beta(\Delta k)^n \tag{2}$$

(k is purposefully written without a subscript since it is not known whether mode I, the tensile mode, or mode II, the in-plane shear mode, or a combination is operating. Mode III, the out-of-plane shear mode, is impossible under the plane strain assumption.) Δk can only be a function of the boundary conditions (applied loads and displacements) and the geometry as long as the nominal stress field is independent of material properties. (Δk is a weak function of Poisson's ratio, which is ignored here.) When the tip of the crack lies in the compressive region (ignoring the initial transient crack growth) k is a minimum which is zero from the above discussion. When the tip of the crack is in the tensile region k is a function of the average normal contact force σ_n, the coefficient of friction μ, the length of the crack in the tensile region and the depth of the crack below the surface (since these quantities define the boundary conditions and geometry and since the stress field does not depend on the elastic constants, as shown below). It is reasonable to assume that the maximum k will occur when the crack lies at some constant critical depth d and when some constant critical effective crack length C_e is in the tensile region. (Transient crack growth therefore occurs in the period when $C < C_e$). Thus

$$\Delta k = k(\sigma_n, \mu, d, C_e) \tag{3}$$

Since Δk is not a function of C, eqn. (3) can be substituted into eqn. (2) and the result is easily integrated:

$$C = \beta k^n(\sigma_n, \mu, d, C_e)N + C_e \tag{4}$$

If ζ is defined as the number of contacts per unit length and S is the sliding distance, then $N = \zeta S$ or

$$C = \beta k^n(\sigma_n, \mu, d, C_e)\zeta S + C_e \tag{5}$$

Gupta and Cook [6] showed that the real area of contact is almost proportional to the applied normal load. In addition, the increase of the real area of contact is almost solely due to an increase in the number of contacts. Therefore, the number of contacts is essentially proportional to the overall normal load L for a metal with a given hardness:

$$\zeta = \alpha L \tag{6}$$

Defining $\delta = \alpha\beta$, eqn. (5) becomes

$$C = \delta k^n(\sigma_n, \mu, d, C_s)LS + C_s \tag{7}$$

Furthermore, the worn volume V must be Cd times some crack breadth which must be of the order of C_s. Equation (7) becomes

$$V = \{\delta k^n(\sigma_n, \mu, d, C_s)LS + C_s\}dC_s \tag{8}$$

In the past, it was often assumed (*e.g.* ref. 6) that σ_n was equal to the hardness. As was discussed in the overview paper [1] there is no direct experimental support for this view, although it may not be unrealistic to assume that σ_n will increase in some manner with hardness. If we let $\sigma_n = \xi H$ as a first approximation, eqn. (8) may be rewritten as

$$V = \{\delta k^n(\xi H, \mu, d, C_s)LS + C_s\}dC_s \tag{9}$$

Since k has units of stress × length$^{1/2}$ and must be directly proportional to the nominal stress, we may normalize k by $\sigma_n(\xi H)$ and the square root of the half-contact length a to get a dimensionless $\bar{k}$. Equation (9) becomes (using $\bar{d} = d/a$ and $\bar{C}_s = C_s/a$)

$$V = [\delta\{\bar{k}(\mu, \bar{d}, \bar{C}_s)\xi H\sqrt{a}\}^n LS + C_s]\, dC_s \tag{10}$$

Some discussion of the implications of this model is now possible. It can be seen that the volume worn is linearly proportional to the normal load and to the distance slid. This is a well-established experimental result.

However, the influence of hardness is the reverse of that predicted by the adhesion theory if the crack propagation rate (*i.e.* β and/or n) and the number of contacts (*i.e.* α) are not affected by the mechanism responsible for the increase in hardness. In this case, increasing H will increase V by a large factor. This may be one reason why harder materials sometimes wear faster than softer materials.

As to the use of eqn. (10), we can see that it is necessary to evaluate several constants and one function. ξ is hard to find, but may be taken to be 1 in the absence of more information. δ will be difficult to evaluate since α is hard to find. β and n can be evaluated from standard fatigue data. μ must currently be taken as a parameter of the sliding pair. The "fracture mechanics constants" d and C_s and the "fracture mechanics function" k will be evaluated in the following section.

Evaluation of the fracture mechanics constants and function

The method of evaluation will be to calculate k for many possible values of d and C_s. Then C_s and d can be found by inspection.

The method of calculating k is a boundary integral method. Consider a body subjected to a stress field $\sigma(x, y)$ in the absence of a crack. If a crack is present, evaluation of σ at the crack surface will generally yield non-zero tractions on the crack surface (which will be here called "pseudo-stresses"). However, superposition of a stress field which exactly cancels these tractions,

which is zero at any free surface of the body and which causes no displacement at points where displacement boundary conditions are specified will provide the exact solution, by uniqueness. If the stress field that is to be superposed is not zero at some free surface or causes a non-zero displacement at a point where displacement is specified, the superposition will not provide an exact solution since the boundary conditions at the edges of the body will not be met, but hopefully the solution will be useful.

In the implementation of the method, only the stresses in the vicinity of the crack tip are needed. It is well known that the elastic stresses in the vicinity of a crack tip can be written in terms of the distance r from the crack tip and the angle θ from the crack centerline as

$$\sigma_{rr} = \frac{k}{\sqrt{2r}} f_1(\theta)$$

$$\sigma_{\theta\theta} = \frac{k}{\sqrt{2r}} f_2(\theta) \tag{11}$$

$$\sigma_{r\theta} = \frac{k}{\sqrt{2r}} f_3(\theta)$$

If $k'(x)$ is defined as the influence function [7] (the stress intensity factor per unit force for a self-equilibrating pair or point forces on opposed faces of the crack), the stresses in the vicinity of the crack tip are

$$\sigma_{rr} = \frac{1}{\sqrt{2r}} \int_{-c_0}^{0} k'(x)\sigma(x, y)\,dx\, f_1(\theta)$$

$$\sigma_{\theta\theta} = \frac{1}{\sqrt{2r}} \int_{-c_0}^{0} k'(x)\sigma(x, y)\,dx\, f_2(\theta) \tag{12}$$

$$\sigma_{r\theta} = \frac{1}{\sqrt{2r}} \int_{-c_0}^{0} k'(x)\sigma(x, y)\,dx\, f_3(\theta)$$

and comparison of eqns. (11) and (12) shows that

$$k = \int_{-c_0}^{0} k'(x)\sigma(x, y)\,dx \tag{13}$$

Since it was shown above that the material in the region of interest is elastic, the stress field σ is taken to be the elastic solution due to a set of normal and tangential loads elliptically distributed over the contact area. The solution is given by Smith and Liu [8]. With all distances (x and y) normalized by the contact half-length a and all stresses normalized by the maximum normal applied stress* p_0 and with the (x, y) coordinate system of

*Note that $\sigma_n = \frac{p_0}{2} \int_{-1}^{1} (1 - x^2)^{1/2}\,dx = \frac{p_0\pi}{4}$.

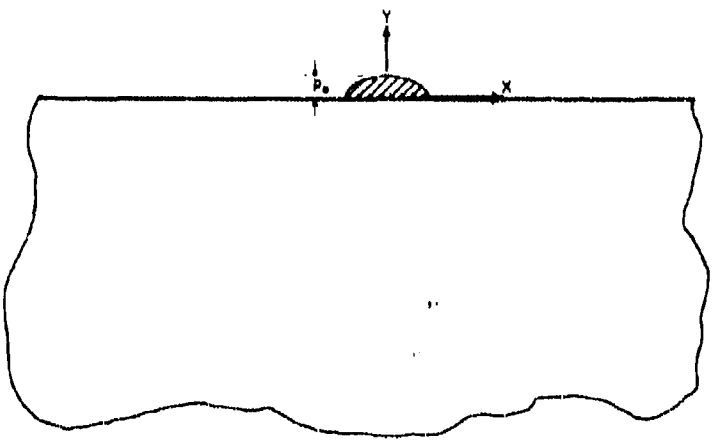

Fig. 3. Elliptically distributed loads on a half-space.

Fig. 3, the first step is to define non-dimensional squared radii from the contact corners:

$$R_1 = (1+x)^2 + y^2$$
$$R_2 = (1-x)^2 + y^2 \tag{14}$$

and two factors (which are difficult to name but which appear often):

$$\psi = \frac{\pi}{R_1 (R_2/R_1)^{1/2} \{2(R_2/R_1)^{1/2} + (R_1 + R_2 - 4)/R_1\}^{1/2}} \frac{1 - (R_2/R_1)^{1/2}}{}$$
$$\phi = \frac{\pi}{R_1 (R_2/R_1)^{1/2} \{2(R_2/R_1)^{1/2} + (R_1 + R_2 - 4)/R_1\}^{1/2}} \frac{1 + (R_2/R_1)^{1/2}}{} \tag{15}$$

Finally the stresses are given: for $y < 0$ (note that the bar is used to denote a normalized dimensionless quantity, here σ/p_0)

$$\bar{\sigma}_{xx} = \frac{\mu}{\pi}\{(2x^2 - 2 - 3y^2)\psi + 2\pi x + 2(1 - x^2 - y^2)x\phi\} +$$
$$+ \frac{y}{\pi}\{(1 + 2x^2 + 2y^2)\phi - 2\pi - 3x\psi\} \tag{16}$$

$$\bar{\sigma}_{yy} = \frac{\mu}{\pi} y^2\psi + \frac{1}{\pi} y(\phi - x\psi)$$

$$\bar{\sigma}_{xy} = \frac{\mu}{\pi}\{(1 + 2x^2 + 2y^2)y\phi + 2\pi y + 3xy\psi\} - \frac{y^2}{\pi}\psi$$

where μ is the coefficient of friction; for $y = 0$

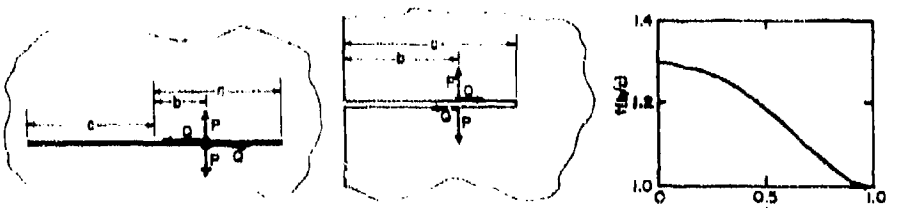

(a) (b) (c)

Fig. 4. Stress intensity factors for point loads on a crack face. (a) Lower bound (infinite solid) (note $k = 3 - 4\nu$ in plane strain, where ν is Poisson's ratio). At the right-hand end

$$k_I = \frac{1}{2\pi\sqrt{c}}\left\{P\left(\frac{c+b}{c-b}\right)^{1/2} + Q\frac{k-1}{k+1}\right\} \qquad k_{II} = \frac{1}{2\pi\sqrt{c}}\left\{Q\left(\frac{c+b}{c-b}\right)^{1/2} - P\frac{k-1}{k+1}\right\}$$

(b) Upper bound (edge crack in a semi-infinite solid):

$$k_I = \frac{2P f(b/c)}{\pi[c\{1-(b/c)^2\}]^{1/2}} \pm 2\% \qquad k_{II} = \frac{2Q f(b/c)}{\pi[c\{1-(b/c)^2\}]^{1/2}} \pm 2\%$$

(c) The graph is used to evaluate $f(b/c)$.

$$\begin{aligned}
\bar{\sigma}_{xx} &= 2\mu\{x - (x^2-1)^{1/2}\} && x > 1 \\
&= 2\mu\{x + (x^2-1)^{1/2}\} && x < -1 \\
&= 2\mu x - (1-x^2)^{1/2}\} && |x| < 1 \\
&= 0 && |x| > 1 \\
\bar{\sigma}_{yy} &= -(1-x^2)^{1/2} && |x| < 1 \\
&= 0 && |x| > 1 \\
\bar{\sigma}_{xy} &= \mu(1-x^2)^{1/2} && |x| < 1
\end{aligned} \tag{17}$$

The function k' is more difficult than the stresses to specify. First, no solutions were found in the literature for point forces on the face of the crack in Fig. 1 and so an infinite body solution was used with consequently a failure to meet the boundary conditions at the free surface to either side of the contact. Second, the "pseudo-stresses" given by eqn. (16) correspond to forces which tend to close the crack. The cancelling forces must thus tend to open the crack. This will slightly open the end of the crack which lies at the edge of the compressive region and make it impossible to define C_e exactly; k' is a function of C_e.

Thus as an approximation upper and lower bounds were calculated. The stress intensity factors were calculated using the formulae from Tada *et al.* [9] for the two configurations shown in Fig. 4. The factor from Fig. 4(a) is a lower bound on the stress intensity factor for the tip of interest since it assumes that the end carries one-half of the load. The stress intensity factor from Fig. 4(b) is an upper bound since it assumes that the end carries no load.

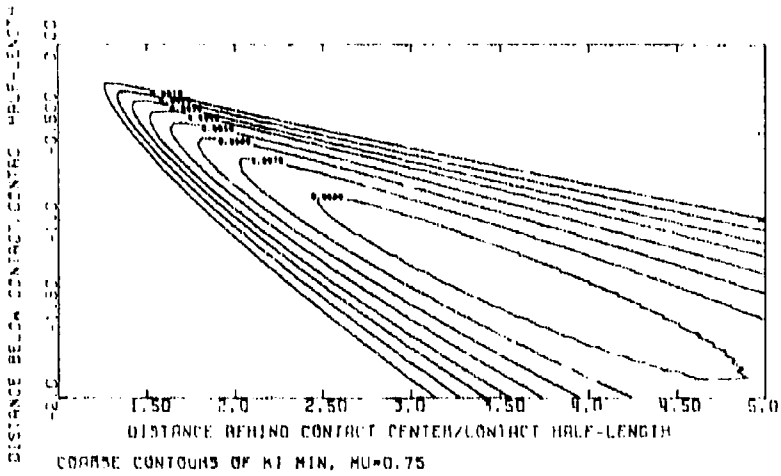

Fig. 5. A "coarse" contour plot of the lower bound on k_1, with a coefficient of friction of 0.75.

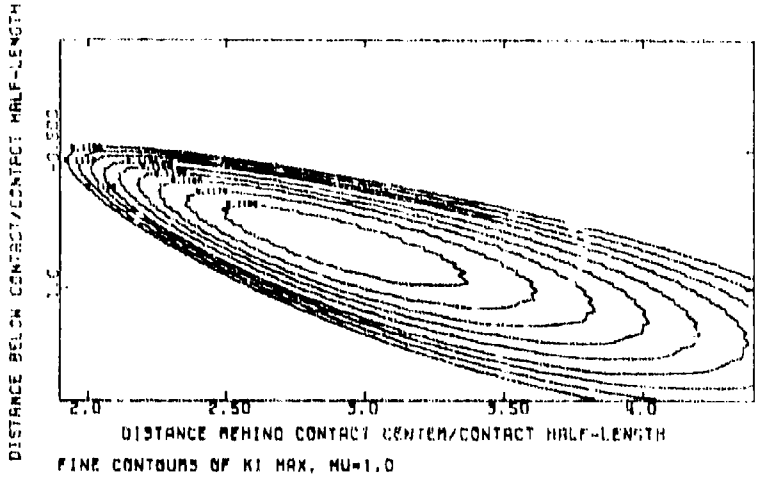

Fig. 6. A "fine" contour plot of the upper bound on k_1, with a coefficient of friction of 1.0.

It is apparent that an analytical integration of eqn. (13) would be at best difficult, tedious and prone to error. Thus, the integration was carried out numerically for selected cases of $\mu = 0.5$, 0.75 and 1. Poisson's ratio was 1/3 in all the calculations. The calculations are not sensitive to the value of Poisson's ratio.

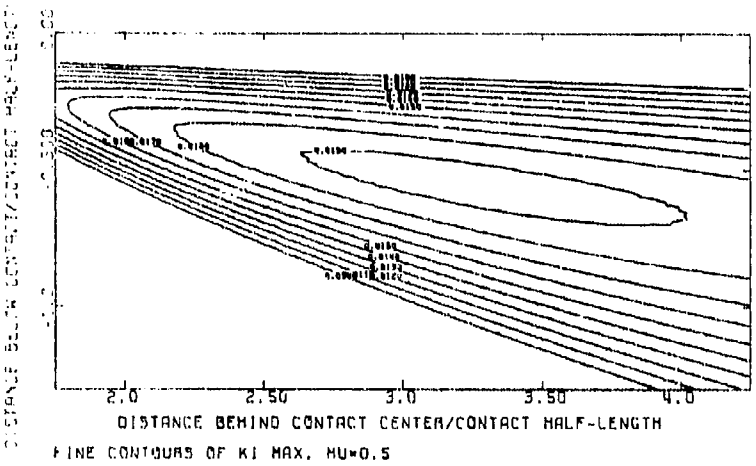

Fig. 7. A "fine" contour plot of the upper bound on $\bar{K}_I$, with a coefficient of friction of 0.5.

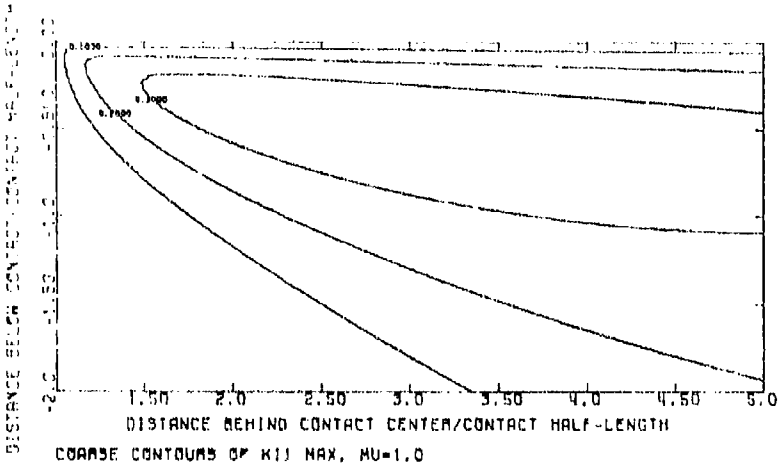

Fig. 8. A "coarse" contour plot of the upper bound on $\bar{K}_{II}$, with a coefficient of friction of 1.0.

An equally spaced integration scheme was used, with the number of integration points chosen to be proportional to C_s. This method was chosen over an unequally spaced weighted scheme, since the chosen method did not require re-evaluation of eqns. (16) for each integration point and thus provided a significant saving in computer time. The calculations were carried out for 401 values of C_s and 251 values of d, starting from $x = -1.0$ and $y = 0.0$ and decreasing x and y by intervals of 0.01. Trial computations were

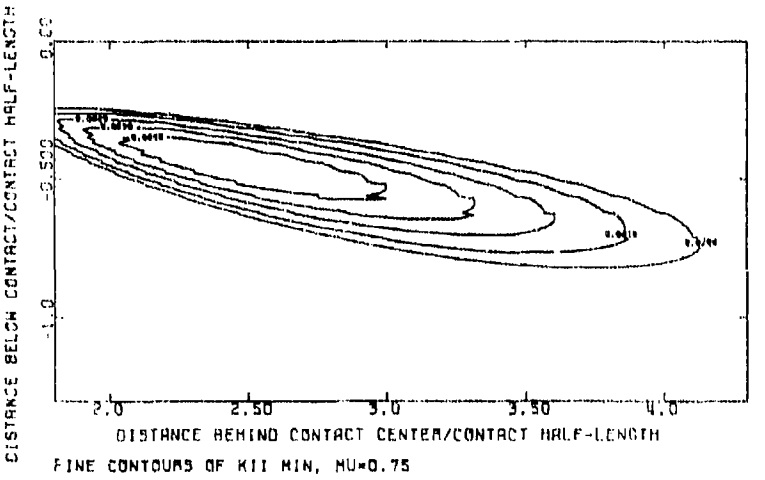

Fig. 9. A "fine" contour plot of the lower bound on F_{II}, with a coefficient of friction of 0.75.

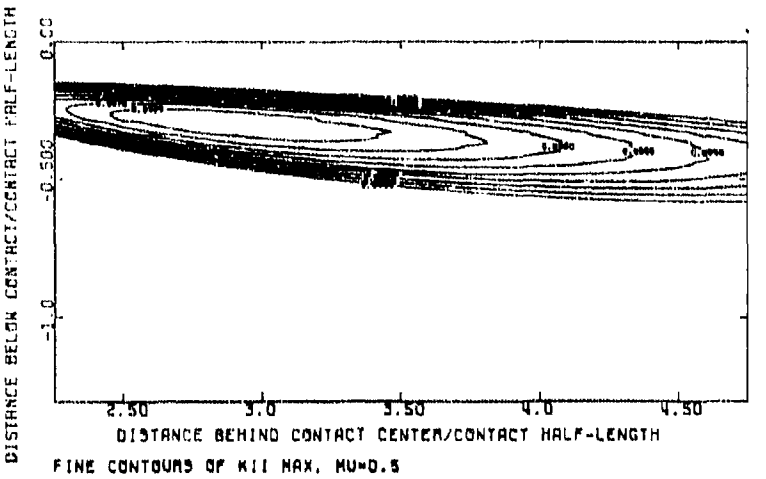

Fig. 10. A "fine" contour plot of the upper bound on F_{II}, with a coefficient of friction of 0.5.

carried out decreasing x and y by intervals of 0.025, and the final computations differ from these by 10 - 15%. We do not feel that a decrease in the stepsize will significantly increase accuracy.

The computation was carried out using a program written in FORTRAN IV on the MIT IBM 370/168 computer. First the stresses were calculated and stored on disk. This program took about 3 min of machine time. Then

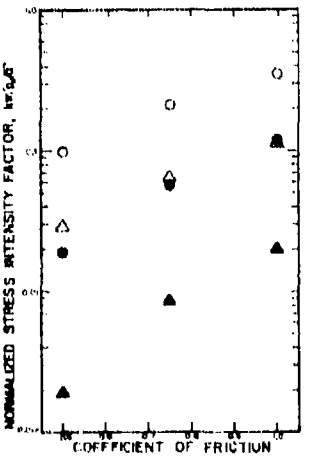

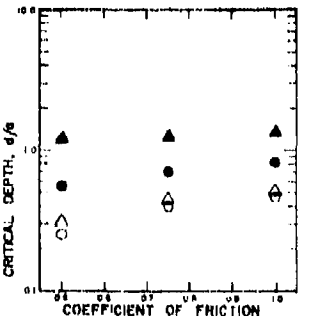

Fig. 11. Normalized stress intensity factors as functions of the coefficient of friction: ● k_I, upper bound; ▲ k_I, lower bound; ○ k_{II}, upper bound; △ k_{II}, lower bound.

Fig. 12. The critical depth (depth of propagation of the most favored crack) as a function of coefficient of friction: ● k_I, upper bound; ▲ k_I, lower bound; ○ k_{II}, upper bound; △ k_{II}, lower bound.

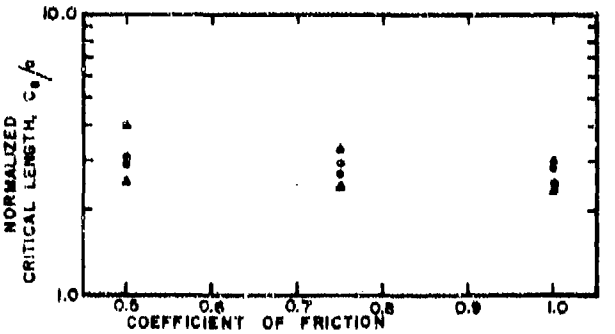

Fig. 13. The effective crack length at point of maximum stress intensity factor as a function of coefficient of friction: ● k_I, upper bound; ▲ k_I, lower bound; ○ k_{II}, upper bound; △ k_{II}, lower bound.

another program was used to calculate upper and lower bounds on either k_I or k_{II} for one value of μ. This program ran for about 40 - 50 min of machine time.

Typical results are presented in Figs. 5 - 10 as contour plots of $\bar{k}$ (k normalised by the maximum contact stress p_0 and the square root of the contact half-length a, and multiplied by π for convenience) *versus* x and y. Figures 11 - 13 show $\bar{k}_I$, $\bar{k}_{II}$, $\bar{d}$ and $\bar{C}_0$ as functions of μ (d and $\bar{C}_0$ are normalized by the contact half-length a). Numbers may be read off from these graphs and substituted into eqn. (10) to predict a wear rate for a sliding pair with a given μ.

Discussion

Figure 14 shows the plastic zone size r_p at the tip of the crack ($r_p = (1/2)(k/Y)^2$). This was calculated by assuming that the average contact stress σ_n is equal to the hardness and the calculation also ignored any variations in the flow stress near the surface. It can be seen that $r_p/d < 1$ in all cases, and in most cases $r_p/d \ll 1$, so that the third condition for linear elastic fracture mechanics to be applicable is met.

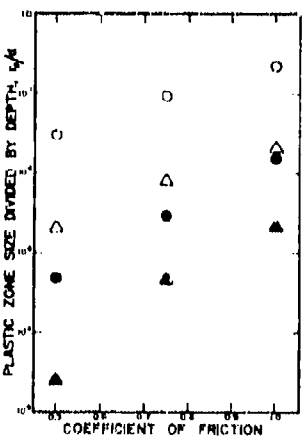

Fig. 14. The plastic zone size divided by critical depth as a function of coefficient of friction: ● k_I, upper bound; ▲ k_I, lower bound; ○ k_{II}, upper bound; △ k_{II}, lower bound.

Of course, several important factors have been ignored. The large deformations present in sliding wear cause anisotropy, especially in that slip planes tend to line up parallel to the surface [1]. Also, experimental results show that significant crack growth is due to the linking up of separate cracks. Neither of these effects was included.

Also, residual stresses are not accounted for in the stress field of eqns. (16) and (17). However, Merwin and Johnson [10] showed that the only possible residual stress is σ_{xx}, which cannot affect a crack on a plane of constant y. Thus residual stresses do not affect crack propagation.

The analysis also contains many other assumptions which are discussed in the body of this paper.

It should be noted that, during preliminary computation, stress intensity factors were calculated for cracks growing in the y direction from the surface. Even very short cracks had stress intensity factors larger than the largest factors for cracks growing in the x direction. Since "surface" cracks have not been observed in ductile metals, we feel that the plowing and smearing action in front of and at the contact prevents such cracks from forming. It should also be noted that such cracks cannot grow into the compression region, and

that they only have large stress intensity factors in the region immediately behind the contact where the compression region is close to the surface. Therefore these cracks cannot link up with other cracks, which is necessary to form a wear particle.

In spite of the many assumptions, the functional relationship of eqn. (10) should hold. The increase of volume worn with increasing hardness for some metals has been documented [11] and eqn. (10) provides a reasonable explanation.

The calculation of stress intensity factors is a weak point in the analysis, owing to the failure to meet the free-surface boundary conditions. This weakness could be remedied in several ways.

The best way would be to find an analytic expression for the stress intensity factor of a crack, parallel to the free surface of a half-space, subjected to two self-equilibrating point loads on the crack faces. Such an expression could be used in the analysis presented above to obtain better estimates of stress intensity factors. The cost of computation would probably be about the same. Unfortunately, the desired stress intensity factor was not found in the literature and we have not attempted to derive it ourselves.

Another way to improve the calculation would be to iterate the solution. Since most of the surface of the half-space is distant from the crack tip, the stresses on that surface due to the point forces on the crack faces are the stresses along a line in an infinite plane due to two opposed forces at a point. As a stress intensity factor, say k_a, is calculated, the program could also calculate the free-surface stresses. Then the state of stress in the half-space due to cancelling of these free-surface stresses (or an approximation) could be used instead of the stresses of eqns. (16) to calculate another stress intensity factor k_b and another set of free-surface stresses, using the same procedure as above. This iteration procedure could be repeated as long as required. Hopefully, the sum $k_a + k_b + \ldots$ would converge to the true value of k. The drawback of this procedure is, of course, the high computation cost.

In any of the schemes presented above, the exact point where the crack goes from compression (closed) to tension (open) is unknown since the point forces applied to the crack tend to open the crack and to lengthen it. In the calculations presented here, the crack was assumed to end at the tension–compression boundary of the nominal stress field. Since the analysis is elastic, giving infinite stresses at the crack tip, it is impossible to balance these stresses against the compressive stress at the end of the crack to calculate the actual end position. Locating the end thus requires a plastic analysis, with attendant difficulty and cost.

Since stress intensity factors were calculated for many cracks, approximately 0.0012% of the calculation time was spent on the crack with the maximum k. The ratio of calculations which did not yield data points in Figs. 9 - 12 to calculations which did is 8×10^4. However, it was necessary to demonstrate that the stress intensity factor is a well-behaved function

with one maximum. Since this has now been demonstrated, a much better ratio of "useless" to "useful" calculations could be obtained, perhaps by using a search method to find the crack with the maximum k. This would reduce the computation cost significantly.

We feel that the calculations of stress intensity factors presented in this paper, while approximate, may be useful. To demonstrate that the solution is not unreasonable, we will use eqn. (2) by substituting $k = \bar{k}p_0\sqrt{a}/\pi$ and solving for a (using $p_0 = 4\sigma_n/\pi$ and assuming that σ_n equals the hardness H):

$$a = \frac{\{(dC/dN)\beta^{-1}\}^{2/n}}{(\bar{k}H)^2}\left(\frac{\pi}{2}\right)^4 \tag{18}$$

Assuming for mild steel $n \approx 4$, $\beta \approx 1.7 \times 10^{-3}$ Pa^{-4} μm^{-1} (10^{-19} lb^{-2} in^7) and $H \approx 1.4$ GPa (2×10^5 lb in^{-2}), then

$$a = 75\left(\frac{dC}{dN}\right)^{1/2}\bar{k}^{-2}\ \mu\text{m} \tag{19}$$

We will use approximate dC/dN values for mild steel [2]: $dC/dN \approx 10^{-2}$ μm pass^{-1} at a coefficient of friction $\mu = 0.5$ and $dC/dN \approx 2.5 \times 10^{-3}$ μm pass^{-1} at $\mu = 0.85$.

Reading from Fig. 11, at $\mu = 0.5$, $0.002 < \bar{k} < 0.1$, which gives $1.9 \times 10^6 > a > 750$ μm. At $\mu = 0.85$, $0.01 < \bar{k} < 0.3$, which gives $3.8 \times 10^4 > a > 42$ μm. The smaller values of a come from the larger values of k.

These values of the half-contact length are extremely large, but the lower values are not more than an order of magnitude out of line since a is often assumed to be on the order of 10 μm. However, the spread is certainly large. The calculations indicate that the larger values of k are the more reasonable. Although these values are k_{II} values, this cannot be taken to show that mode II is the operative mode. In addition, the values of dC/dN were calculated using $d \approx 2$ μm, which is probably too small and yields large values of dC/dN. Smaller values of dC/dN would give smaller values of a. It is also possible that the cancellation of free-surface stresses discussed above would give higher values of $\bar{k}$.

Of course, asperity contacts are not always the same size. Contact size depends on the material, the surface finish, the plastic deformation history, the applied force and the lubricant if one is present. A smooth surface will have a large average contact size, but the number of contacts will be reduced. Since the worn volume depends on $\bar{k}_s^n$ and $\bar{k}$ is proportional to a, the wear rate depends on a^n, but it is only directly proportional to the number of contacts. Thus, a smooth surface with few but large asperity contacts may have a higher wear rate than a rougher surface! It has been shown that rough surfaces quickly become smoother, but higher initial wear volumes have been reported for smooth surfaces compared with rough surfaces under some conditions [11]. This has been attributed to asperity deformation and fracture but both mechanisms could be contributing.

Since contacts differ in size, each contact may tend to propagate a crack at a slightly different depth. Equation (10) was derived assuming that the

contact size was constant and that the change in the stress intensity factor was also constant. For contacts bigger or smaller than a, the change in the stress intensity factor for a crack at a depth d will be less than that predicted by the analysis; eqn. (10) therefore gives an upper bound on the crack propagation rate.

It is also apparent from Fig. 11 that the wear sheet thickness d is an increasing function of μ. In stiff sliding systems where clearances cannot change significantly, wear particles may jam up, increasing μ. This would lead to thicker wear particles, leading to more jamming, and would finally cause seizure. The process would be analogous to an unstable equilibrium; any small perturbation increasing μ would tend to increase both μ and d until seizure occurs.

The final test of eqn. (10) must be whether or not it is useful. To this end, we hope to carry out wear tests on steels (with many inclusions) for which the fatigue constants β and n have been determined. Hopefully the results will correlate with those predicted by eqn. (10).

Conclusions

(1) Linear elastic fracture mechanics can be used to analyze subsurface crack propagation in delamination wear, at least for coefficients of friction greater than 0.5.

(2) In crack propagation controlled wear, increasing hardness will generally increase wear if the contact stress is increased without affecting the crack propagation rate.

(3) Wear is proportional to the normal load and to the distance slid in crack propagation controlled wear.

(4) For a given size of asperity contact, there is one depth and one effective crack length for which the stress intensity factor is a maximum, *i.e.* $k(x, y, \mu, \sigma_n)$ is a smooth function with one maximum.

(5) Wear particle thickness is a function of the coefficient of friction. This leads to a possible explanation of seizure.

Acknowledgments

The work reported here was sponsored by the Defense Advanced Research Projects Agency through the Office of Naval Research under contract N00014-67-A-0204-0080. We are grateful to Dr. Edward van Reuth and Lt. Richard S. Miller for their support and guidance.

References

1 N. P. Suh, An overview of the delamination theory of wear, Wear, 44 (1977) 1 - 15.
2 S. Jahanmir and N. P. Suh, Mechanics of subsurface void nucleation in delamination wear, Wear, 44 (1977) 17 - 38.
3 G. Augustsson, Strain field near the surface due to surface traction, S.M. Thesis, Department of Mechanical Engineering, MIT, 1964.

4 S. P. Timoshenko and J. N. Goodier, Theory of Elasticity, McGraw-Hill, New York, 1951.
5 N. P. Suh, Microstructural effects in wear of metals. In R. J. Jaffey (ed.) Fundamental Aspects of Structural Alloy Design, Plenum Press, New York, 1976.
6 P. K. Gupta and N. H. Cook, Junction deformation model for asperities in sliding interaction, Wear, 20 (1972) 73 - 87.
7 R. C. Labbens, J. Heliot and A. Pellissier-Tanon, Weight functions for three-dimensional symmetrical crack problems. In Cracks and Fracture, Am. Soc. Test. Mater. Spec. Tech. Publ. STP 601, 1976.
8 J. O. Smith and C. K. Liu, Stresses due to tangential and normal loads on an elastic solid with application to some contact problems, J. Appl. Mech., 20 (1953) 157 - 166.
9 H. Tada, P. C. Paris and G. R. Irwin, The Stress Analysis of Cracks Handbook, Del Research Corp., Hellertown, Pa., 1973.
10 J. E. Merwin and K. L. Johnson, An analysis of plastic deformation in rolling contact, Proc. Inst. Mech. Eng., London, 177 (1963) 241 - 252.
11 S. Jahanmir, A fundamental study on the delamination theory of wear, Ph.D. Thesis, Department of Mechanical Engineering, M.I.T., 1976.

Wear, 44 (1977) 57 - 64

THE RELATIONSHIP BETWEEN CRACK PROPAGATION RATES AND WEAR RATES

J. R. FLEMING and N. P. SUH

Department of Mechanical Engineering, Massachusetts Institute of Technology, Cambridge, Mass. 02139 (U.S.A.)

(Received March 30, 1977)

Summary

In order to check qualitatively the validity of the analysis of crack propagation in delamination wear, wear experiments were performed with 7075-T6 and 2024-T3 aluminum alloys. The former alloy has a higher hardness (by 25%) and a faster crack propagation rate (3 - 10 times) in normal fatigue tests than the latter. The preliminary test results show that the wear rate of 7075-T6 aluminum is also greater than that for 2024-T3 aluminum, indicating that the wear rate correlates with the crack propagation rate.

Introduction

The analyses done for delamination wear [1, 2] imply that the crack propagation rate is the rate controlling mechanism for steady state sliding wear when the coefficient of friction is large enough to create a tensile region of appreciable size behind a moving asperity. When the coefficient of friction is very small, the crack propagation rate parallel to the surface is so small that a large number of cracks must be nucleated and therefore the crack nucleation rate, which is governed by the magnitude of the normal load and adhesive force, may be the rate controlling process. In a previous paper, the case of delamination wear which is controlled by crack propagation was considered in terms of linear elastic fracture mechanics. An equation was derived to predict wear in the case where the crack propagation rate controls the wear rate. Unfortunately, insufficient information about the parameters appearing in the equation is available, so that the validity of the derivation cannot be checked directly by comparing predictions with wear experiments. However, some of the assumptions of the analysis may be checked. The purpose of this paper is to present preliminary experimental results which may shed some light on the validity of these major assumptions.

The wear equation was derived by assuming that delamination crack propagation is similar to fatigue crack propagation. This assumption was

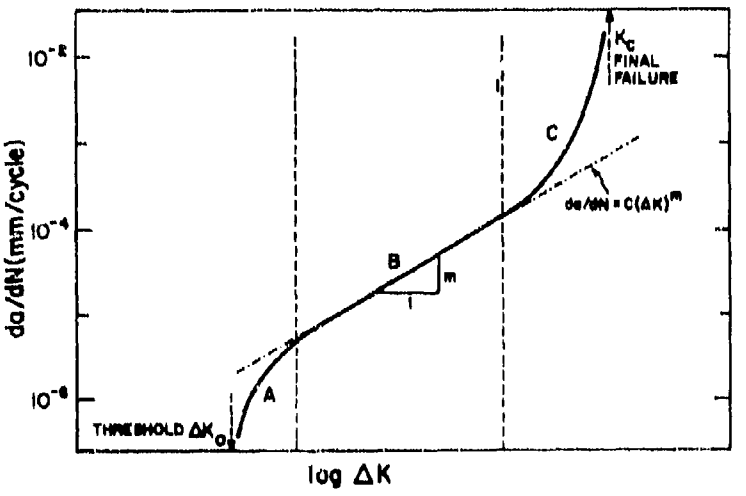

Fig. 1. A typical plot of the crack extension per cycle *vs.* the logarithm of the change in the stress intensity factor (from ref. 3). The primary mechanisms may be divided into three regimes: regime A, non-continuum mechanisms, showing a large influence of (i) microstructure, (ii) mean stress and (iii) environment; regime B, continuum mechanisms (striation growth), showing little influence of (i) microstructure, (ii) mean stress, (iii) dilute environment and (iv) thickness; regime C, "static mode" mechanisms (cleavage, intergranular and fibrous), showing a large influence of (i) microstructure and (ii) thickness but little influence of the environment.

based on the fact that both types of cracks are subjected to cyclic loading. Fatigue cracks certainly grow cyclically. Since the stress in front of a sliding asperity contact is compressive and the stress behind such a contact is tensile, then as asperities slide along a surface each point below the surface undergoes cyclic loading. Furthermore, delamination cracks have been often observed at various stages of growth; thus delamination cracks grow incrementally rather than in one step as in static fracture.

It still remains to be proved that fatigue crack growth rates and delamination crack growth rates can be correlated. In order to introduce such proof, it is first necessary to discuss the characteristics of fatigue crack growth.

It has long been known that, if the crack extension per loading cycle da/dN is plotted against the logarithm of the change in stress intensity factor ΔK at the tip of the crack, the shape of the curve is independent of the material. A typical curve is shown in Fig. 1 (from ref. 3). There are three regimes of growth: a threshold regime (region A), a steady growth regime (region B) and a static mode regime (region C). In the threshold regime the average crack extension per cycle is of the order of atomic dimensions or less. Thus continuum mechanics does not apply in this region and the cracks grow in spurts, *i.e.* they do not grow in some cycles and they grow by several atomic diameters in other cycles. In the static mode regime the crack exten-

sion per cycle is on the order of part size; continuum mechanics applies but, since the stress intensity factor at the tip of a crack increases significantly in each cycle owing to the large extension, the relationship between the crack extension and the logarithm of the stress intensity factor is non-linear.

In the steady growth regime cracks grow at a constant extension per cycle and the stress intensity factor increases slowly. Fatigue striations are produced. It has been shown empirically that the relationship between Δk and da/dN in the steady growth regime is of the form

$$\frac{da}{dN} = C(\Delta k)^m \tag{1}$$

where C and m are material properties; m is usually of the order 3 - 4.

Equation (1) was used in the previous paper [1] to derive a wear equation by assuming that delamination crack growth is described by eqn. (1). Several questions arise in connection with this assumption. Since most fatigue data are taken under mode I (tensile) conditions and since it is not known whether delamination cracks grow by mode I, by mode II (in-plane shear) or a by combination, can eqn. (1) be used at all ? If the correlation between fatigue and delamination exists, do delamination cracks grow in region B where eqn. (1) applies ? These questions will be considered in the discussion. We will now turn to the demonstration of a correlation between fatigue crack growth rates and wear rates.

Experimental materials

The ideal method of demonstrating the correlation would be to select a material and to treat it to obtain widely different fatigue crack growth rates while keeping all other properties as constant as possible. However, this is almost impossible. It has been shown that fatigue crack growth rates correlate well with the Young's modulus but do not correlate at all with such parameters as the yield strength [4, 5]. This indicates that, although the material at the tip of a growing crack is plastic, the elastic properties dominate the crack propagation in cyclic loading situations where linear elastic fracture mechanics is valid.

The significance of this finding is that it is difficult to obtain different fatigue crack growth rates without other major changes, such as changing the major constituent of the alloy. Yet some changes in fatigue crack growth rates are found in aluminum alloys.

Hahn and Simon [6] collected crack growth rate data for various aluminum alloys. The data were generated at many laboratories under varying conditions. The two alloys for which the most data were available were 7075-T6 and 2024-T3. Hahn and Simon found that the data agreed quite well and showed that the fatigue crack propagation rate of 7075-T6 was three times that of 2024 in dry air, five times that of 2024 in wet air and ten times that of 2024 if Δk was proportional to the yield stress. Plots of da/dN for the two aluminums are shown in Fig. 2.

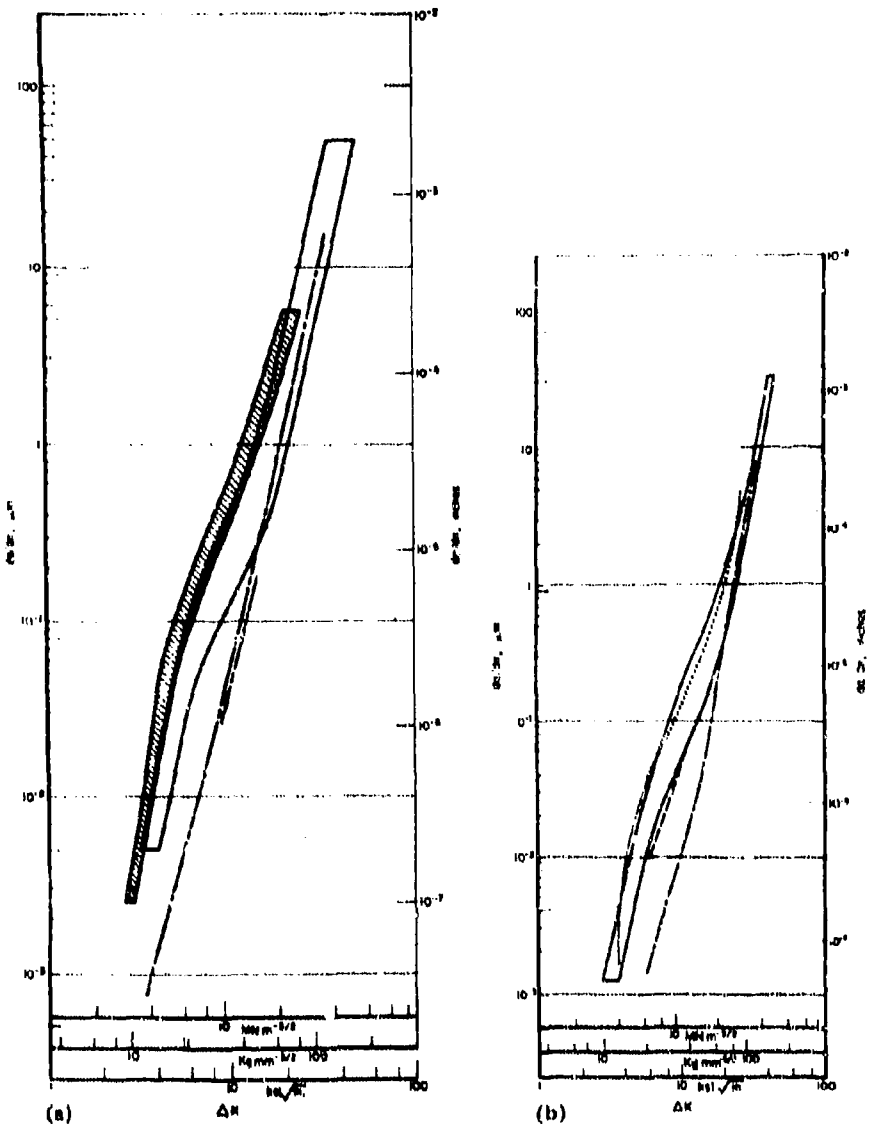

Fig. 2. Plots of da/dN *vs.* log Δk for (a) 7075-T6 and (b) 2024-T3 aluminum (from ref. 6). (a) (1) Dry atmospheres and high cyclic frequencies, — · · — dry argon, 143 Hz, — · — dry air, 57 Hz; (2) dry atmospheres and intermediate cyclic frequencies, ▭ band defined by the mean values of nine different studies in dry air or laboratory air at 0.5 - 30 Hz; (3) corrosive atmospheres and intermediate cyclic frequencies; the shaded band is defined by the mean value of six different studies in humid air, water or NaCl solution at 0.5 - 30 Hz. (b) (1) Vacuum or dry atmospheres and high cyclic frequencies, — · — 5% r.h., 57 Hz, · · · vacuum; (2) laboratory air, ▭ band defined by eight different investigations; (3) moist atmospheres, — · · — over 90% r.h. and distilled water, · · · 100% r.h.

Therefore it was considered useful to study the wear rates of the two aluminums. The alloys have similar microstructures; in both cases the precipitates are intermetallic compounds and the precipitate size and spacing are approximately the same [7]. Yet in order to be able to interpret the experimental data it is necessary to consider the effect of the differences in the hardness and the crack propagation rate on the wear behavior.

The hardness of 7075-T6 is approximately 5/4 times that of 2024-T3. Making the rough assumption that the deformation rate is controlled by the hardness and that crack nucleation is similar in both materials, the crack nucleation rate of 7075-T6 should be 4/5 times that of 2024-T3. Also, since the number of asperity contacts depends almost linearly on the applied normal load [8], the stress at an asperity contact is roughly constant and is probably related to the hardness; thus the number of asperity contacts or loading cycles for 7075-T6 should be about 4/5 times that of 2024-T3.

The stress intensity factor of a delamination crack is proportional to the stress at an asperity contact, and the location of the propagating crack (*i.e.* the distance from the surface to the location where the stress intensity factor is a maximum) depends sensitively on the traction at the asperity contact [1]. However, it is not known how this contact stress is related to the hardness. Thus it is not certain whether Δk in wear is proportional to the yield strength. If we assume that the maximum Δk is nearly the same for both alloys, the delamination crack propagation rate in 7075-T6 should be 3 - 10 times that of 2024-T3 at a given value of Δk. Considering the differences in nucleation rate and number of loading cycles as well as the crack propagation rate the wear rate of 7075-T6 should be (3 - 10) (4/5) (4/5) or 2 - 7 times that of 2024-T3.

Specimen preparation and testing

As-received 9.5 mm (3/8 in) bars of 7075-T6 aluminum and 6.4 mm (0.252 in) bars of 2024-T3 aluminum were turned and polished to a diameter of 6.35 mm (0.25 in). The polishing was performed using successively finer grits, ending with 0.5 μm diamond paste. This was done to ensure a smooth surface, to minimize subsurface damage and to minimize transient wear due to asperity deformation.

The specimens were tested using a cylinder-on-cylinder geometry. Each specimen was placed in a lathe chuck and was rotated against a stationary AISI 52100 steel slider of diameter 6.35 mm (0.25 in). The normal and tangential loads were monitored by strain gages on the slider support bar, which were connected to a Sanborn recorder.

The sliding pair was enclosed in a chamber which was evacuated before the test. During the test the chamber was filled with argon gas. The argon was dried by passing it through calcium carbonate before entering the chamber. During the test the chamber was vented through a bubbler to ensure a small positive pressure within the chamber.

TABLE 1

Results of wear tests on 7075-T6 and 2024-T3 aluminum*

Material	Test time (min)	Weight loss (mg)
2024-T3	5.0	0.35
	7.5	0.44
	10.0	0.46
	12.5	0.57
	15.0	0.70
7075-T6	5.0	0.15
	7.5	0.30
	10.0	0.30
	12.5	0.44
	15.0	0.64

*1 kg normal load; 2 m min $^{-1}$ sliding speed; coefficient of friction 0.3 - 0.38.

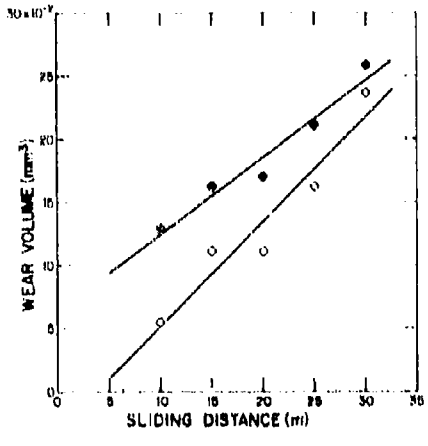

Fig. 3. The worn volume *vs.* the sliding distance for 7075-T6 (◇) and 2024-T3 (◆) aluminum with an assumed density of 2.7 g cm^{-3}.

All tests were run at a sliding speed of 2 m min $^{-1}$ and a normal load of 1 kg. Tests were performed on each alloy for sliding distances of 10, 15, 20, 25 and 30 m. Wear was measured by weighing each specimen before and after the test to an accuracy of 0.01 mg. The results are tabulated in Table 1.

Results and discussion

In all cases, the steady state coefficient of friction varied from 0.3 to 0.38 during the test.

Figure 3 shows the volume worn as a function of the sliding distance. Least-square fits to the data are also shown. The 7075 specimen, despite its

being harder than the 2024 specimen, exhibits a higher wear rate by a factor of 1.34 (0.83×10^{-2} mm^3 m^{-1} and 0.62×10^{-2} mm^3 m^{-1} respectively). This indicates that there is a correlation between the fatigue crack propagation rate and the wear rate (or the delamination crack propagation rate) even though the wear rate ratio is not as high as expected. This is probably because the assumptions used to predict the wear rate ratio are extremely crude and because microstructural differences were ignored.

Figure 3 also shows that the amount of wear of 7075 was less than that of 2024 even though the rate was higher for 7075. This is probably due to the smaller size of the original 2024 rods; the 2024 was polished less. Tests could not be run at higher sliding distances since the geometrical changes due to wear became too large.

It is still impossible to answer the first question about the mode of crack propagation and the values of C and m. However, something may be said about the applicability of eqn. (1), *i.e.* whether delamination cracks grow in region B of Fig. 1. Jahanmir and Suh [2] calculated that delamination cracks in mild steel grow at about 10^{-5} mm cycle^{-1}. We have not yet been able to calculate approximate crack propagation rates in aluminum in a similar manner from wear test results; however, it is reasonable to assume a crack propagation rate of about 10 times that of steel, or of 10^{-4} mm/cycle. This is in region B for the curves in ref. 6 for aluminum. Thus eqn. (1) is probably applicable although we cannot apply it to wear until more is known about the mechanics of interaction as discussed in ref. 1.

Conclusions

Preliminary experimental results indicate that:

(1) wear rates may be correlated with crack propagation rates; and that

(2) delamination cracks may propagate in a manner described by an equation of the form $da/dN = C(\Delta k)^m$.

Acknowledgments

The work reported here was sponsored by the Defense Advanced Research Projects Agency through the Office of Naval Research under contract No. NO0014-67-A-0204-0080. We are grateful to Drs. Edward van Reuth, Arden L. Bement and Richard S. Miller and Lt. Commander K. Petrovic for their support.

References

1 J. R. Fleming and N. P. Suh, Mechanics of crack propagation in delamination wear, Wear, 44 (1977) 39 - 56.

2 S. Jahanmir and N. P. Suh, Mechanics of subsurface void nucleation in delamination wear, Wear, 44 (1977) 17 - 38.
3 R. O. Ritchie, Influence of microstructure on near-threshold fatigue crack propagation in ultra-high strength steel, presented at the Metals Society Conf. "Fatigue 1977", Cambridge, Gt. Britain, March 28 - 30, 1977.
4 S. Pearson, Fatigue crack propagation in metals, Nature (London), 211 (1966) 1077 - 1078.
5 J. M. Barsom, E. J. Imhof and S. T. Folfe, Fatigue crack propagation in high yield strength steels, Eng. Fract. Mech., 2 (1971) 301 - 317.
6 G. T. Hahn and R. Simon, A review of fatigue crack growth in high strength aluminum and the relevant metallurgical factors, Eng. Fract. Mech., 5 (1973) 523 - 540.
7 Metals Handbook, Vol. 1, 8th edn., Am. Soc. Metals, Metals Park, Ohio, 1961.
8 P. K. Gupta and N. H. Cook, Statistical analysis of mechanical interaction of a rough surface, J. Lubr. Technol., 94 (1972) 19 - 26.

Wear, 44 (1977) 65 - 75

WEAR OF COPPER-BASED SOLID SOLUTIONS

J. J. PAMIES-TEIXEIRA, N. SAKA and N. P. SUH
Massachusetts Institute of Technology, Cambridge, Mass. 02139 (U.S.A.)
(Received January 2, 1977)

Summary

The effect of solute atoms on sliding wear was studied by alloying OFHC copper with chromium, silicon and tin. The hardness was found to increase linearly with the atomic solute content although the rate of hardening was different for different solutes.

Microscope observations show that the principal mode of wear is indeed delamination. The results further show that both the wear rate and the friction coefficient are reduced when the solute content is increased. The reduction in the friction coefficient is a consequence of reduced plowing contribution to the tangential component of the surface traction. Both the increase in hardness and the decrease in the friction coefficient reduce the wear since both affect the subsurface deformation rate and consequently the crack nucleation rate. The lower coefficient of friction also reduces the crack propagation rate and the thickness of the wear sheets.

Introduction

The limitations and shortcomings of the adhesion theory [1, 2], such as the inability to explain the effect of microstructure on wear, have been elaborated in previous papers. Subsurface deformation, crack nucleation and crack propagation are the basic processes of delamination wear [3]. They can occur sequentially if the metal can deform plastically and is free of pre-existing voids and cracks, or simultaneously if the material contains those imperfections. It is well established that these processes are structure sensitive, thus implying that the microstructure plays an important role in determining the wear properties of materials.

Generally, hardness is considered to be the most important property in determining the wear rate. The adhesion theory attributes the lower wear rates of harder materials to the reduction of the real area of contact and thus a smaller number of welded junctions. The delamination theory, however, postulates that the hardness is important since it affects the rate of plastic deformation and the surface traction at each asperity which in turn controls

the subsurface deformation, crack nucleation and crack propagation processes. Furthermore, the delamination theory of wear predicts adverse effects if the hardness is increased by introducing inclusions which act as crack nucleation sites.

Thus, raising the hardness while suppressing crack nucleation and crack propagation is a good method for decreasing the wear rates of a material. The objective of the present paper is to investigate the effect of hardening via substitutional solid solution, without any appreciable amount of second phases which promote crack nucleation. The results show that such a manipulation of the microstructure decreases the wear rate as predicted by the delamination theory.

Experimental materials and procedures

Materials preparation

OFHC copper, copper–chromium (0.58 and 0.81 at.% Cr), copper–silicon (2.3 and 8.6 at.% Si) and copper–tin (1.4, 3.4 and 5.7 at.% Sn) alloys were investigated. The copper–chromium alloys were supplied by the American Metal Climax Inc. Copper–silicon and copper–tin solid solutions were prepared by melting OFHC Cu with the desired amount of solute in an induction furnace under a dry and purified argon atmosphere. Graphite was used both as a susceptor and as a mold in the case of copper–tin alloys. For copper–silicon alloys, aluminum oxide molds were used to avoid the reaction between silicon and graphite. The temperature was monitored by means of an optical pyrometer to an accuracy of ±5 °C. After reaching the desired temperature (1150 °C for Cu–Sn and 1450 °C for Cu–Si), it was maintained for 1 h to allow good mixing of the two components of the alloy. The cooling was very slow until the solvus temperature was reached and then the cooling rate was increased to minimize precipitation during cooling.

The cast rods with a diameter of 17 mm were then encapsulated in Vycor tubes under vacuum and homogenized at 800 °C for 50 h. The temperature was controlled to within ±3 °C. After homogenization, the rods were swaged down to a diameter of approximately 7 mm and then machined to a diameter of 6 mm in two passes at a spindle speed of 214 rev min^{-1} and a feed rate of 0.06 mm rev^{-1}. The machined rods were polished with emery papers of different grit size. After final polishing with 4/0 emery paper the specimens were vacuum sealed in Vycor tubes and were recrystallized. Other details are given in Table 1, and representative microstructures are shown in Fig. 1.

After heat treatment, the specimens were finished with 3 μm diamond lapping compound. Then they were washed with soap and water, rinsed with alcohol and dried with an air blower. The specimens were then weighed to an accuracy of 0.01 mg and tested.

TABLE 1

Experimental materials: copper solid solutions*

Alloy	Composition		Recrystallization treatment		Grain size (μm)
	Wt.%	At.%	Temperature (°C)	Time (min)	
OFHC Cu	—	—	360	250	28
Cu Sn	2.5	1.4	790	120	35
Cu Sn	6.0	3.4	790	60	40
Cu Sn	10.0	5.7	790	30	30
Cu Si	1.0	2.3	860	300	75
Cu Si	4.0	8.6	860	300	90
Cu Cr	0.47	0.58	1070	5	450
Cu Cr	0.66	0.81	1070	5	485

*The purity of the materials used was: OFHC 99.98%; Sn 99.89%; Si 99.9999%.

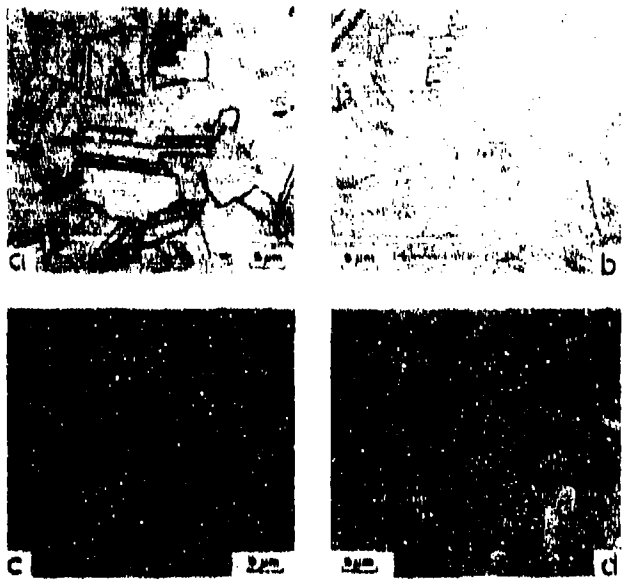

Fig. 1. Optical micrographs showing the representative microstructures of solid solutions: a) OFHC copper, (b) Cu–5.7 at.% Sn, (c) Cu–8.6 at.% Si and (d) Cu–0.81 at.% Cr.

Wear tests

Wear tests were carried out on a lathe using a cylinder-on-cylinder geometry. The specimens were rotated by the spindle of the lathe and the stationary slider was held in a holder connected to a lathe tool dynamometer. The slider was made of AISI 52100 steel (Brinell hardness 560 kg mm^{-2}) and was polished to the same conditions as the specimens. The dynamometer was

attached to the carriage of the lathe and the normal force was applied by the transverse motion of the carriage. Both normal and friction forces were measured by a strain gage assembly and were monitored by a Sanborn 321 Recorder. The normal load was 2 kg in all cases. The tests were carried out for 100 min (which for the applied load was sufficient to reach the steady state delamination process). In order to avoid temperature effects, all the tests were carried out at a sliding speed of 200 cm min^{-1}. To minimize surface oxidation during tests, the sliding surfaces were enclosed in a chamber which was evacuated before each test and filled with purified argon during the test. A schematic drawing of the apparatus is shown in Fig. 2.

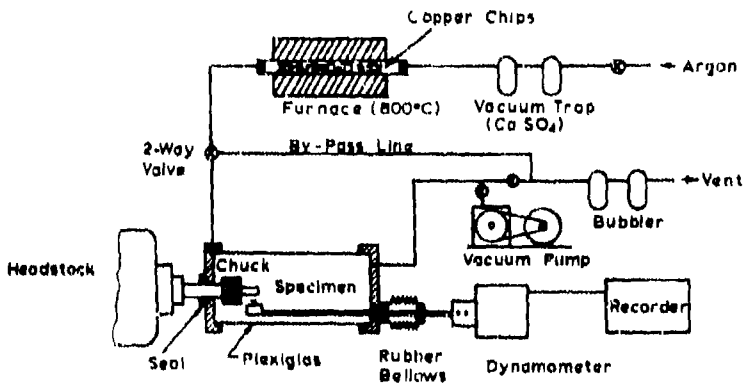

Fig. 2. A schematic diagram of the experimental set-up used for wear tests.

Metallography

The wear track surface and subsurface were observed in a scanning electron microscope (SEM). For wear track observations no special preparation was required. For subsurface observations the specimens were mounted in plastic mounts and polished on silicon carbide papers until the desired location in the wear track was reached. Next, metallographic polishing was carried out in a vibrating polisher with a slurry of 0.05 μm alumina powder. Then the specimens were etched with potassium dichromate solution. The polishing and etching were checked in an optical microscope and when the conditions were satisfactory the specimens were removed from the mounts, cleaned and observed in the SEM.

Experimental results

Figure 3 shows that the Vickers hardness of the solid solutions increases linearly with increase of the solute content. It can also be seen that different elements produce different hardening for the same atomic content of solute.

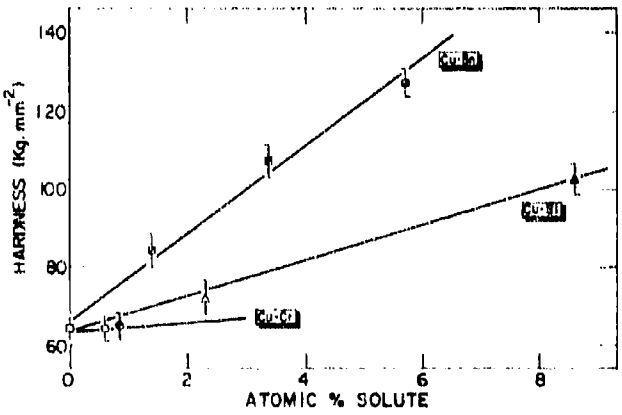

Fig. 3. The Vickers microhardness under a 200 g load *vs.* the atomic per cent of solute. Each point represents an average of five measurements and the bars represent the standard deviation.

A good improvement is obtained for Cu–5.7 at.% Sn solid solution whose hardness is twice that of OFHC copper. The addition of silicon to copper is not as effective as that of tin but there is still an increase of about 60% for Cu–8.6 at.% Si. In Cu–Cr alloys, no hardening was noticed because of the low atomic content of Cr used owing to the limited solid solubility of chromium in copper. These results are in good agreement with the work done on solid solution hardening of copper-based alloys [4, 5].

An immediate consequence of the alloying was changes in the friction coefficient for different compositions. Figure 4 shows that the friction

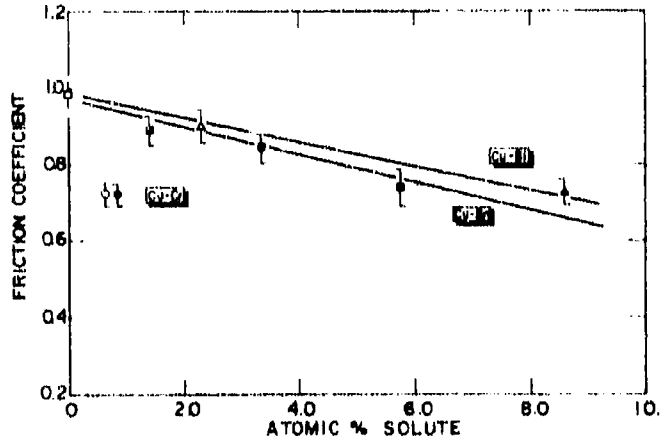

Fig. 4. The friction coefficient as a function of the atomic content of solute. The friction coefficient was calculated using the steady state tangential force. The sliding speed was 2 m min^{-1}.

coefficient decreases linearly with the increase in the atomic content of solute in the cases of Cu–Sn and Cu–Si. However, for Cu–Cr alloys the friction coefficient is lowered by adding only a small percentage of chromium and does not decrease as the chromium percentage increases.

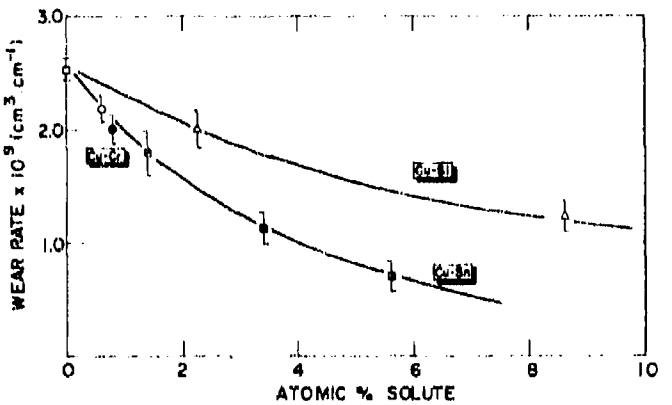

Fig. 5. The wear rate as a function of the atomic per cent of solute. The normal load was 2 kg and the duration of the tests was 100 min.

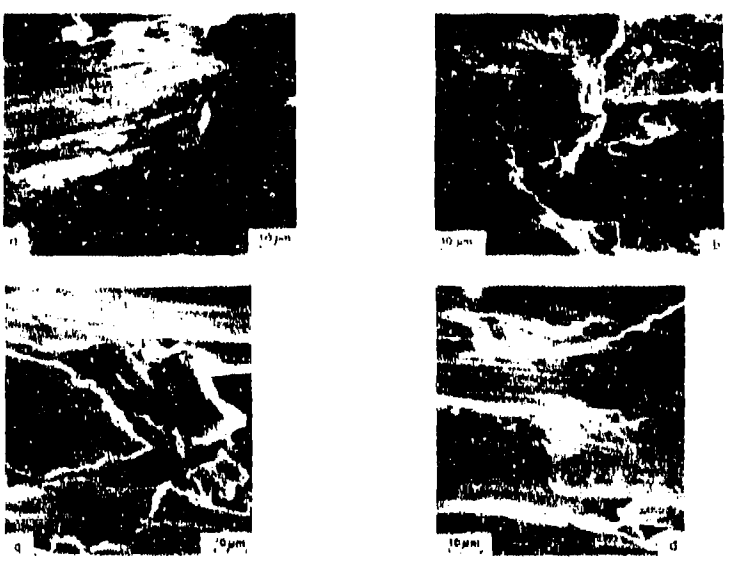

Fig. 6. Scanning electron micrographs of wear tracks: (a) OFHC copper, (b) Cu–5.7 at.% Sn, (c) Cu–8.6 at.% Si and (d) Cu–0.81 at.% Cr. The normal load was 2 kg at a sliding speed of 2 m min^{-1} and the sliding distance was 200 m.

The effect of composition on the wear rates is shown in Fig. 5. The wear rate is decreased as the amount of solute increases, but the decrease is different for different solutes, particularly for silicon and tin. In the case of Cu–Cr alloys there is uncertainty in defining a curve since the experimental points are very close.

Microscope examination was conducted to check whether or not the delamination process occurred. Figure 6 shows scanning electron micrographs of some of the materials tested. The sliding direction in all micrographs is from the right to the left. The micrographs clearly show that delamination wear sheets have formed. It is also interesting to note that the top surface of the particles is very smooth.

Figure 7 shows scanning electron micrographs of the subsurface of the same specimens as in Fig. 6. The sliding direction is again from the right to the left. These micrographs indicate that cracks tend to propagate parallel to the surface and then to extend to the surface. The depth at which cracks propagate seems to be different for specimens with different compositions. This difference is more striking between micrographs (a) and (b) in Fig. 7;

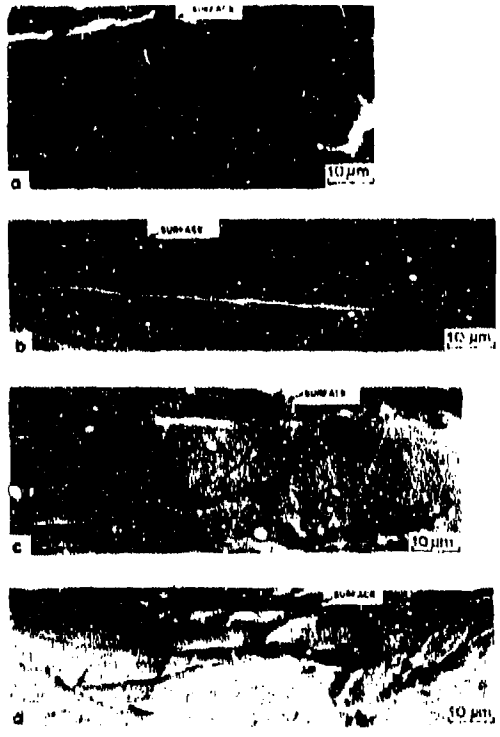

Fig. 7. Scanning electron micrographs of the subsurfaces. The materials and test conditions are the same as in the previous figure.

the former (OFHC Cu) shows cracks propagating at a depth of the order of 50 μm, and the latter (Cu–5.7 at.% Sn) shows cracks at a depth of the order of 15 μm.

Discussion

The microscope observations of the worn specimens show three facts: (a) that wear sheets formed by cracking (Fig. 6); (b) that there was extensive subsurface deformation; and (c) that there are subsurface cracks running parallel to the surface (Fig. 7). These observations confirm that delamination wear was occurring.

The experimental results presented in the last section show that the addition of solutes to copper increases the hardness, as shown in Fig. 3; the presence of solutes also decreases both the wear rate and friction coefficient as shown in Figs. 5 and 4, respectively. We shall first consider these results in terms of the mechanics of subsurface deformation, crack nucleation and crack propagation. Then the metallurgical aspects will be considered.

Measurements to quantify the subsurface deformation have been made in the past [6] and plastic strains as high as 16 or greater have been found for situations similar to those in this study; these strains are much larger than those encountered in normal bulk deformation and can only be explained in terms of the effect of the high hydrostatic pressure acting near the asperity–surface contact and of cyclic creep. The mechanism of plastic deformation under cyclic loading due to the normal and tangential components is discussed in the companion paper by Jahanmir and Suh [7].

The process of cyclic creep in a sliding situation can be stated as follows. When two surfaces are brought together, contact is only established at the asperities [1]. As the contact area is very small, local plastic deformation will occur under the asperities. Increasing the hardness increases the load-carrying capacity at each asperity, but to a first order approximation the plastic zone size and the area of contact are not changed. However, the number of contacting points will be decreased, which decreases the real area of contact [8]. Thus the main role of the hardness is in controlling the number of contacting points and the magnitude of the compressive stress below each contact point. When a tangential displacement is imposed on the asperities, a friction force is generated. This combination of normal and tangential tractions results in a zone of compressive stresses below and ahead of the asperities and a zone of tensile stresses behind the asperities. (The size of the zone of tensile stresses, as well as the magnitude of the stresses, is chiefly controlled by the tangential traction and thus by the friction coefficient.) Therefore, the material near the surface will experience a cyclic state of loading each time an asperity passes by. Since the loading history is the same for all asperities, the cyclic loading is characterized by a constant stress amplitude which will be determined by the hardness and friction coefficient. The number of cycles at a given location is given by the number of asperities

that have passed over that location. Although the cyclic stress–strain characteristics of the present materials are not known precisely, the cyclic loading can give rise to a process of cyclic softening and cyclic creep. This may have contributed to the large amount of subsurface deformation that has been observed in addition to the deformation mechanism analyzed elsewhere [7].

Therefore alloying affects the process of subsurface deformation in two ways: (a) it increases the hardness (Fig. 3), which reduces the number of cycles for a given sliding distance; and (b) it reduces the friction coefficient (Fig. 4), which results in a reduction of the cyclic stress amplitude.

As deformation continues, cracks will be nucleated when the conditions for nucleation are satisfied. It has been shown in a previous paper [7] that for two-phase metals the depth at which voids can be formed decreases when the friction coefficient is reduced. However, there are two difficulties with that analysis when extended to single-phase materials. First, the mechanism of crack nucleation is not known precisely for the case of single-phase materials. Secondly, the analysis does not hold for cases where no particles are present. Nevertheless, cracks do nucleate and it is conceivable that the influence of the friction coefficient will be the same. This means that a reduction in the friction coefficient decreases the depth at which cracks are likely to be nucleated, which leads to a reduction in the wear rate.

After cracks are nucleated, they will propagate. The mechanics of crack growth were analyzed in a previous paper [9]; the results show that both the depth and growth rate of the fastest growing crack are reduced when the friction coefficient is reduced. This further implies that the wear particles will be thinner when the friction coefficient is reduced leading to lower wear rates.

Figure 5 shows that the reduction of the wear rate is less in the case of the Cu–Si system than in the case of Cu–Sn. This is due to the fact that in Cu–Si, the friction coefficient is slightly higher (Fig. 4) and the hardness is lower (Fig. 3) than in the case of Cu–Sn. Also Cu–Cr, which has the lowest hardness of all the alloys, exhibits wear rates comparable with Cu–Sn, because its friction coefficient is the lowest among all the alloys (Fig. 4). These results are in agreement with the discussion given above.

Although an explanation of the results has been given in terms of phenomenological quantities such as hardness and friction coefficient, the role of solutes in the delamination wear should be clarified. How solute additions affect the cyclic behavior of the material, crack nucleation and crack propagation are important basic questions. Unfortunately, all those effects are not known at present and even a qualitative explanation is not possible. In any case, crack nucleation and crack propagation do not seem to be the dominant processes in these alloys. If they were, the wear rate would not have decreased as the solute content is increased because any addition of solutes tends to accelerate the crack nucleation and crack propagation processes.

The variations in the friction coefficient as a function of composition also support the delamination theory. Two mechanisms have been proposed

to explain the generation of friction forces: adhesion at the contacting asperities [2] and plowing of softer metal by hard asperities [10]. The adhesion model explains the friction coefficient in terms of the ratio of the energy of adhesion to the hardness. Although the effect of alloying on the surface energy is not known precisely, it is reasonable to assume that it changes linearly with the composition over a narrow range. The percentage change in surface energy by the rule of mixture is then about the same as the atomic per cent of the solute. This leads to a range of values of 900 - 1100 erg cm $^{-2}$ for all alloys. With that assumption, the change in surface energy alone cannot explain the variations observed in the friction coefficient. In contrast, if plowing is important a variation in the friction coefficient as hardness changes would be expected. Figure 8 shows that the friction coefficient decreases linearly with the increase in the hardness. This result follows the same trend as results reported in the past for cubic metals under abrasive conditions, when plowing is the important mechanism [11]. Although the degree of plowing is much smaller in the present work, the same mechanism still seems to be operating. Nevertheless, the effect of surface energy cannot be neglected altogether since Fig. 8 does not show a unique relationship between friction coefficient and hardness; also Cu–Cr alloys exhibit low friction coefficients in spite of low hardness.

Further work must be done to clarify the effect of solutes on the cyclic creep behavior of materials and the crack nucleation and crack propagation processes. The main finding of this work is that adding solutes to pure metals decreases the wear rate because of the increase in hardness and the reduction in friction coefficient.

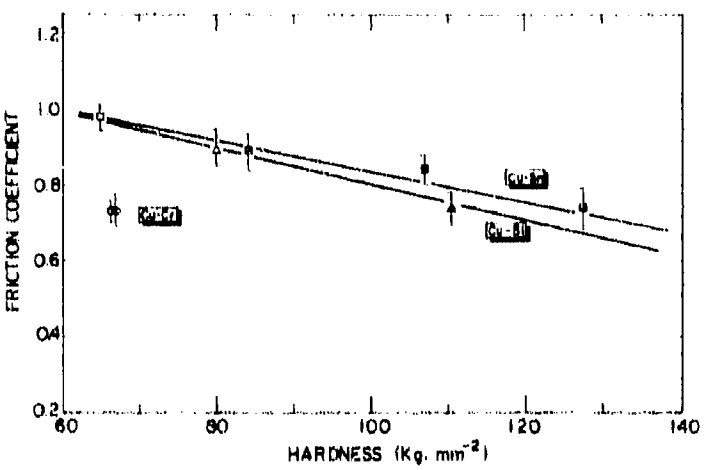

Fig. 8. The friction coefficient as a function of hardness. The normal load was 2 kg and sliding speed was 2 m min^{-1}.

Conclusions

Microscope observations conducted on worn specimens show that wear in copper-based solid solutions occurs as postulated by the delamination theory of wear. An increase in solute content improves wear and friction behavior of those materials. The effect of solute addition on the wear rate is twofold: (a) it reduces the friction coefficient which reduces the deformation rate, the depth of crack nucleation and crack propagation rate; and (b) it increases the hardness which decreases the plastic deformation rate and the number of loading cycles per unit sliding distance. Furthermore, the reduction in the friction coefficient is basically due to the increase in hardness which decreases the tendency for the hard asperities to plow the softer metal, although the effect of adhesion cannot be ignored.

References

1 J. F. Archard, Contact and rubbing of flat surfaces, J. Appl. Phys., 24 (8) (1953) 981 - 988.
2 E. Rabinowicz, Influence of surface energy on friction and wear phenomena, J. Appl. Phys., 32 (8) (1961) 1440 - 1444.
3 N. P. Suh, The delamination theory of wear, Wear, 25 (1973) 111 - 124.
4 R. Fleischer, Solution hardening, Acta Metall., 9 (1961) 996 - 1000.
5 R. Fleischer, Substitutional solution hardening, Acta Metall., 11 (1963) 203 - 209.
6 G. Agustsson, Strain field near the surface due to surface traction, S.M. Thesis, Department of Mechanical Engineering, MIT, 1974.
7 S. Jahanmir and N. P. Suh, Mechanics of subsurface void nucleation in delamination wear, Wear, 44 (1977) 17 - 38.
8 P. K. Gupta and N. H. Cook, Statistical analysis of mechanical interaction of rough surfaces, J. Lubr. Technol., 94 (1972) 19 - 24.
9 J. R. Fleming and N. P. Suh, Mechanics of crack propagation in delamination wear, Wear, 44 (1977) 39 - 56.
10 F. P. Bowden, A. J. W. Moore and D. Tabor, The plowing and adhesion of sliding metals, J. Appl. Phys., 14 (1943) 80 - 91.
11 P. J. Alison and H. Wilman, The different behavior of hexagonal and cubic metals in their friction, wear and work hardening during abrasion, Br. J. Appl. Phys., 15 (1964) 281 - 289.

Wear, 44 (1977) 77 - 86

WEAR OF TWO-PHASE METALS

N. SAKA, J. J. PAMIES-TEIXEIRA and N. P. SUH
Massachusetts Institute of Technology, Cambridge, Mass. 02139 (U.S.A.)
(Received February 1, 1977)

Summary

The effect of the second-phase particle structure on the wear properties of two-phase metals was investigated by using precipitation-hardened copper chromium alloys (Cu–0.58 at.% Cr and Cu–0.81 at.% Cr) aged for different periods of time at 500 °C. The hardness of these materials was found to increase initially with the aging time and then to decrease; the maximum value was reached after about 100 min of aging. Metallographic examination of worn specimens indicated that the wear process proceeded by subsurface deformation, crack nucleation and crack propagation, *i.e.* by delamination. The friction coefficient was found to be constant for both alloys and for all aging times. In the early stages of precipitation both the wear rate and the wear coefficient decreased. As the aging continued the wear rate and the wear coefficient increased even though the hardness also increased. The wear coefficient remained constant for the overaged alloys. The decrease in both the wear rate and wear coefficient in the early stages of precipitation is due to the fact that particles are small and coherent and require a large amount of subsurface deformation for crack nucleation. With further aging, the particles grow and become incoherent, increasing the wear rate due to easier crack nucleation. For the case of the overaged alloys, the wear coefficient tends to become constant because the wear process is controlled by the crack propagation rate which is found to be independent of the aging time for both alloys.

Introduction

According to the delamination theory [1], the wear of metals is a result of several sequential and independent processes, namely subsurface deformation, crack nucleation and crack propagation. As discussed in the overview paper [1], the microstructure of metals plays an important role in the mechanics of these processes and thus in the wear properties of metals. Although these processes operate sequentially, normally one of them is the dominant process; the relative importance of each process is determined by the microstructure.

For particle-free solid solutions, it has been found that subsurface deformation tends to be the rate controlling process [2]. Also, it has been shown that the hardness and the friction coefficient play a major role in the overall wear process because they control the subsurface deformation and the location of nucleation and propagation of subsurface cracks. In dispersion-hardened metals, incoherent dispersoids act as pre-existing cracks owing to the absence of bonding with the matrix; thus the wear rate is controlled by the density of dispersoids and by the crack propagation rate [3]. Consequently, although the hardness increases with the density of dispersoids, the wear rate also increases.

In this paper the wear properties of metals with both coherent and incoherent second-phase particles are investigated to clarify the importance of the crack nucleation process in delamination wear. By aging precipitation-hardenable copper–chromium alloys for different periods of time, different particle structures were obtained [4, 5]. The results presented in this paper show that the wear rate is a strong function of particle structure and of the bonding quality of the interface between second-phase particles and the matrix.

Materials and experimental procedures

Two different compositions (Cu–0.58 at.% Cr and Cu–0.81 at.% Cr) of precipitation-hardenable copper–chromium alloys were used in this investigation. These alloys were supplied by the American Metal Climax, Inc., in the form of 12.7 mm (0.5 in) diameter rods. Initially the materials were solutionized for a period of 50 h in evacuated Vycor tubes at 1070 °C and were then quenched in water.

The solutionized materials were then swaged down to a diameter of 7 mm (0.28 in) and machined to a diameter of 6.4 mm (0.25 in). After machining, the specimens were recrystallized at 1070 °C for 5 min, aged at 500 °C for different periods of time in evacuated Pyrex capsules and were then quenched in water. Representative microstructures are shown in

Fig. 1. Optical micrographs showing representative microstructures of precipitation-hardened Cu–0.81 at.% Cr alloy for aging times of (a) 5 min, (b) 1000 min and (c) 10 000 min. The aging temperature was 500 °C.

TABLE 1

Experimental materials

Parameter	Alloy	Aging time (min)		
		100	1 000	10 000
Volume fraction $V_v \times 10^3$	Cu–0.58 Cr	5.19	5.25	5.31
	Cu–0.81 Cr	6.96	6.97	7.09
Mean free path λ (μm)	Cu–0.58 Cr	68.9	70.49	71.8
	Cu–0.81 Cr	51.84	53.02	53.00
Particle size d (μm)	Cu–0.58 Cr	0.54	0.55	0.58
	Cu–0.81 Cr	0.55	0.56	0.58

Fig. 1. Quantitative measurements characterizing the particle structure of the overaged alloys are shown in Table 1.

Unlubricated wear tests were carried out using the cylinder-on-cylinder geometry. The slider was made of AISI 52100 steel (BHN 560) and its diameter was 6.4 mm (0.25 in). The surface speed during wear tests was in all cases 200 cm min^{-1} and the duration of test was 100 min, which corresponds to a sliding distance of 200 m. Other details of the test procedures are given in ref. 2.

Results

Figure 2 shows the variation in the hardness of the copper–chromium supersaturated solid solutions aged for different times as a function of the aging time. The hardness is 65 kg mm^{-2} for solid solutions and 140 kg mm^{-2} for peak aged alloys. The aging time for the maximum hardness is different for the two alloys whereas the maximum hardness is about the same. These results are in good agreement with previous work on precipitation hardening in these alloys [6].

Figure 3(a) shows the friction coefficient as a function of the aging time. It can be seen that the friction coefficient is fairly constant for all treatment times for both of the alloys. Thus the increase in hardness resulting from the aging treatment does not seem to affect the friction coefficient.

In Figure 3(b) the wear rate, which is defined as the volume of material lost per unit sliding distance, is plotted as a function of the aging time. It can be seen that the wear rate initially decreases by a factor of three for both Cu–Cr alloys and then increases approximately linearly; the slopes seem to be the same for both alloys. It is interesting to note that the minimum wear rate does not correspond to the maximum hardness (in Fig. 3 the peak hardness is indicated by arrows A and B for Cu–0.58 Cr and Cu–0.81 Cr, respectively).

To check the effect of microstructural parameters the wear coefficient (a dimensionless number obtained from the wear rate by multiplying by the

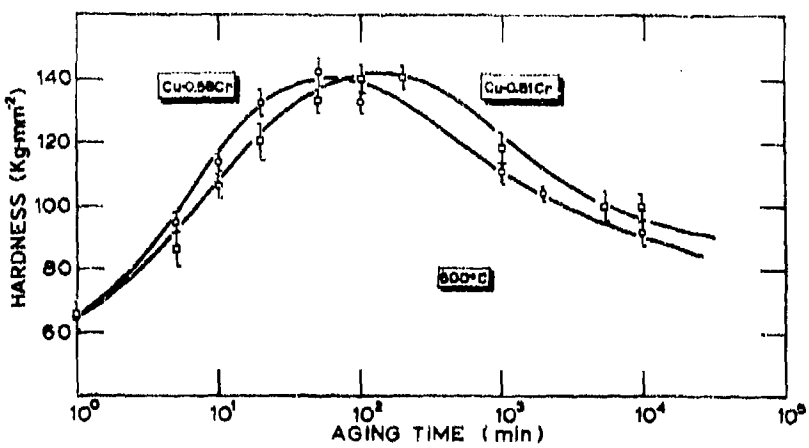

Fig. 2. The Vickers microhardness under a 200 g normal load as a function of aging time. The specimens were subjected to an aging treatment at 500 °C and were water quenched at the end of the treatment.

hardness and dividing by the normal load) is plotted in Fig. 3(c). It is seen from Fig. 3(c) that the wear coefficient decreases in the early stages of aging but, after some time of aging (in the present case about 5 min), it increases rapidly and then levels off asymptotically to a constant value.

As the microstructural differences between the two Cu–Cr alloys are characterized by the volume fraction and the mean free path of particles (and thus also by the particle size), plots of wear resistance (the inverse of wear coefficient) as a function of the volume fraction and the inverse of mean free path are shown in Figs. 4(a) and 4(b), respectively. The wear resistance decreases with an increase in the volume fraction and with the inverse of the mean free path of particles for the overaged alloys. These two curves are similar to plots of uniaxial strain to fracture *versus* the same parameters [7].

Figure 5 shows micrographs of wear tracks of the precipitation-hardened alloys aged for 5 and 10 000 minutes. The sliding direction is from left to right. It can be seen that the surface details are similar to those found elsewhere [2]. The subsurface features for the same alloys are shown in Fig. 6 where some second-phase particles can be seen in the overaged alloys. However, it is interesting to note that in Fig. 6(a) (the specimen aged for 5 min) subsurface cracks are very close to the surface, while for the specimen aged for 10 000 min cracks are formed at a larger depth.

As an example of the morphology of wear particles, scanning electron micrographs of particles collected from the Cu–0.81 at.% Cr alloy aged for 10 000 min are shown in Fig. 7. It is clear from the micrographs that the particles are indeed in the form of sheets, as predicted by the delamination theory of wear. An interesting feature of these particles is their lamellar

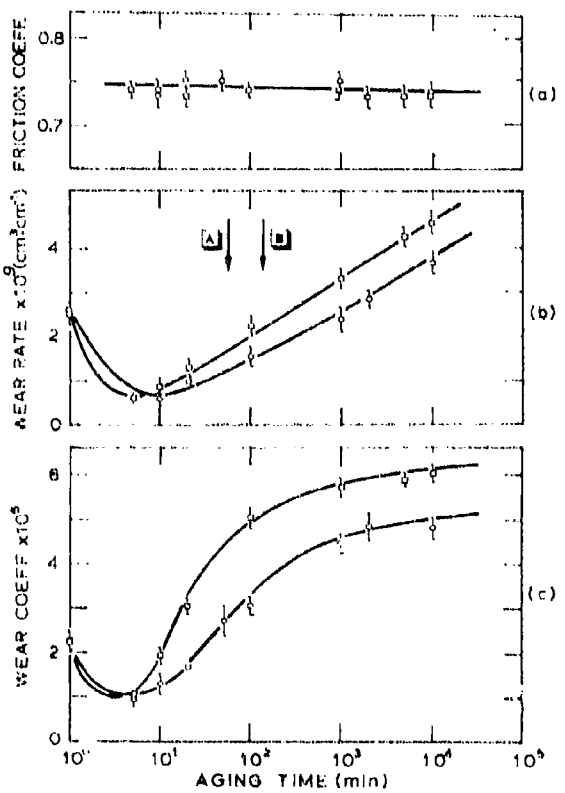

Fig. 3. Friction and wear properties of precipitation-hardened Cu–Cr alloys as a function of the aging time: (a) friction coefficient, (b) wear rate and (c) wear coefficient. The normal load was 2 kg and the duration of the tests was 100 min at a sliding speed of 200 cm min^{-1}.

structure. Such a feature seems to be caused by the presence of a number of cracks above the depth at which the cracks tend to propagate fastest.

Discussion

Metallographic observations of the surface (Fig. 5), of the subsurface (Fig. 6) and of wear particles (Fig. 7) clearly show that wear occurs by processes of subsurface deformation, crack nucleation and crack propagation, as postulated by the delamination theory of wear.

The material in the subsurface is deformed incrementally by the moving asperities which impose cyclic loading that results from normal and tangential tractions. The important parameters controlling the subsurface deformation are the hardness and the friction coefficient (see ref. 2). As the hardness

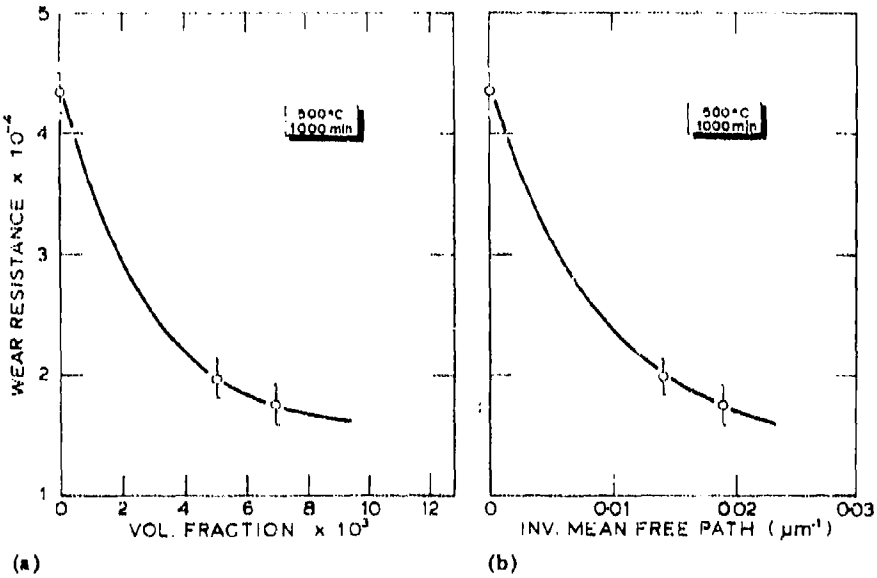

Fig. 4. The wear resistance (reciprocal of the wear coefficient) *vs.* (a) the volume fraction and (b) the mean free path of Cu–Cr alloys for 1000 min of treatment.

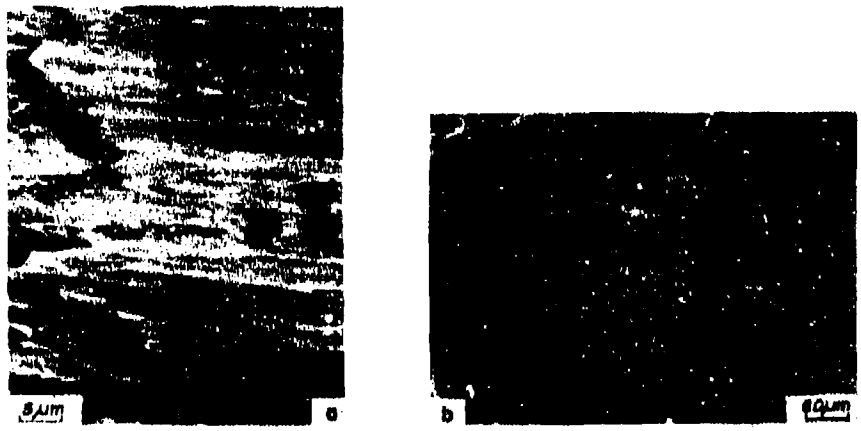

Fig. 5. Scanning electron micrographs of wear tracks of the precipitation-hardened Cu–0.81 at.% Cr alloy for an aging time of (a) 5 min and (b) 10 000 min. The sliding direction is from left to right.

is increased less subsurface deformation will accumulate. Since the friction coefficient is constant for both alloys and for all treatment times (Fig. 3(a)), the location of the subsurface crack nucleation sites and the crack propagation depth will not be affected significantly by the aging process. Therefore

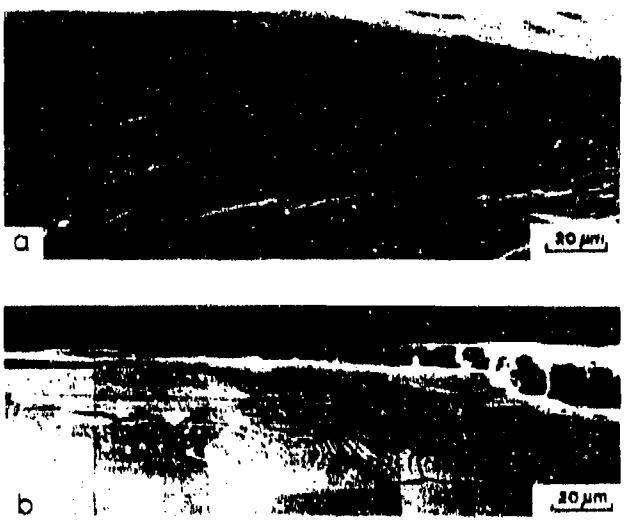

Fig. 6. Scanning electron micrograph of the subsurface of precipitation-hardened Cu–0.81 at.% Cr alloy aged for (a) 5 min and (b) 10 000 min.

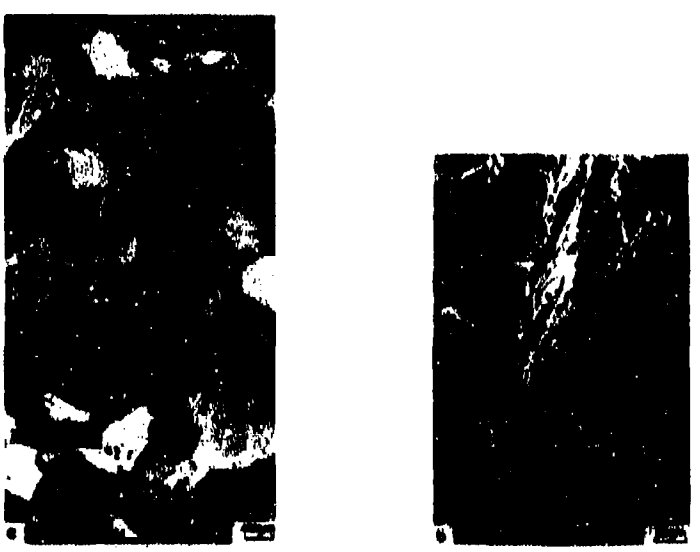

Fig. 7. Scanning electron micrographs of wear particles collected from wear tests on the specimen of Cu–0.81 at.% Cr aged for 10 000 min.

the wear process is not affected by the tangential component of the surface traction.

In Fig. 3(b) the wear rate is shown to decrease in the early stages of precipitation. This is due to an increase in the hardness and a consequent reduction of deformation. However, with further aging the wear rate increases even though the hardness increases. This result cannot be explained in terms of subsurface deformation alone and thus the crack nucleation and crack propagation processes have to be considered.

As deformation accumulates cracks will be nucleated when two conditions are simultaneously satisfied: (a) the tensile stress at the interface should be equal to the strength of the particle–matrix interface; and (b) the elastic energy released upon decohesion of the interface should be enough to overcome the surface energy of the void. According to Argon and his coworkers [8], in materials with particles much smaller than 20 nm in diameter cavities can never be formed by particle–matrix separation because the energy condition is not satisfied. For particles of about 20 nm cracks can nucleate by particle fracture, although the energy condition is difficult to satisfy and is probably the necessary and sufficient condition. If the particles are substantially greater than 20 nm, the energy criterion is easily satisfied and cracks can be formed spontaneously as soon as the critical tensile stress at the interface is reached. Based on a solution by Merwin and Johnson [9] adapted to the sliding situation, Jahanmir and Suh [10] have found that, for an elastic perfectly plastic matrix, tensile radial stresses are developed at the particle–matrix interface. These stresses are maximum at some distance from the surface. Further, they have shown that, for particles greater than 1 μm, cracks can be nucleated after only a limited number of cycles.

The wear rate is also affected by the coherency of particles. In the early stages of precipitation, since particles are coherent [11], the stress required to separate the particle from the matrix will be large. Therefore crack nucleation requires large amounts of subsurface deformation in order to develop a sufficient interfacial stress between the matrix and the particle. Since the increased hardness decreases the deformation rate, the wear coefficient (and thus the wear rate) is decreased. The steep increase of the wear coefficient shown in Fig. 3(c) after reaching a minimum value is due to the loss of coherency requiring less stress for decohesion of a particle from the matrix and is also due to the increased particle size. The deformation rate still decreases but the deformation required for nucleation decreases even faster. Further, as the interparticle spacing decreases during the early stages of aging, cracks have to propagate smaller distances in order to join with neighboring cracks. This explains why the wear coefficient of Cu–0.81% Cr alloy should be greater than that of Cu–0.58% Cr alloy because the former has a larger volume fraction of second-phase particles and possibly has a smaller interparticle spacing.

After the maximum hardness is reached, the volume fraction of particles does not increase with aging time anymore and coarsening of particles occurs, which increases the interparticle spacing. Crack nucleation at this point tends

to be relatively easy and the overall wear rate is controlled by the crack propagation rate. In this case two parameters have to be considered: the crack growth rate and the interparticle spacing. Since the hardness does not change very much for the overaged alloys, the number of asperities passing by will be about the same, and since the matrices of both alloys are exactly the same (the aging treatment was carried on at the same temperature), the crack growth rate must be the same to a first order approximation. A rough estimation of the crack growth rate can be made which is similar to that made in a previous paper [10]. Assuming that the material is deleminated by successive layers, the crack growth rate is calculated as the ratio of the mean free path to the number of cycles required to remove one layer. Such a calculation leads to a range of values between 4×10^{-4} and 6×10^{-4} μm cycle^{-1} for both alloys, and the wear rate depends basically on the mean free path of a particle (or the interparticle spacing). Thus, when the overall wear process is controlled by the crack growth rate, the wear coefficient tends to level off toward asymptotic values, as the aging treatment is continued and the mean free path becomes roughly constant. This explains the leveling-off of the wear coefficient when the transition from crack nucleation rate controlled wear to crack propagation controlled wear occurs. The effect of the mean free path is also shown by the difference in the wear rate of Cu–0.81 at.% Cr and Cu–0.58 at.% Cr. As a higher volume fraction implies a smaller mean free path for the same particle size, the curve for Cu–0.81% Cr should be higher than that for Cu–0.58% Cr, as shown in Figs. 4(a) and 4(b).

The arguments presented above are very qualitative, especially for the case of the early stages of precipitation. Quantitative measurements of precipitate shape, size and spacing using transmission electron microscopy, together with an analysis of the mechanics of crack nucleation such as that presented in an earlier paper [10], should give a quantitative relationship between the microstructure and the wear rates of two-phase metals. Meanwhile the empirical evidence and discussion presented in this paper should provide guidelines for the design of two-phase alloys for good wear properties.

Conclusions

(1) An increase in the hardness improves the wear properties of precipitation-hardened alloys only as long as the decreased deformation rate is not outweighed by the increased crack nucleation rate (which increases owing to increased incoherency at the particle–matrix interfaces).

(2) The maximum wear resistance occurs at aging times shorter than those which yield maximum hardness in the systems studied because crack nucleation occurs easily near the maximum hardness.

(3) As aging proceeds, with the alloy continuing past maximum hardness into the overaging regime, and particles grow, cracks are easily nucleated at

small subsurface deformation, the wear coefficient rapidly increases and the crack propagation rate begins to control the wear rate.

(4) The wear rate increases as the mean free path between incoherent second-phase particles decreases in overaged alloys owing to the increased number of cracks joining between particles.

(5) For good wear resistance it is desirable to have a large volume fraction of very small and coherent particles.

References

1 N. P. Suh, An overview of the delamination theory of wear, Wear, 44 (1977) 1 - 16.
2 J. J. Pamies-Teixeira, N. Saka and N. P. Suh, Wear of copper-based solid solutions, Wear, 44 (1977) 65 - 75.
3 N. Saka and N. P. Suh, Delamination wear of dispersion-hardened alloys, ASME Paper No. 76-WA/Prod.-29.
4 A. Kelly and R. B. Nicholson, Prog. Mater. Sci., 10 (3) (1963).
5 H. K. Hardy and T. J. Heal, Prog. Met. Phys., 5 (1954).
6 W. Koster and W. Knorr, Property changes during age-hardening of a copper–chromium alloy, Z. Metallk., 45 (1954) 350 - 356 (in German).
7 B. I. Edelson and W. M. Baldwin, The effect of second phases on the mechanical properties of alloys, Trans. Am. Soc. Met., 55 (1962) 230 - 250.
8 A. S. Argon, J. Im and R. Safoglu, Cavity formation from inclusions in ductile fracture, Metall. Trans., 6A (4) (1975) 825 - 837.
9 J. E. Merwin and K. K. Johnson, An analysis of plastic deformation in rolling contact, Proc. Inst. Mech. Eng., London, 177 (25) (1963) 676 - 690.
10 S. Jahanmir and N. P. Suh, Mechanics of subsurface void nucleation in delamination wear, Wear, 44 (1977) 17 - 38.
11 R. O. Williams, Precipitation process in copper–chromium alloys, Trans. Am. Soc. Met., 52 (1960) 530 - 544.

Wear, 44 (1977) 87 - 99

SURFACE TOPOGRAPHY AND INTEGRITY EFFECTS ON SLIDING WEAR*

S. JAHANMIR** and N. P. SUH

Department of Mechanical Engineering, Massachusetts Institute of Technology, Cambridge, Mass. 02139 (U.S.A.)

(Received February 1, 1977)

Summary

The effect of surface roughness and integrity on the sliding wear of metals was investigated experimentally. The results are consistent with the delamination theory of wear. The initial wear rate was influenced by the surface roughness and the applied load but the steady state wear rate was independent of the initial roughness. Under low applied loads delamination of smooth surfaces commences soon after sliding is initiated, whereas the delamination of rough surfaces is delayed until the original asperities are worn. Consequently, under low loads the initial wear rate of a smooth surface is higher than that of a rougher surface. The opposite is found under high loads since original asperities are removed immediately. It is also shown that machining damage to the surface or the subsurface (in the form of deformation, voids and cracks) accelerates the initial wear rate of the machined surface.

Introduction

Surface topography and surface integrity are two major surface characteristics which affect the wear behavior of machined surfaces. The surface roughness and the surface waviness are two topographical parameters which respectively describe the short range and the long range geometric deviations of a surface from the nominal geometric shape. The term surface integrity is used to characterize the quality of the surface and the subsurface material in terms of plastic deformation, cracks, structural heterogeneity by phase transformations, and residual stresses, all of which may be affected by surface preparation methods.

*Part of the results presented in this paper was also presented at the CIRP meeting in Germany in 1975.

**Present address: Department of Mechanical Engineering, University of California, Berkeley, Calif. 94720, U.S.A.

The effect of surface roughness and surface integrity on wear behavior is investigated experimentally in this paper. The experimental results are shown to be consistent with the delamination theory of wear. The effect of surface waviness on wear has been analyzed elsewhere [1] and it will be reviewed in the discussion section of this paper.

The wear behavior at the initiation of sliding interaction, before a steady state condition is reached, is referred to as the run-in phenomenon. Queener *et al.* [2] have shown that run-in wear depends on the original surface roughness when wear tests were conducted under lubricated conditions. Rowe *et al.* [3, 4] have shown that run-in also occurs in dry wear testing and that the sliding surfaces become smoother during running-in. However, when the steady state wear is reached the surfaces become very rough. These observations are all consistent with the mechanisms of the delamination theory of wear [5 - 7]. According to the theory, the initial smoothing is associated with the removal of machining marks [8]. However, when steady state wear by delamination is established, the wear surfaces become rough owing to the craters left after wear sheets lift off the surface.

The quality of a machined surface is related to the degree of damage generated in a surface layer during machining. A study by Abrahamson *et al.* [8] has shown that subsurface damage introduced during machining increases the initial wear rate. Scott *et al.* [9] and Allen [10] showed that surface integrity has an important effect on the life of ball bearings. Even though the effect of surface integrity on fatigue life has been studied extensively by Field and his associates [11 - 13], its effect on sliding wear was not investigated previously.

Experimental procedure

Wear tests were carried out on a lathe using a cylinder-on-cylinder testing geometry. The 0.6 cm diameter specimens were rotated at a surface speed of 3 cm s^{-1} and the stationary AISI 52100 pins (0.6 cm in diameter) were pushed against the specimens by normal loads of 0.106 and 0.850 kg. A series of tests was carried out by manually moving the slider parallel to the axis of the specimen. This was performed under a load of 0.907 kg for 10 revolutions. The tests were run under argon flowing into a chamber surrounding the contacting surfaces. All tests were run dry and at room temperature.

The materials tested were commercial cold-rolled AISI 1018 steel (hardness 84 kg mm^{-2}) and 70/30 brass (hardness 46 kg mm^{-2}). A variety of surface finishes were generated by turning. The surface finishes ranged from 1.2 to 10.4 μm (c.l.a.). They were generated by turning at 319 rev min^{-1} with a 0.13 mm depth of cut at various feed rates. Some specimens were prepared with cutting tools having a range of positive and negative rake angles to study the effect of subsurface damage generated by machining. Another series of specimens was prepared by orthogonal turning lubricated with lard oil, using tools with positive and negative rake angles.

The effect of surface roughness

The process of asperity deformation during the initial stages of sliding is shown in Fig. 1. The sliding direction was perpendicular to the machining marks in Fig. 1(a) and parallel to these in Fig. 1(b). The wear track on the rough surface (*i.e.* 3.4 μm c.l.a.) has become smooth and there is no evidence of adhesive or transferred particles.

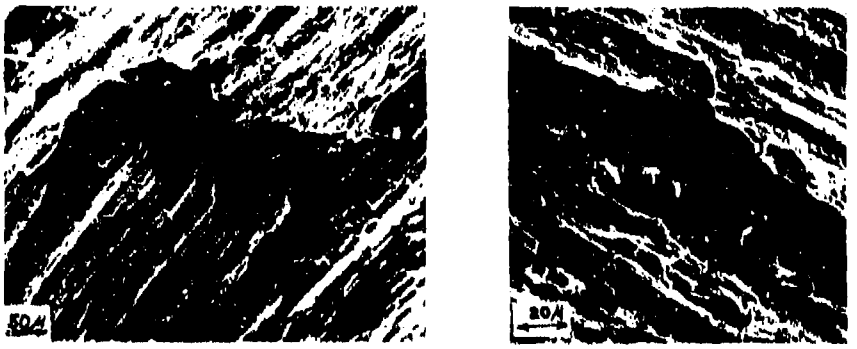

(a) (b)

Fig. 1. Plastic deformation of the original asperities for AISI 1018 steel (cylinder-on-cylinder geometry): (a) sliding perpendicular to the machining marks, 2.0 μm c.l.a. surface finish, after ten passes under a normal load of 0.91 kg; (b) sliding parallel to the machining marks, 3.3 μm c.l.a. surface finish, after 0.25 m of sliding under a normal load of 0.35 kg.

The results of wear tests on samples with varying roughness and normal loads are presented in Fig. 2. Under a load of 0.850 kg (Fig. 2(a)) the rough surfaces have a slightly larger total weight loss than the smoother surface. The small difference in weight loss is probably due to the large weight of the original asperities of the rougher surfaces. However, once the asperities are removed and steady state delamination is reached, the wear rate of all surfaces is the same.

Figure 2(b) shows that under a 0.106 kg normal load, the smoother surface has a greater total weight loss than the rough surface. However, the steady state delamination rate of both surfaces is the same. The difference in wear is due to the difference in the time delay before the onset of delamination. The 1.2 μm c.l.a. surface started delamination after 9 m of sliding, whereas delamination of the 2.7 μm c.l.a. surface began after 32 m of sliding. This was not observed under large loads because the contact stress was sufficient to remove the original asperities and to initiate delamination almost immediately.

The result of the wear test on AISI 1020 steel performed by Abrahamson *et al.* [8] with a pin-on-disk machine is given in Fig. 3. These

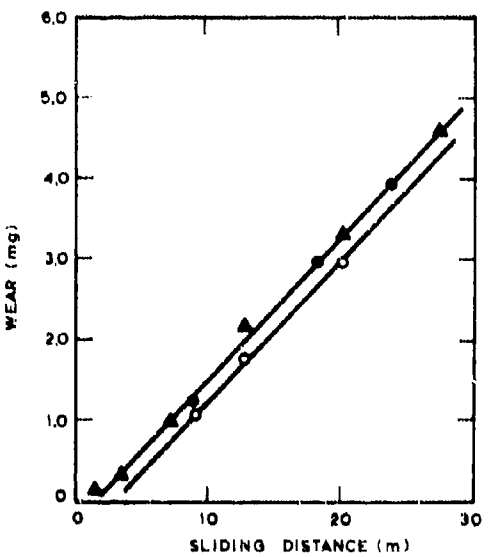

(a)

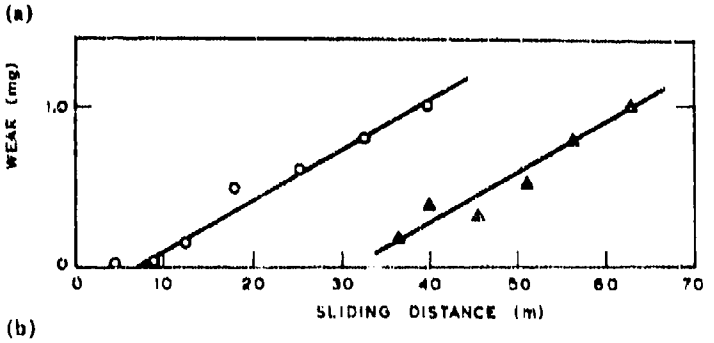

(b)

Fig. 2. The effect of original roughness of machined surfaces on weight loss: (a) normal load of 0.850 kg, AISI 1018 steel, ○ 2.1 μm c.l.a., ▲ 6.0 μm c.l.a., ● 7.8 μm c.l.a.; (b) normal load of 0.106 kg, 0.12 μm c.l.a., ▲ 2.7 μm c.l.a.

tests were run under conditions similar to the ones reported here, the only exception being that the pin-on-disk tests were done at an average surface speed of 7.8 cm s^{-1}. The similarity of the two sets of results, *i.e.* of Figs. 2 and 3, indicates that the effects on wear of the surface roughness and especially of the normal load are independent of the testing geometry.

These tests show that the surface roughness does not affect the steady state wear rate but only influences the initial wear behavior of machined surfaces. The fact that the rough surfaces under low loads wear less than smooth surfaces has interesting practical implications in the design and preparation of sliding surfaces. These results suggest that rough sliding surfaces under low contact stresses will last longer than smoother surfaces.

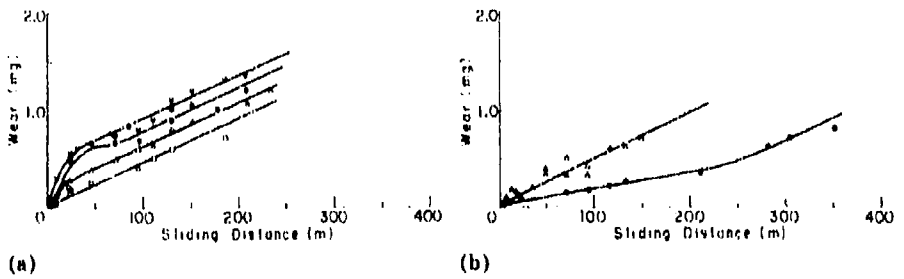

Fig. 3. Weight loss as a function of sliding distance for AISI 1020 steel (pin-on-disk geometry) [7]: (a) under a normal load of 0.30 kg, □ 0.1 μm c.l.a., ^ 0.3 μm c.l.a., V 1.1 μm c.l.a., ● 4.8 μm c.l.a; (b) under a normal load of 0.075 kg, ^ 0.3 μm c.l.a., ● 4.8 μm c.l.a.

Furthermore, under normal sliding conditions where lubricants are used the rough surfaces will also retain the lubricant and the wear behavior may be improved even further.

It should be emphasized that the rough surface is better than the smooth surface under light loads only if there is no subsurface damage (generated by machining). Otherwise, the large asperities delaminate catastrophically and produce large wear particles which could then cause abrasive wear of the sliding components. This was observed when specimens generated by a worn tool were wear tested under a low (0.75 kg) normal load. In these specimens the wear data were scattered and the delayed delamination associated with rough surfaces was not observed.

The effect of surface integrity

According to the delamination theory, steady state sliding wear of metals occurs by subsurface deformation and by void and crack nucleation and propagation. Therefore, if the prepared surface contained any surface or subsurface damage (*i.e.* deformation, voids and cracks), one would expect a larger initial wear rate. This is shown in Fig. 4 for an as-drawn surface and for a polished surface. The initial weight loss of the as-drawn surface is higher because of the surface damage generated during drawing, as shown in Fig. 5(a). (The as-drawn surface was lightly polished with a no. 4/0 emery paper to remove the surface oxides.) The polished surface was prepared by polishing off 0.06 mm with no. 2 emery paper and a final polish with a 4/0 emery paper. This process generated a relatively damage-free surface, as observed in Fig. 5(b), which led to a lower weight loss than that for the as-drawn specimen.

The effect on wear of subsurface damage generated by machining is shown in Fig. 6. The two series of specimens were machined using a sharp and a chipped cutting tool, as shown in Fig. 7. The chipped tool was still

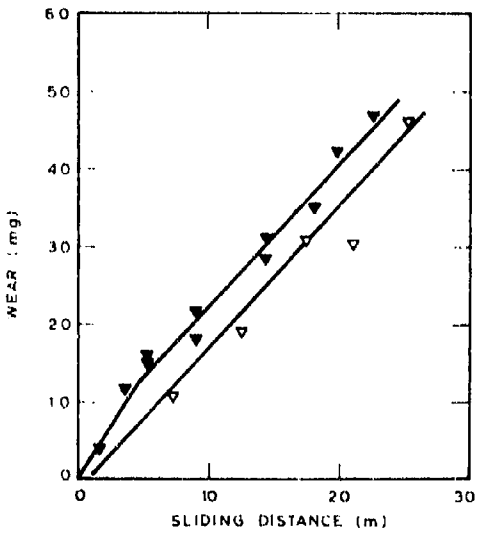

Fig. 4. The effect of surface damage on wear of 1018 steel under a normal load of 0.85 kg: ▼ as drawn, ▽ polished.

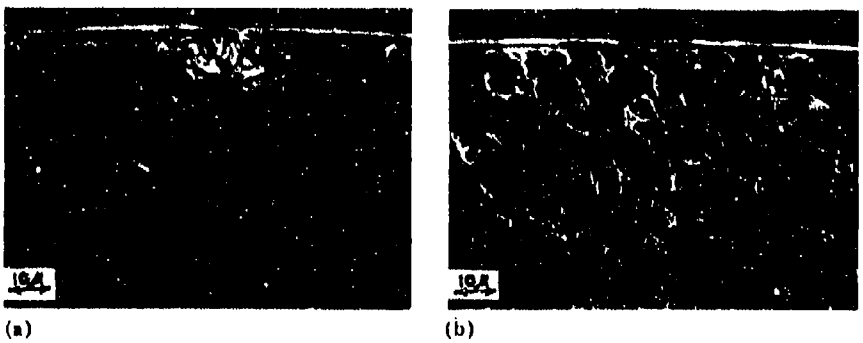

(a) (b)

Fig. 5. Sections perpendicular to the surface showing the typical microstructure of 1018 steel: (a) as drawn, (b) after polishing.

capable of producing fine surface finishes and from a machinist's point of view it was still useful. The difference in the initial weight loss of the two series of specimens is due to the larger subsurface damage generated by the chipped tool (10 μm deep) compared with that of the sharp tool (2 μm deep), which is observed in Figs. 8(a) and 8(b) respectively. It is interesting that the subsurface deformation caused by the chipped tool was sufficient to generate wear sheets (Fig. 9) on the machined surface.

Machined surfaces could also contain subsurface damage if machining parameters such as the rake angle, cutting tool radius or depth of cut were

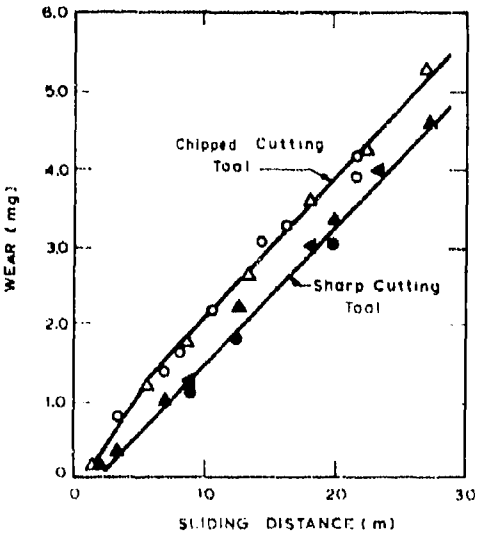

Fig. 6. The effect of subsurface machining damage on wear of 1018 steel: ○ 1.4 μm c.l.a., ^ 4.8 μm c.l.a., ● 2.1. μm c.l.a., ▲ 6.0 μm c.l.a., ◀ 7.8 μm c.l.a.

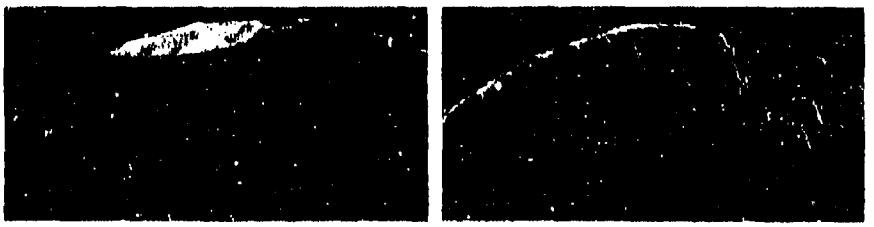

(a) (b)

Fig. 7. Scanning electron micrographs of the rake face of (a) a chipped cutting tool and (b) a sharp cutting tool.

not selected properly. Turley [14, 15] has shown that the depth and the degree of deformation in 70/30 brass increases as the rake angle decreases. At large negative rake angles the tool does not cut, but rather it slides over the surface causing plowing and subsurface deformation. The depth of deformation also increases with the depth of cut and with the cutting tool radius.

Figure 10 shows the wear of steel specimens prepared with three different tools: 40° rake; 8° rake; and 1.3 mm honed radius, 40° rake. The figure shows that all specimens have the same wear rate. This is probably due to the fact that all the tools had positive rake angles and, since steel is much harder than brass, the damage caused by machining with different cutting

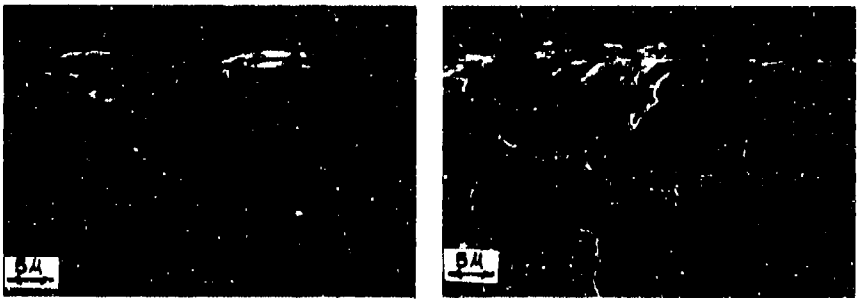

(a) (b)

Fig. 8. Sections perpendicular to the surface, showing typical subsurface damage of 1018 steel: (a) machined with a chipped tool, 4.8 μm c.l.a.; (b) machined with a sharp tool, 6.0 μm c.l.a.

Fig. 9. Wear sheets on the machined surface of a 3.3 μm c.l.a. surface finish, prepared with a chipped cutting tool.

tools might have not been sufficient to affect the wear behavior. Therefore 70/30 brass specimens were prepared by orthogonal turning with +25°, +5° and −15° rake angles. The results of the wear tests on the brass indicated that there was not a large difference between the wear rates of the samples cut with positive and negative rake angle tools. Subsurface observations of the machined surfaces showed that the depth of deformation was 25 μm for the +25° tool and 30 μm for the −15° tool. Since this difference was not large, it did not lead to a substantial difference in the wear rate of the samples.

The depth of deformed layers reported by Turley ranged from 600 μm for a +25° tool to 900 μm for a −15° tool. Such a difference in the deformed

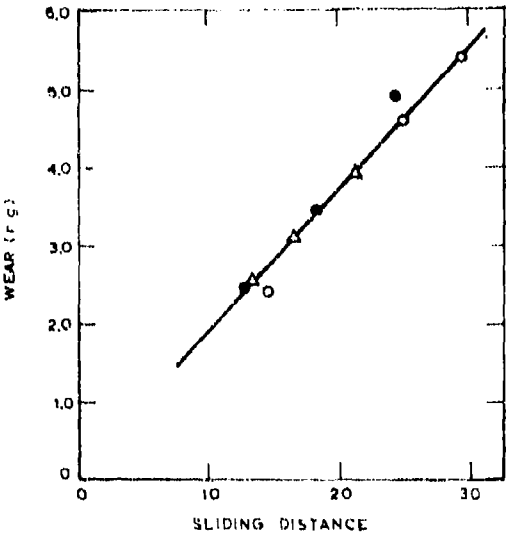

Fig. 10. Wear of 1018 steel specimens machined with three different cutting tools under a normal load of 0.85 kg: ● 40° rake angle, 1.3 μm c.l.a.; ○ 8° rake angle, 2.5 μm c.l.a.; △ 1.2 mm honed radius, 40° rake angle, 2.0 μm c.l.a.

regions generated by the two tools should result in a large difference in the initial wear rates. Since the degree of machining damage in the brass samples of this investigation did not differ between samples, no difference in the wear behavior was observed.

The deformation depth in brass observed by Turley was much more than the deformation depth reported here, probably because of the difference in the machining conditions. Turley's specimens were prepared by planing, whereas the specimens tested at MIT were prepared by turning. This indicates that the choice of machining operation and machine tools may be an important factor in the preparation of surfaces for sliding applications, since each type of machining generates a different type of damage in the finished product.

Discussion on surface roughness and integrity

The results presented here substantiate the predictions of the delamination theory in regard to surface roughness and integrity. The significance of this investigation is not only in the verification of the delamination theory but also in the practical implications of the results. It has been shown that specification of surface roughness alone is not sufficient; the surface integrity, surface preparation method and machining variables must also be properly specified for sliding surfaces.

A recent investigation [16] has shown that burnishing, which is the final surface preparation procedure in some applications, decreases the initial

wear rate of sliding surfaces. In burnishing, the original machining marks are deformed and fractured and some of the surface damage is removed. This process is very similar to the running-in of surfaces. Since the steady state wear rate is smaller than the transient wear rate, the burnished surface will have a lower wear rate (provided that burnishing conditions are selected such that subsurface void formation is prevented). In fact, if burnishing is done under a large load, the resulting surface will be rougher than the original surface [16] probably because of sliding wear by delamination.

The topography of a surface is generally characterized by both surface roughness and surface waviness. Surface roughness is the short range deviation of a surface profile from an average profile, whereas the waviness is the long range deviation. The investigation in this paper considered only the influence of surface roughness on wear. The effect of surface waviness on wear should not be disregarded, since in a recent paper [1] it has been shown that waviness can cause seizure of two geometrically constrained sliding surfaces. The approximate analysis indicates that, owing to the waviness, large wear particles may be generated by high local friction forces. These particles may then wedge in between the two geometrically constrained sliding surfaces and cause seizure.

The surface integrity considered in this paper has been limited to surface and subsurface damage caused by deformation and by void and crack nucleation. However, in general, machining can damage the surface and the subsurface by generating microstructural defects (*i.e.* deformation, voids and cracks), mechanical changes (*i.e.* residual stress) and metallurgical changes (*i.e.* phase transformation). Based on the results presented here it can be concluded that microstructural defects decrease the wear life of a machined surface. However, the effect of mechanical and metallurgical changes on wear have not been investigated; they will be discussed here in terms of the delamination theory of wear.

It has been shown [11 - 13, 17, 18] that, in grinding and orthogonal turning, surface integrity depends on such machining conditions as the speed, the cutting fluid, the type of grinding wheel and the size of the wear land. Cutting with sharp tools and at moderate speeds produces very little subsurface damage, whereas cutting with a worn tool or at high speeds degrades the surface integrity [17]. Since phase transformation near the surface depends on the temperature generated during machining, which in turn depends on the cutting speed, three distinct behaviors can be observed in turning high strength steels. Low speed cutting with a worn tool primarily causes microstructural defects and does not cause any observable metallurgical changes. Machining at moderate speeds with a worn tool generates a surface layer softer than the bulk (probably overtempered martensite). However, machining at higher speeds with a worn tool generates a harder surface but a softer subsurface. The hard surface layer is generated by the high rate of heating and cooling near the surface which produces untempered martensite. The softer subsurface is overtempered martensite. Similar metallurgical changes have also been observed for ground surfaces [11 - 13].

It is conceivable that the microstructural defects generated by an improper selection of machining parameters would lead to a larger initial wear of the surface. However, if no subsurface cracks are nucleated but the surface becomes harder or softer, prediction of the wear behavior becomes more difficult. A harder surface may resist deformation and delamination, but if any large wear particles are generated, abrasive wear will be the controlling mechanism and wear will be accelerated. A softer surface is less resistant to deformation, abrasion and plowing. It has been shown that the prediction of wear behavior cannot be based on the hardness alone, and that the microstructure must also be considered [19]. Since at this time no information is available on the wear behaviors of untempered or overtempered martensite, the effect of a near-surface phase transformation on the wear of steel cannot be resolved.

Machining also alters the mechanical state of the surface layer by introducing residual stresses. The nature of the residual stress depends on the type of machining and on the parameters. It has been found that grinding at low speeds and at small depth of cut produces a compressive residual stress, whereas grinding at higher speeds and at larger depth of cut produces a tensile residual stress at the surface [12]. In some turning operations, however, the near-surface residual stresses were observed to be always tensile, and the depth and their magnitude increased with the size of the wear land [18]. A large tensile residual stress can be detrimental in such applications as fatigue and sliding, since crack nucleation and crack propagation could occur more readily. In contrast, a compressive residual stress can be beneficial only if no subsurface microstructural defects (voids and cracks) have been generated during machining.

The above discussion and the result of tests indicate that surface roughness and integrity are important parameters in the wear behavior of machined surfaces. For a surface with a given set of microstructural characteristics, the effect of surface roughness on wear depends on the nature of the application, on the operating conditions and on whether or not the surface is lubricated. For example, in the case of lubricated sliding several unique situations are possible. In situations such as in a journal bearing, the retention of lubricants by the asperities can be an important consideration, especially if the applied normal load is small. The other extreme is the case of gears where the load is applied through a "line" contact and therefore the normal stress is high. In this case, the lubrication of the interface is no problem, since only a small part of the surface is in sliding contact at any time and lubricant is easily supplied to the surface while it is not in contact. The initial asperities on these gear surfaces will be removed instantaneously and these removed asperities will accelerate the subsequent wear process through abrasion. Therefore it is a desirable practice to lap the surfaces of gears before they are put into service. In short, since smoother surfaces are not necessarily better than rougher surfaces and since manufacturing cost increases with surface finish, decisions on desirable surface topography should be made after consideration of all the important factors involved.

Further work is clearly needed to develop a systematic way of characterizing and specifying the surface topography and integrity.

Conclusions

Based on the investigations presented in this paper, the following conclusions were made.

(1) Surface roughness influences only the initial wear behavior and not the steady state wear rate.

(2) At low normal loads rough sliding surfaces have smaller wear than smoother surfaces, provided that the surfaces are free from machining damage.

(3) Subsurface damage associated with machining operations could increase the initial delamination wear rate of the sliding surfaces.

(4) The choice of machining operation and variables are important factors in the preparation of surfaces for sliding applications.

Acknowledgments

The work reported in this report was sponsored by the Defense Advanced Research Projects Agency through the Office of Naval Research under contract N00014-67-A-0204-0080. We are grateful to Dr. Edward van Reuth and to Lt. Richard S. Miller for their personal support and guidance of our work.

References

1 N. P. Suh and T. Nagao, Implications of wear theories on surface quality and functional requirements, CIRP Ann. Int. Inst. Prod. Eng. Res., 25 (2) (1976) 513 - 519.
2 C. A. Queener, T. C. Smith and W. L. Mitchel, Transient wear of machine parts, Wear, 8 (1965) 391 - 400.
3 G. W. Rowe, H. Kallszer, G. Trmal and A. Cotter, Running-in of plane bearings, Wear, 34 (1975) 1 - 14.
4 H. Kallsser and G. W. Rowe, Surface integrity after severe wear or grinding, Proc. Int. Conf. on Surface Technology, Carnegie-Mellon University, Pittsburgh, Pa., May 1 - 3, 1973, pp. 333 - 347.
5 N. P. Suh, The delamination theory of wear, Wear, 25 (1973) 111 - 124.
6 N. P. Suh, S. Jahanmir, E. P. Abrahamson, II, and A. P. L. Turner, Further investigation of the delamination theory of wear, J. Lubr. Technol., 96 (1974) 631 - 637.
7 S. Jahanmir, N. P. Suh and E. P. Abrahamson, II, Microscopic observations of the wear sheet formation by delamination, Wear, 28 (1974) 235 - 249.
8 E. P. Abrahamson, II, S. Jahanmir and N. P. Suh, The effect of surface finish on the wear of sliding surfaces, CIRP Ann. Int. Inst. Prod. Eng. Res., 24 (1975) 513 - 514.
9 R. L. Scott, R. K. Kepple and M. H. Miller, The effect of processing-induced near-surface residual stress on ball bearing fatigue. In J. Bidwell (ed.), Rolling Contact Phenomena, Elsevier, New York, 1962, pp. 301 - 316.

10 S. Allen, Effect of surface condition of instrument ball bearings, Proc. Int. Bearing Symp., Draper Laboratory, Cambridge, Mass., June 5 - 7, 1973.
11 M. Field and J. F. Kahles, The surface integrity of machined and ground high strength steels, DMIC Rep. 210, 1964, pp. 54 - 68.
12 M. Field, W. P. Koster, J. B. Kohls, R. E. Snider and J. Maranchik, Jr., Machining of High Strength Steels with Emphasis on Surface Integrity, Air Force Machinability Data Center, Cincinnati, Ohio, 1970.
13 M. Field, J. F. Kahles and J. T. Cammett, A review of measuring methods for surface integrity, Ann. CIRP, 21 (1972) 219 - 238.
14 D. M. Turley, Deformed layers produced by machining 70/30 brass, J. Inst. Met., 96 (1968) 82 - 86.
15 D. M. Turley, Dislocation substructures and strain distributions beneath machined surfaces of 70/30 brass, J. Inst. Met., 99 (1971) 271 - 276.
16 R. Rajasekariah and S. Vaidynathan, Increasing the wear resistance of steel components by ball burnishing, Wear, 34 (1975) 183 - 188.
17 J. A. Bailey, S. Jeelani and S. E. Becker, Surface integrity in machining AISI 4340 steel, ASME Paper No. 76-WA/Prod-33.
18 C. R. Liu and M. M. Barash, The mechanical state of the sublayer of a surface generated by chip-removal process, Parts 1 and 2, ASME Paper No. 75-WA/Prod-9, 10.
19 S. Jahanmir, E. P. Abrahamson, II and N. P. Suh, The effect of second-phase particles on wear, Proc. 3rd North American Metalworking Research Conf., Carnegie Press, 1975, pp. 854 - 864.

Wear, 44 (1977) 101 - 108

BEHAVIOR OF MEDIUM CARBON STEEL UNDER COMBINED FATIGUE AND WEAR

T. NAGAO, J. J. PAMIES-TEIXEIRA and N. P. SUH

Department of Mechanical Engineering, Massachusetts Institute of Technology, Cambridge, Mass. 02139 (U.S.A.)

(Received February 1, 1977)

Summary

The combined fatigue-wear life of medium carbon steel (AISI 1045) was investigated under various combinations of loads and sliding wear conditions using a rotating beam test. The direction of the maximum tensile stress due to bending was perpendicular to that due to wear [1]. Tests were also performed with specimens plated with a thin layer of cadmium or nickel-gold. All of the tests were conducted in the high cycle regime. The results show that the fatigue life of all the specimens at a stress level higher than the endurance limit of the specimen was within the experimental scatter of a typical fatigue test. The effect of sliding wear on fatigue life is manifested primarily by the stress field imposed by the slider on the specimen. In the case of plated specimens, the fatigue life was not significantly affected, although the wear rate was decreased by an order of magnitude.

Introduction

Many rotating parts of a machine, *e.g.* components of turbomachinery and vehicles, are often subjected to cyclic bending loads leading to fatigue combined with a sliding action at the surface which leads to wear. When the relative displacement between the slidor and the part is small, this situation is commonly known as fretting fatigue. Fretting fatigue has been investigated extensively, since the reduction of fatigue life due to the combination of fatigue loading and wear is a major problem for aircraft components and high speed machines. However, the question of what happens to these parts when the relative displacement between the slider and the part is large and occurs only along a single direction has not been investigated in the past.

The purpose of this paper is to present the results of a combined fatigue-wear study conducted using AISI 1045 steel under different loads. The combined tests reported in this paper are simpler than fretting fatigue tests and may allow insight into the fretting fatigue problem by sliding the

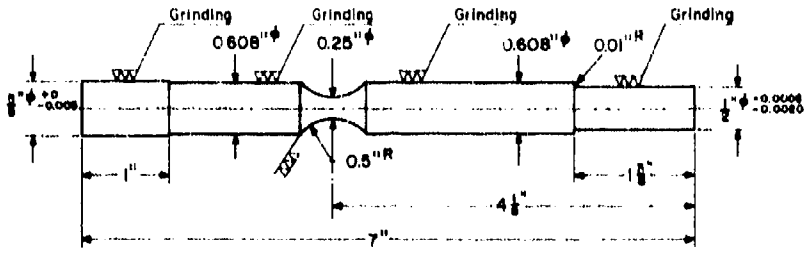

Fig. 1. A schematic diagram of the specimen used for combined fatigue-wear tests.

isolation of the effect of loading conditions from the effect of particles entrapped between fretting parts.

It is obvious that the effect of sliding action will be confined to a zone within about 200 μm of the surface and therefore it will affect only the crack nucleation process of fatigue. Since the wear rate is often slower than the crack propagation rate of fatigue cracks, it is expected that the effect of combined fatigue-wear loading will not be of any significance in the low cycle regime but may be of importance in that part of the high cycle regime where crack nucleation becomes important. Furthermore, since the sliding action may continuously disrupt the formation of a stable oxide layer, it may affect the fatigue life by changing the dislocation behavior near the surface. Although the work reported in this paper does not answer all these questions, it does provide a partial understanding of the problems involved.

Experimental materials and procedures

In order to investigate the behavior of medium carbon steels under combined fatigue-wear loading, AISI 1045 steel was used. The material was received in the form of cylindrical rods 16 mm (5/8 in) in diameter. Specimens were then machined to the final configuration shown in Fig. 1. The straight parts of the specimen were ground in standard grinding machines to provide maximum concentricity. The testing region was machined with a rotary lathe cutting tool of 12.7 mm (1/2 in) radius. Then the necked zone was polished to a minimum diameter of 6.4 mm with emery paper of sequentially reduced grit size, and finished with 6 μm particle size diamond lapping compound. Some of the specimens were then plated with a layer of cadmium or with a flash of nickel followed by a layer of gold. The initial thickness of the plating was about 0.1 μm for cadmium and 0.05 μm for nickel followed by 0.5 μm of gold.

Fatigue and combined fatigue-wear tests were carried out by rotating the specimens on a lathe. The fatigue geometry used was the classical cantilever rotating beam with the load applied at the end. The fatigue load as well as the normal load on the slider was applied by dead weights. The load on the slider was in all cases 0.3 kg. The friction force was measured by

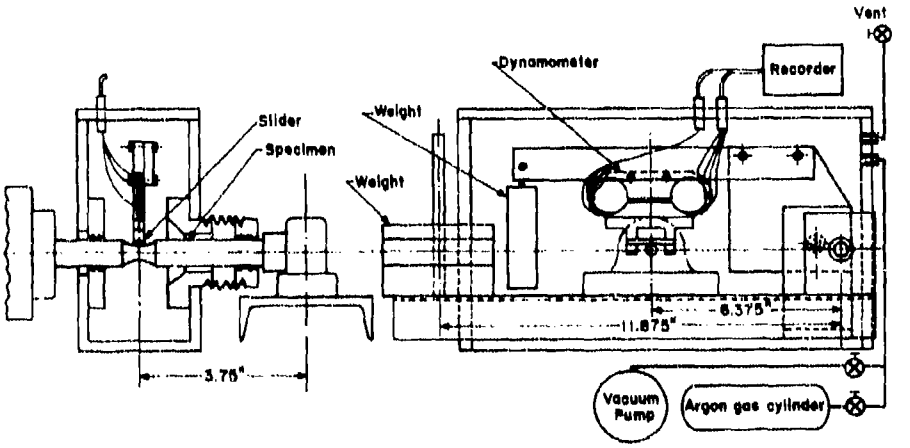

Fig. 2. A schematic diagram of the experimental set-up used to carry out the combined fatigue-wear tests.

means of a strain gage assembly to which the slider was attached. The sliders were in the form of cylindrical pins of 3.2 mm (1/8 in) of AISI 52100 steel (BHN 560).

Tests were run both in air and in argon atmosphere. For the tests under controlled atmosphere, the specimen and slider were enclosed in a chamber, which prior to the test was evacuated and filled with argon gas (Fig. 2). The tests were run until complete failure at a speed of 1000 rev min^{-1}.

Results

A series of different tests was carried out with AISI 1045 steel to show the effect of sliding wear on the fatigue life. Ordinary fatigue tests were also done to provide a reference. Combined fatigue-wear tests were carried out with unpolished, polished and coated specimens. The fatigue stresses were calculated based on the true diameter of each specimen and using the concentration factor of 1.07 [2].

In Fig. 3, the resulting S–N curves are shown. In the range of higher stresses (greater than 35 kg mm^{-2}), and thus shorter life, no remarkable difference was found between the plain fatigue and the fatigue-wear specimens, whereas for the lower stresses some differences exist. First, combined fatigue wear reduces the life by about a factor of two. Second, the reduction in life is more apparent in the case of combined fatigue wear with polished specimens.

Figure 4 shows both the test zone and the fracture surface of a specimen which failed at 8.0×10^5 cycles under a stress amplitude of 34.5 kg mm^{-2}. Figure 5 shows similar features but for a specimen subjected to combined fatigue wear. The stress amplitude in this case was 32 kg mm^{-2} and

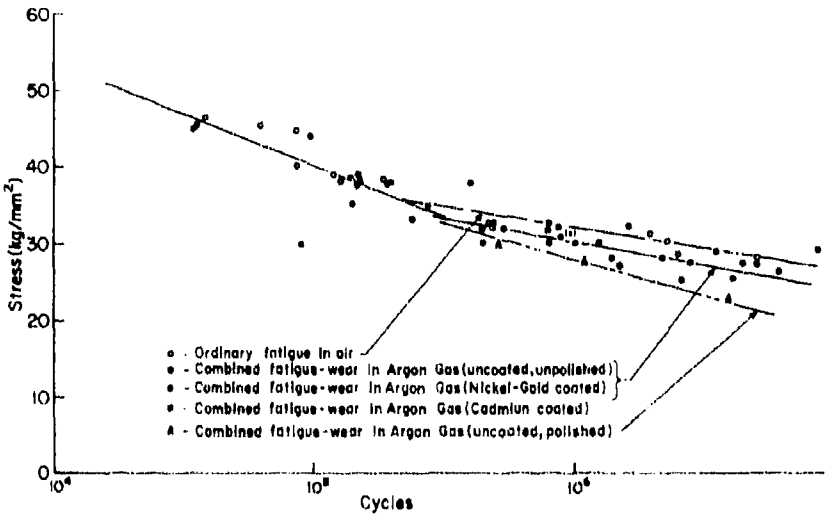

Fig. 3. S N curves for combined fatigue-wear tests. The stresses were calculated using the actual diameter of each specimen.

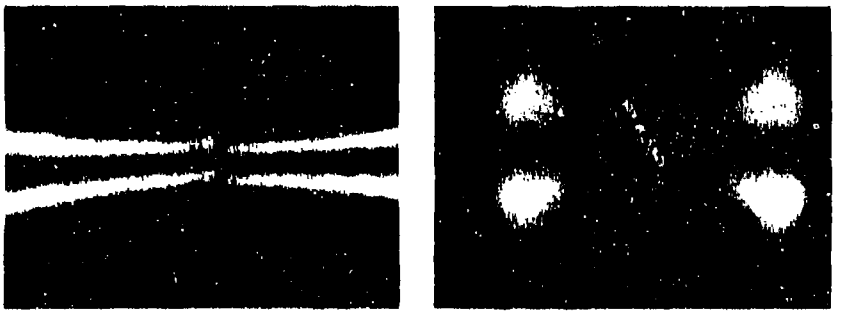

Fig. 4. A fractured specimen in plain fatigue loading. The stress amplitude was 34.5 kg mm $^{-2}$ and the number of cycles to failure was 8.0×10^5.

the number of cycles to failure was 4.33×10^5 cycles. These two micrographs look basically similar, the only difference being the presence of a wear track.

Figure 6 shows the wear volume, calculated from measurements of the width and depth of the wear track, as a function of the number of cycles. Although there is some scatter, it is clear that the wear rate of coated specimens, particularly the nickel–gold coated specimen, is reduced by an order of magnitude, whereas the reduction for cadmium coated specimens is only a factor of 3.

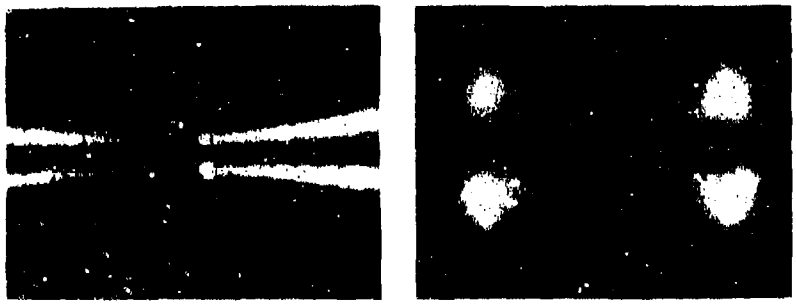

Fig. 5. A specimen fractured in the combined fatigue-wear test. The stress amplitude was 32 kg mm^{-2} and the number of cycles to failure was 4.33×10^5.

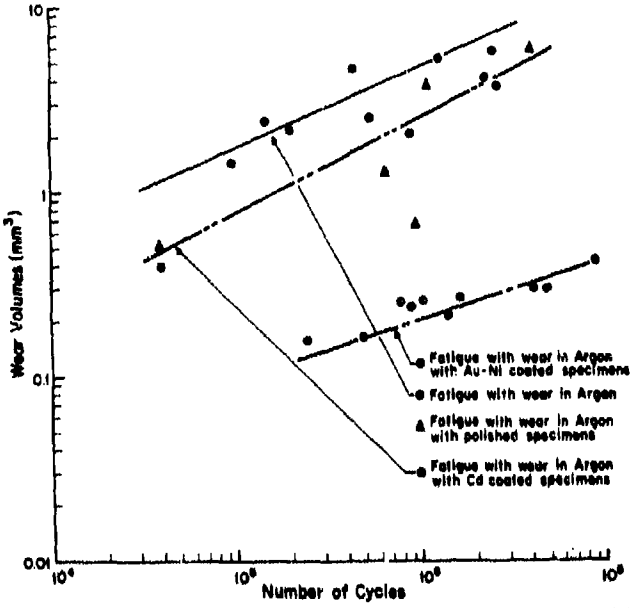

Fig. 6. The logarithm of the wear volume as a function of the logarithm of the number of cycles to failure. The wear volume was calculated by measuring the depth and width of the wear tracks.

Discussion

The results in the last section show that the fatigue life is reduced when sliding wear is imposed on the fatigue loading. It can be explained in terms of the accelerated crack nucleation rate due to the sliding action.

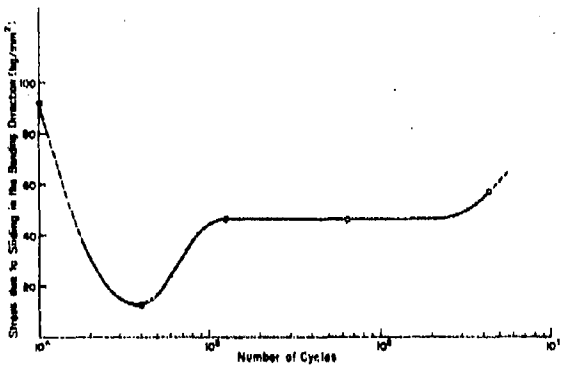

Fig. 7. The stress due to sliding in the direction of bending stresses as a function of the number of cycles to failure.

The sliding action imposes a cyclic state of loading on the material near the surface [3]. Under this cyclic loading the matrix can undergo plastic deformation and cyclic creep along shear bands in the direction of sliding, creating sufficient stress for debonding of the interface between the matrix and any hard particles or inclusions. The mechanics of void formation in the sliding situation are discussed in a companion paper [4]. These cracks may propagate both in the direction of sliding, leading to delamination wear, and in the radial direction leading to the fatigue failure. Fleming and Suh showed that there is a location below the surface where the crack growth rate is a maximum owing to the sliding action [5]. The cracks nearest to the surface are likely to be propagated in the transverse (*i.e.* radial) direction owing to the fatigue loading, because the direction and the magnitude of the normal stress due to bending are respectively perpendicular and proportional to the radius. In contrast, the stress field (based on the apparent contact) in the specimen under the slider is compressive in all directions, except near the trailing edge of the slider where the normal stresses are tensile. Therefore, the stress imposed on the specimen along the maximum bending stress direction will cause the specimen to undergo two cycles of loading for each revolution of the specimen.

In order to clarify the effect of the contact loading on the overall of cyclic loading, the stress history of the specimens was examined through a stress analysis for an elastic specimen [2]. Figure 7 shows the time dependent change of stress in the axial direction due to the load on the slider; this stress was calculated in terms of the measured geometry of worn specimens and sliders. Figure 8 is a schematic diagram of the loading history of the specimen at the contact point. It illustrates the fatigue loading cycle (Fig. 8(b)), the loading cycle in the bending plane due to the load on the slider (Fig. 8(c)) and the result of a superposition of Figs. 8(b) and 8(c) (Fig. 8(d)). It is clear that the actual number of fatigue loading cycles is doubled owing to the load applied by the slider during the early phase of the fatigue testing

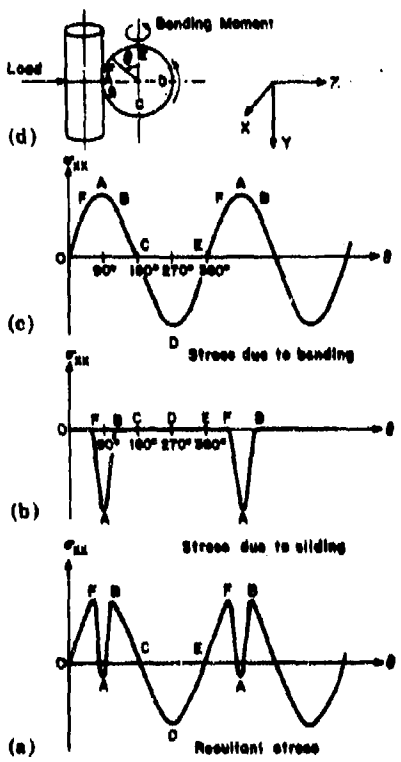

Fig. 8. A schematic diagram illustrating the loading history of a given point at the surface: (a) slider and specimen, (b) bending loading cycle, (c) sliding action loading cycle and (d) resultant of loading in (b) and (c).

when the crack length is short. Since initial crack growth is the dominant factor in fatigue life, doubling the number of cycles implies a reduction in the resulting fatigue life by a factor of approximately 2. This is in agreement with the results shown in Fig. 3 for the curves for plain fatigue and for combined fatigue wear.

Another feature of Fig. 3 is the greater reduction in the fatigue life for the tests run on polished specimens than that for the unpolished ones. This is probably due to the fact that the polishing removed the prestrained surface layer from the specimen. This layer contained compressive residual stresses which opposed the tensile stress due to bending.

The results for the coated specimens shown in Fig. 3 show that no improvement in the fatigue life was obtained by coating. However, the wear resistance of the specimen was greatly improved, especially for the case of the nickel–gold plated specimens (Fig. 6). According to the delamination theory of wear, the coating should reduce the wear rate of the specimen as

a result of the reduction of the subsurface deformation in the direction of sliding [6], which in turn results in a decrease in the crack nucleation and propagation rates. However, a reduction in the wear rate does not mean that the crack nucleation process due to the sliding action is completely suppressed. The mere fact that the fatigue life with coated specimens is worse than the fatigue life of plain fatigue specimens indicates that, even with coating, the crack nucleation process due to the sliding action dominates the crack nucleation process due to the fatigue loading. Further, it may be concluded that the reduction in the crack nucleation rate due to sliding obtained by coating is not substantial enough to improve the fatigue life in combined loading. Thus, the fatigue life is always reduced when crack nucleation occurs owing to the sliding action.

It should be recognized, however, that the above arguments are qualitative and that the stress analysis is rather simplistic. Nevertheless, the results are explainable in terms of loading cycles.

Conclusions

The main conclusions that can be drawn from this work are as follows.

(1) The load applied by the slider increases the crack nucleation rate near the surface and doubles the actual number of fatigue loading cycles, thus leading to a reduction in fatigue life by a factor of 2.

(2) The coating on the specimens is very effective in reducing the wear rate but does not improve the fatigue life because crack nucleation is not suppressed completely.

References

1 J. O. Smith and C. K. Liu, Stresses due to tangential and normal loads on an elastic solid with applications to contact stress problems, J. Appl. Mech., 20 (1953) 157 - 166.
2 R. E. Peterson, Stress Concentration Factors, Wiley-Interscience, New York, 1974.
3 J. J. Pamies-Teixeira, N. Saka and N. P. Suh, Wear of copper-based solid solutions, Wear, 44 (1977) 65 - 75.
4 S. Jahanmir and N. P. Suh, Mechanics of subsurface void formation in delamination wear, Wear, 44 (1977) 17 - 38.
5 J. R. Fleming and N. P. Suh, Mechanics of crack propagation in delamination wear, Wear, 44 (1977) 39 - 56.
6 S. Jahanmir and N. P. Suh, Sliding wear resistance of metallic coated surfaces, Wear, 40 (1976) 75 - 84.

Wear, 44 (1977) 109 - 125

WEAR OF METALS AT HIGH SLIDING SPEEDS

N. SAKA, A. M. ELEICHE* and N. P. SUH

Department of Mechanical Engineering, Massachusetts Institute of Technology, Cambridge, Mass. 02139 (U.S.A.)

(Received March 10, 1977)

Summary

High speed sliding wear of AISI 1020 steel, AISI 304 stainless steel and commercially pure titanium (75A) was studied using a pin-on-ring geometry. All the tests were carried out in air without any lubricant. The sliding speed was 0.5 - 10.0 m s^{-1} and the normal force was 49.0 N (5 kgf).

The friction coefficient of all the materials tested decreased with the sliding speed; this appears to be a consequence of oxide formation. The wear rate of 304 stainless steel increased monotonically with speed, whereas the wear rate of 1020 steel and titanium first decreased and then increased and again decreased, with a maximum occurring at about 5 m s^{-1}. The complex variation of the wear rate as a function of speed is explained in terms of the dependence of the friction coefficient, hardness and toughness of the materials on temperature. Microscope examinations of the wear track, the subsurface of worn specimens and the wear particles indicate that the wear mode was predominantly by subsurface deformation, crack nucleation and growth processes, *i.e.* the delamination process, similar to the low speed sliding wear of metals. Oxidative and adhesion theories proposed in the past to explain the high speed sliding wear of metals are found to be incompatible with the experimental observations.

Introduction

The papers presented so far in this issue of *Wear* emphasize subsurface deformation, crack nucleation and crack growth as important processes in the low speed sliding wear of metals. Both the metallographic and the empirical evidence presented clearly support this view. In these papers the experimental conditions were chosen so that the temperature rise was minimal; hence thermal aspects could be neglected. However, it is well

*Present address: Department of Mechanical Engineering, School of Engineering, Cairo University, Egypt.

known that at temperatures above about one-half of the absolute melting point of materials thermal aspects become important. The effect of temperature on surface traction, subsurface deformation, crack nucleation and crack propagation cannot be neglected, and oxidation plays an increasingly important role in high speed (or high temperature) sliding wear.

Wear of metals at high temperatures due to high loads and/or speeds is of special practical and theoretical interest. This problem is of interest in a variety of applications such as cutting tools, metal forming dies, automotive and aircraft brakes, guide rails for high speed vehicles, and lubricated sliding systems under starvation conditions. Yet, theoretical understanding of the wear mechanism at high speed and/or high loading conditions is quite inadequate.

Several theories of sliding wear of metals at high speeds have been proposed in the past. In one theory [1] it was hypothesized that the increased wear rate is due to the loss of hardness with the temperature rise, in accordance with the adhesion theory [2]. In another theory [3 - 6] it was assumed that as a result of the temperature rise the surface oxidizes (provided that oxygen is present) and the oxide layer is peeled off by external forces once it reaches a critical thickness. In this model the wear rate is determined by the diffusion of oxygen atoms through the oxidized layers. In a third model it is assumed that the oxides act as abrasive particles and thus contribute to abrasive wear [7].

The basic question is whether these mechanisms are the dominant mechanisms responsible for wear. In this sense, there are several limitations to the above theories although they may be valid in a narrow range of loads and speeds for specific materials. The limitations of the adhesion theory discussed in preceding papers also apply to high speed sliding wear. Firstly, the wear particles are generally platelike, much larger in size than predicted by current theories, and have metallic luster. Secondly, large scale subsurface deformation cannot be explained on the basis of these theories. Thirdly, the theories predict that the wear rate increases monotonically with sliding speed because of the temperature rise. This is contrary to several experimental observations; some observations have shown that the wear rate increases with speed [8], whereas some other observations show, surprisingly, that the wear rate decreases with speed [9]. Indeed, the wear rate may exhibit maxima and minima provided the range of speed is sufficiently wide. Finally, the effect of the friction coefficient on the wear rate has been essentially ignored. The only place where the friction coefficient appears is in the calculation of thermal energy generated due to friction. Unlike low speed sliding wear, the friction coefficient decreases substantially with speed and may have a pronounced effect on the wear rate.

With that background, it is clear that the wear of metals at high sliding speeds takes place by a mechanism different from that predicted by the existing theories. The purpose of this paper is to investigate critically the mechanism of wear at high sliding speeds and to explore the possibility that delamination wear might take place under such conditions.

Materials and procedures

AISI 1020 steel, AISI 304 stainless steel and commercially pure titanium (75A) were chosen for study. The choice of the materials was based on several considerations. As these three materials have three different crystal structures, the effect of crystal structure should be reflected in the wear data. AISI 1020 steel and titanium were chosen to investigate the effect of phase transformations, if any, induced by frictional heating. AISI 304 stainless steel is oxidation resistant and does not transform to other crystal structures at high temperature. Therefore, when its wear rate is compared with the more easily oxidized 1020 steel, it should provide information about oxidative wear. Further, as the thermal and other physical properties of these alloys are readily available, calculation of the temperatures of the sliding surfaces is easier. Other details about the materials are given in Table 1 and the microstructures are shown in Fig. 1.

TABLE 1

Experimental materials

Component	Material	Approximate composition	Hardness (MPa)	Density (10^3 kg m^{-3})
Specimen	AISI 1020 steel	0.2% C, 0.4% Mn	2300	7.78
	AISI 304 stainless steel	0.08% C, 18% Cr, 8% Ni	2920	8.03
	75A titanium	0.29% Fe, 0.05% C 0.06% N, 0.20% O	2350	4.50
Slider	AISI 52100 steel	1.02% C, 0.35% Mn 0.28% Si, 1.45% Cr 0.025% P, 0.025% S	7260	7.83
	AISI 4150 steel	0.5% C, 0.8% Mn 1% Cr, 0.2% Mo	9320	7.78

Figure 2 shows the schematic arrangement of the experimental set-up used for the wear tests. The sliding system consisted of a rotating AISI 52100 steel ring (0.2 m in diameter and 40 mm wide) mounted on a variable speed lathe. The normal load was applied by a dead weight and the tangential traction was measured by a dynamometer–Sanborn recorder assembly. The temperature was measured by iron–constantan thermocouples located on the specimen near the sliding interface and was recorded throughout the test by a multichannel recorder. The specimens were machined to conform to the surface of the ring. The pin-on-ring geometry used here has many advantages over other sliding configurations. First, conformity of the sliding surfaces enables a calculation of the nominal normal pressure, which remains constant during the entire test. Second, the sliding velocity (which determines the rate of heat generation) at the contact is the same over the entire

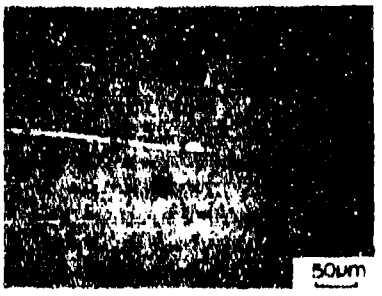

(a)

(b)

(c)

Fig. 1. Microstructures of experimental materials: (a) AISI 1020 steel, (b) AISI 304 stainless steel and (c) 75A titanium.

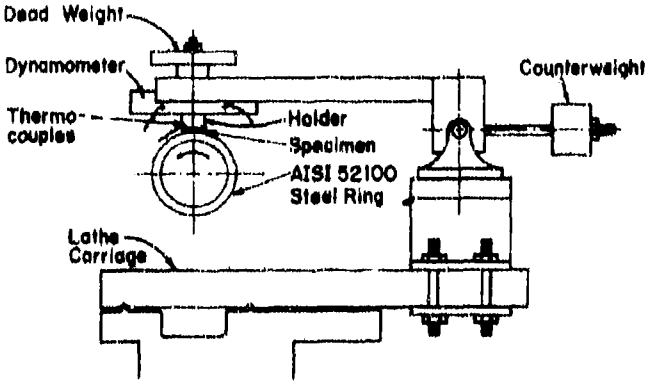

Fig. 2. Schematic diagram of the experimental set-up.

contact area. Finally, it is possible to calculate the surface temperature with simple assumptions because the sliding geometry does not change during the wear test and the heat flow into the specimen is at the most two dimensional.

The specimens were approximately 25 mm high, 25.4 mm long and 6.35 mm thick. The nominal contact area was a portion of a cylinder and was about 1.6×10^{-4} m^2. The specimens were prepared by machining at small depths of cut with a copious supply of lubricant. Both the specimen and the ring were polished to 4/0 emery grade but no attempt was made to measure the surface roughness. The specimen and the ring were cleaned with trichloroethylene before testing. The specimens were weighed to an accuracy of 0.01 mg before testing.

The majority of the tests were carried out under a normal force of 49.0 N in the speed range 0.5 - 10.0 m s^{-1}. The duration of the test was 1800 s. All tests were done in air without any lubricant. The temperature of the specimen was measured along the sliding interface at three locations and away from the surface at two locations. After testing, the specimens were brushed lightly and the weight was measured to an accuracy of 0.01 mg. Both the surface and the subsurface were examined metallographically. Selected specimens were cut, polished, etched with standard etchants and observed in a scanning electron microscope (SEM). Wear particles were collected during the test and were examined in an optical microscope. Several tests were also carried out on 1020 steel and 304 stainless steel at lower loads with a different slider in the same range of speeds and the results are tabulated in Table 2.

TABLE 2

Additional test results for AISI 1020 steel and AISI 304 stainless steel*

Test no.	Surface speed (m s^{-1})	Normal force (N)	Sliding distance (km)	Friction coefficient	Volume loss (10^{-9} m^3)	Wear rate ($\times 10^{-12}$ m^3 m^{-1})
AISI 1020 steel						
1	2.59	16.87	18.73	0.70	17.60	0.94
2	5.56	14.22	20.71	0.57	70.43	3.40
3	9.50	13.33	15.72	0.62	56.29	3.58
4	0.47	33.32	0.95	1.11	2.05	2.16
5	2.69	33.36	4.39	0.80	23.65	5.39
6	8.75	30.06	1.88	0.47	44.21	23.51
AISI 304 stainless steel						
1	2.43	11.76	17.70	0.96	76.46	4.32
2	5.35	11.11	18.91	0.86	91.78	4.85
3	8.74	13.33	16.72	0.73	50.18	3.00
4	2.57	35.53	9.51	0.81	123.26	12.96
5	5.13	31.78	3.28	0.84	39.35	12.18
6	8.65	29.86	7.53	0.86	73.85	9.37

*An AISI 4150 steel disc of 0.1 m in diameter and 0.64 cm thick was used as the slider.

Results

Figure 3 shows the friction coefficient as a function of the logarithm of the sliding speed. The friction force usually fluctuated during the first few minutes of the test, especially at low sliding speeds and loads. However, steady state conditions were soon reached and the tangential traction remained constant thereafter. Friction coefficients plotted in this figure and those shown in Table 2 are calculated using the steady state tangential force. It can be seen that the friction coefficient decreases gradually with an increase in speed and that its value at high speeds is about a one-half of its value at low speeds in the speed range investigated. It can also be seen that the friction coefficient for AISI 1020 steel is higher than that for the other two materials.

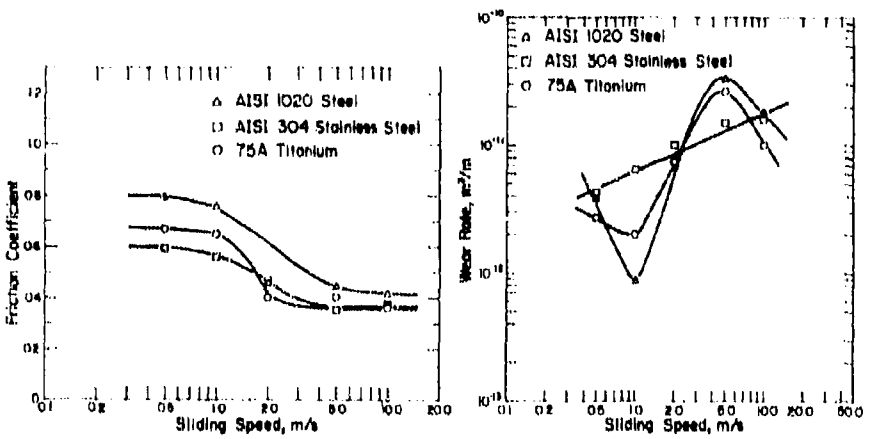

Fig. 3. The friction coefficient *vs.* the logarithm of the sliding speed. The friction coefficient was calculated using the steady state values of the tangential traction. Each point represents an average of three values.

Fig. 4. The logarithm of wear rate *vs.* the logarithm of the sliding speed. The normal force was 49.0 N and the duration of the test was 1.8×10^5 s. Each point represents an average of three values.

The wear rate as a function of the sliding velocity is shown in Fig. 4. The wear rate of 304 stainless steel increases monotonically with the sliding speed whereas the wear rate of both 1020 steel and 75A titanium first decreases, then increases and reaches a maximum and then decreases again. Both maxima are at a speed of about 5 m s^{-1}. The wear rate of 304 stainless steel, which is more oxidation resistant than 1020 steel, is about the same as that of 1020 steel. In fact, the stainless steel exhibits a higher wear rate than the other two metals at lower sliding speeds. These results are somewhat different from previous investigations in that a minimum and a maximum were observed in the wear rates in this work.

To investigate the effect of temperature rise on the friction and wear properties, the temperature of the specimen was monitored continuously. The temperature exhibited an initial transient for a period of about 5 min and then reached a steady state value which depended on the sliding speed, the normal load and the material. Thus for most of the test it appears that the surface temperature remained constant. The steady state surface temperature was estimated by using a fin model (see Appendix). The estimated surface temperatures are plotted in Fig. 5 as a function of the sliding speed for all the materials. As it is not the intent of this work to do a rigorous heat transfer analysis, only approximate surface temperatures are shown. The analysis of the temperature of a sliding system has been carried out by a number of investigators in the past and great differences exist between various theories. Thus it always becomes necessary to resort to the experimental measurement of temperature. In estimating the surface temperature the fact that oxide layers with different heat transport properties from the parent metal are present on the surface was ignored.

Using the temperatures thus calculated, if the friction coefficient and wear rates are replotted as functions of the average surface temperature, the general shape of these curves remains the same as in Figs. 3 and 4 because the temperature is essentially a monotonically increasing function of the sliding speed even though the friction coefficient decreases somewhat. It can be clearly seen from Figs. 4 and 5 that the wear rates are not monotonically increasing function of temperature, as they should be if oxidative or adhesive wear were the dominant modes of wear.

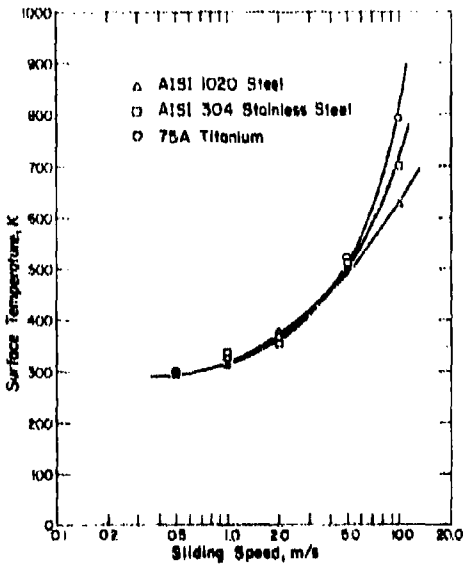

Fig. 5. Average surface temperature as a function of the logarithm of the sliding speed. The surface temperature was calculated by the fin equation.

Metallographic examination of wear tracks and the subsurface of worn specimens was conducted to investigate the mechanism of wear particle formation. Micrographs of the surfaces of worn specimens are shown in Fig. 6. The wear track is much rougher than the initial polished surface and extensive oxidation took place during the test. It can be seen from the above figure that large plastic deformation of the surface took place as a result of sliding. In fact, the material flowed so extensively that a "mushrooming" effect was observed at speeds greater than 1 m s^{-1}.

Scanning electron micrographs of the subsurface, shown in Fig. 7, clearly indicate that large scale subsurface deformation took place as a result of sliding. Large subsurface cracks oriented nearly parallel to the surface indicate that crack nucleation and growth took place, similar to the low speed delamination wear process. As these materials have inclusions of one kind or another, it is expected that crack nucleation can take place readily.

Wear particles were collected during the test to investigate their nature, size and shape. Figure 8 shows that a majority of the particles have metallic luster although some oxidation took place, especially in the case of 1020 steel. The particles are essentially platelike and several hundred micrometers

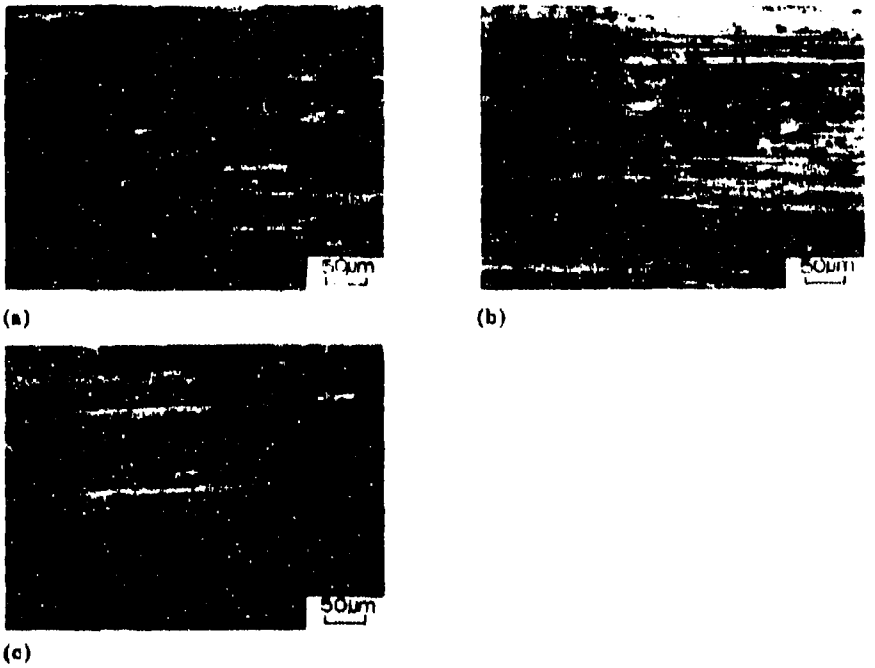

(a) (b)

(c)

Fig. 6. Surfaces of worn specimens: (a) AISI 1020 steel, (b) AISI 304 stainless steel and (c) 75A titanium. The normal force was 49.0 N, sliding speed was 5 m s^{-1} and the duration of the test was 1.8 × 10^3 s. Sliding direction is from right to left.

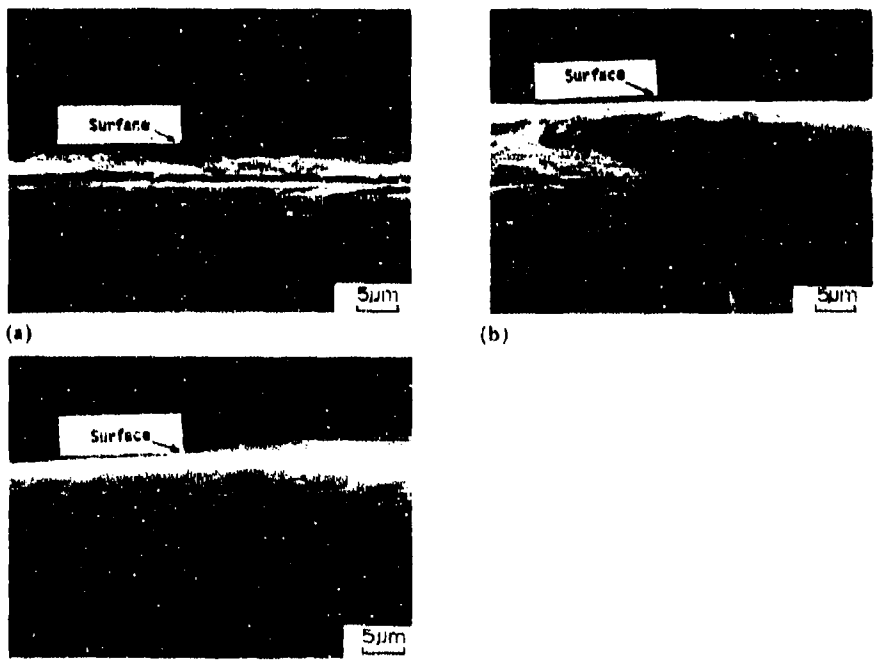

Fig. 7. Scanning electron micrographs of the subsurface: (a) AISI 1020 steel, (b) AISI 304 stainless steel and (c) 75A titanium. Experimental conditions were the same as given in Fig. 6. Sliding direction is from left to right.

in diameter. These wear particles are similar to the particles collected from low speed sliding tests on a variety of steels [10] and copper and copper alloys [11]. It appears that although oxidation and delamination take place simultaneously, particle removal from the surface seems to be by crack nucleation and growth processes.

Discussion

Micrographs of worn surfaces (Fig. 6), scanning electron micrographs of subsurfaces (Fig. 7) and characteristic wear particles shown in Fig. 8 clearly indicate that the mode of wear particle formation at the speed of 5 m s^{-1} was by subsurface deformation, crack nucleation and propagation. The metallic luster of the wear particles indicates that the wear particles were formed by crack growth in the subsurface rather than along the oxide–metal interface. However, it can also be seen from Fig. 8 that some oxidation took place either during the subsurface crack growth or after the wear sheet was formed.

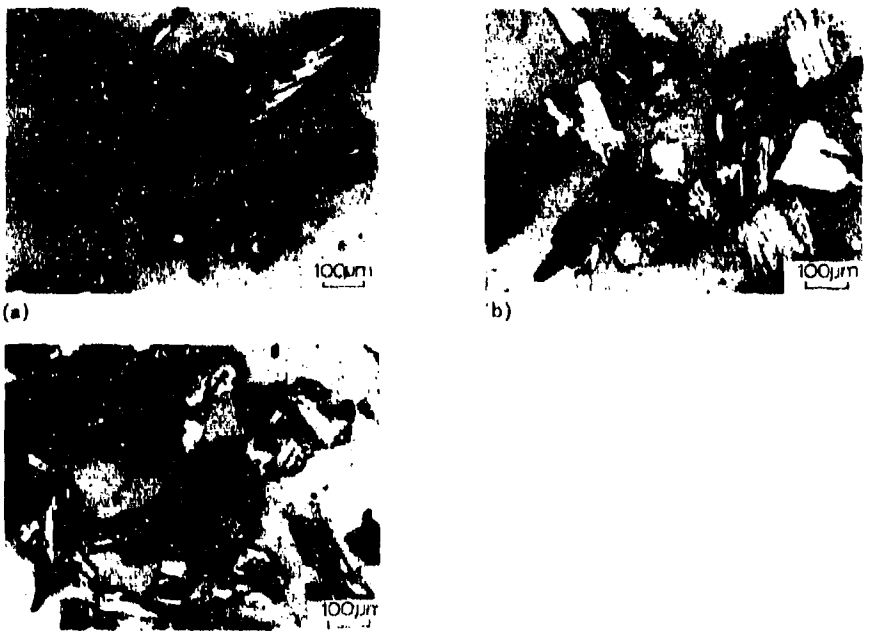

Fig. 8. Wear particles of (a) AISI 1020 steel, (b) AISI 304 stainless steel and (c) 75A titanium. Experimental conditions were the same as given in Fig. 6.

Although the mechanism of delamination seems to be reasonably well established, the complex dependence of the wear rate on the sliding speed needs further explanation. In delamination wear of metals, the overall wear rate is determined by the subsurface deformation, crack nucleation and propagation processes. Generally the slowest of these processes determines the overall wear rate. The material properties that determine the rates of these processes are the friction coefficient, hardness, inclusion density, inclusion matrix bond strength and toughness. The effect of these properties on the overall wear rate has already been discussed in the previous papers. Therefore, only the effect of temperature on these properties and thus on the overall wear rate will be discussed here.

Before a discussion of how the temperature rise due to frictional heating can result in an increased or decreased wear rate, the variation of friction coefficient with sliding speed (or temperature) needs to be considered. The reduction of the friction coefficient as a function of the sliding speed (or temperature) has been explained in the past on the basis of oxide formation [12 - 15]. Above a critical temperature, when the oxidation rate becomes appreciable, a thin layer of oxide spreads on the surface. If the thickness of the oxide film is of the order of 100×10^{-10} m and if the

hardness of the oxide is not greatly different from the metal, it adheres well to the surface below and thus acts as a solid lubricant. While it is recognized that oxidation is responsible for the reduction in the friction coefficient, it is not clear at present what functional relationships exist between the friction coefficient and such operational parameters as speed, load etc. Since the friction coefficient at high sliding speeds (approximately 0.3) is still higher than the value for oxide–oxide contact (approximately 0.1), it appears that metal–metal and oxide–metal contact is taking place. The sharp transition in the friction coefficient around a sliding speed of 1 m s^{-1} is probably because of the extensive oxidation accompanying the temperature rise which was reflected in the response of the thermocouples.

It has been explained in the previous papers that the subsurface deformation accumulates as a result of repeated cyclic loading by the moving asperities of the slider. Although the cyclic deformation characteristics of the materials are not known precisely, it can be assumed to a first approximation (based on a previous finding [16]) that soft metals accumulate more subsurface deformation for a given sliding distance than hard metals, mainly owing to the larger number of asperity contacts. The amount of deformation depends on the normal load, a flow stress parameter such as the hardness, and the friction coefficient. Therefore, more deformation is expected to be accumulated at high temperature than at low temperature because of the loss of hardness. However, the subsurface deformation rate should decrease with the decrease in friction coefficient. Since the hardness of metals decreases almost exponentially with temperature and the friction coefficient does not seem to decrease (see Fig. 3) that rapidly, the deformation rate increase due to the lower hardness should outweigh the decrease due to the lower friction coefficient; the deformation rate should, therefore, increase with temperature. Thus, large wear rates are expected at high temperatures if the subsurface deformation rate is the rate controlling mechanism.

Metals lose hardness as the temperature is raised because of several thermally activated microstructural changes. Allotropic transformations, recovery, recrystallization and grain growth, loss of coherency and dissolution of second phase particles are only a few examples. To identify the exact mechanism it is necessary to study the problem case by case. In the case of single-phase single-component systems, in the absence of phase transformation, loss of hardness is basically due to thermally activated dislocation motion. Although the exact mechanism of softening at high temperatures is not isolated in the materials tested, some speculations can be made. In the 1020 steel, both dispersion of Cottrell atmospheres and dissolution of carbide particles contribute to softening. In the case of the single-phase 304 stainless steel it may be due to extensive cross slip, whereas in the case of titanium operation of secondary slip systems at high temperature together with cross slip can be given as possible reasons.

As discussed earlier, two conditions have to be satisfied for crack nucleation around inclusions: (a) the normal tensile stress across the

interface should be greater than the bond strength of the interface; and (b) the elastic energy released should be greater than or equal to the energy of the new surfaces. In the case of alloys with second phase particles larger than 25 nm in diameter, cracks nucleate at the particle–matrix interface when the stress condition is satisfied, since the energy condition is always satisfied [17, 18]. Additional preferential sites for crack nucleation at high temperature are triple points and grain boundaries, especially when undesirable impurities segregate or preferential precipitation takes place at the grain boundaries. It can be expected that crack nucleation will be difficult at high temperatures for several reasons. First, it is difficult to develop large normal stress at the particle–matrix boundary because of extensive cross slip. Secondly, because of dynamic recovery and even recrystallization at high temperatures the stored elastic energy will be smaller than in room temperature deformation. However, if the strength of a particle–matrix interface decreases with temperature, it may favor crack nucleation.

The analysis of crack nucleation presented previously [19] was for the case when the recovery effects were negligible, *i.e.* for the case when the test temperatures are below about one-half of the absolute melting temperature of the materials. At these temperatures deformation takes place predominantly by dislocation glide and is homogeneous. However, at high temperatures other modes of deformation such as grain boundary sliding and diffusion creep become important (and may even be dominant); the crack nucleation problem should then take into consideration these modes of deformation along with the glide mode. Further, the stress criterion given previously may not even be applicable at high temperature; instead a critical strain criterion seems more reasonable. Nevertheless, the stress and energy criteria seem to be applicable for the conditions used in this investigation because the temperatures are not very high.

Once the cracks are nucleated, they grow by the repeated loading imposed on the crack tip by the moving asperities. In the linear elastic fracture mechanics approach adopted in a previous paper [20] it was assumed that crack growth rate can be expressed as a power function of the stress intensity factor. When that assumption is valid, the wear rate of hard materials should be higher than that of soft materials if the wear is controlled by crack growth rates. If the same assumption is valid for high speed (or temperature) sliding, the wear rate should be lower at high sliding speeds than at low sliding speeds because the hardness at high speeds (or temperature) will be lower. This does not seem to be the case for speeds less than 5 m s^{-1}, as can be seen from Fig. 4. This implies first that the crack growth rate does not control wear and/or that the linear elastic fracture mechanics analysis of high speed sliding crack growth rates is not valid. It appears that both of these are possibilities.

It appears, therefore, that the overall wear rate is a complicated function of the friction coefficient, the hardness, the bond strength of the particle–matrix interface, the crack growth rates etc. It is difficult at present

to predict the effect of all these parameters on the wear rate. However, several qualitative conclusions can be drawn from Figs. 3 and 4. It appears that type 304 stainless steel exhibits an increasing wear rate as a function of the sliding speed throughout the test range because of a reduction in hardness. Further, the reduction in friction coefficient does not appear to compensate for the decrease in hardness. Similar argument also can be given for the 1020 steel and for the titanium for speeds between 1 and 5 m s^{-1}. The decrease in wear beyond a speed of 5 m s^{-1} may be due to an increase in toughness. The reason for such an increase may be due to the dissolution of carbides. Similarly, in the case of titanium it is conceivable that at high temperatures secondary slip systems operate making the material more ductile. The increase in the wear rate below 1 m s^{-1} can be explained on the basis of the conventional oxidation and abrasion processes. The surfaces of the 1020 specimen and the slider were found to be covered with red iron oxide. Thus, it appears that the oxide particles acted as abrasives although the oxide particle formation need not be by the oxidative wear mechanism.

Many other factors, probably less important, have been neglected in the above discussion. For example, large thermal stresses could be induced in the specimen because of the large temperature gradients. In the polyphase alloys large thermal stresses can be induced even in the absence of a temperature gradient because of different thermal properties of different phases. In the case of polycrystalline h.c.p. metals, which are generally anisotropic with respect to thermal expansion coefficients, thermal stresses can be induced because of different expansions in adjacent grains. Also strain rate effects are neglected in the discussion. However, it is well known that at high strain rates even ductile metals behave like brittle solids. In any case these factors may affect the subsurface deformation, crack nucleation and growth processes somewhat but they will not change the mechanism of wear itself. Despite these limitations, microscope examination of wear tracks, of the subsurface and of wear particles clearly indicates that the mode of wear was by delamination. Adhesion and oxidative theories of wear seem to be incompatible with observations. A quantitative description of wear behavior awaits developments in the mechanical aspects of cyclic deformation, crack nucleation and growth processes at high temperatures.

Conclusions

As a result of the present study on the high speed sliding wear of metals under unlubricated conditions in air, the following conclusions can be drawn.

(1) The friction coefficient for AISI 1020 steel is always higher than that of AISI 304 stainless steel and that of commercial titanium. The friction coefficient is only weakly affected by the normal load and decreases with increasing speed; the reduction for 1020 steel is the largest.

(2) The wear rate of stainless steel increases monotonically with the speed, whereas it goes through a maximum in the neighborhood of 5 m s^{-1}

for both 1020 steel and titanium. The drop in wear rate occurs because of both a low friction coefficient and an increased resistance of the material to crack nucleation and propagation, as a result of temperature rise.

(3) Metallographic examination of the wear tracks, the subsurface of worn specimens and the morphology of wear particles (collected during the test) indicates that the mechanism of wear was subsurface deformation, crack nucleation and propagation, *i.e.* the delamination mechanism.

(4) Oxidative, adhesion and abrasive wear are not the dominant modes of wear under the conditions observed although they may operate simultaneously with the delamination wear.

Acknowledgments

This work was supported by the Defense Advanced Research Projects Agency through the Office of Naval Research under Contract No. N0014-67-A-0204-0080, NR229-011. The authors are grateful to Drs. Arden L. Bement, Edward van Reuth and Richard S. Miller for their support and guidance.

References

1 J. K. Lancaster, The influence of temperature on metallic wear, Proc. Phys. Soc., London, Sect. B, 70 (1957) 112 - 118.
2 J. F. Archard, Contact and rubbing of flat surfaces, J. Appl. Phys., 24 (1953) 981 - 988.
3 T. F. J. Quinn, Role of oxidation in the mild wear of steel, Br. J. Appl. Phys., 13 (1962) 33 - 37.
4 T. F. J. Quinn, Oxidational wear, Wear, 18 (1971) 413 - 419.
5 F. F. Tao, A study of oxidation phenomena in corrosive wear, ASLE Trans., 12 (1969) 97 - 105.
6 N. Tenwick and S. W. E. Earls, A simplified theory for the oxidative wear of steels, Wear, 18 (1971) 381 - 391.
7 E. Rabinowicz, Friction and Wear of Materials, Wiley-Interscience, New York, 1965.
8 S. W. E. Earls and M. G. Hayler, Wear characteristics of some metals in relation to surface temperature, Wear, 20 (1972) 51 - 57.
9 W. Hirst and J. K. Lancaster, The influence of speed on metallic wear, Proc. R. Soc. London, Ser. A, 259 (1960 - 1961) 228 - 241.
10 S. Jahanmir, N. P. Suh and E. P. Abrahamson, II, Microscopic observations of the wear sheet formation by delamination, Wear, 28 (1974) 235 - 249.
11 N. Saka, J. J. Pamies-Teixeira and N. P. Suh, Wear of two-phase metals, Wear, 44 (1977) 77 - 86.
12 R. L. Johnson, M. A. Swikert and E. E. Bisson, Effects of sliding velocity and temperature on wear and friction of several materials, Lubr. Eng., May/June (1955) 164 - 170.
13 M. Cocks, Role of atmospheric oxidation in high speed sliding phenomena, J. Appl. Phys., 28 (5) (1957) 835 - 843.
14 M. B. Peterson, J. J. Florek and R. E. Lee, Sliding characteristics of metals at high temperatures, ASLE Trans., 3 (1960) 101 - 115.

15 E. Rabinowicz, Lubrication of metal surfaces by oxide films, ASLE Trans., 10 (1967) 400 - 407.
16 S. Jahanmir, N. P. Suh and E. P. Abrahamson, II, The delamination theory of wear and the wear of a composite metal surface, Wear, 32 (1975) 33 - 49.
17 K. Tanaka, T. Mori and T. Nakamura, Cavity formation at the interface of a spherical inclusion in a plastically deformed matrix, Philos. Mag., 21 (1970) 267 - 279.
18 A. S. Argon, Formation of cavities from non-deformable second-phase particles in low temperature ductile fracture, J. Eng. Mater. Technol., 98 (1) (1976) 60 - 68.
19 S. Jahanmir and N. P. Suh, Mechanics of subsurface void nucleation in delamination wear, Wear, 44 (1977) 17 - 38.
20 J. R. Fleming and N. P. Suh, Mechanics of crack propagation in delamination wear, Wear, 44 (1977) 39 - 56.

Appendix

Several theories have been proposed in the past to account for the temperature rise at sliding contacts. Unfortunately, the theories cannot be made use of in practical situations because the assumptions made in those theories are not fully valid. Theoretically calculated values may be several hundred per cent off from the measured values. Thus, frequently it is necessary to resort to experimental measurement of the temperature.

A variety of experimental techniques are available for the measurement of the temperature of sliding contacts. Measurement of the thermoelectric e.m.f. produced by the sliding pair, infrared techniques, physical and chemical changes associated with the temperature rise and the thermocouple technique are some of these. Because of its simplicity, the last technique is used in this work although there are some limitations. In this technique temperature is measured away from the surface and the surface temperature is estimated by either graphical extrapolation or by numerical evaluation using heat conduction equations. Graphical extrapolation generally underestimates the surface temperature because the temperature gradient near the surface is much steeper than in the interior. Thus, numerical methods are generally preferred.

Figure A1 shows the schematic arrangement of the slider, the specimen and the thermocouples. As a result of frictional work, heat is generated at the interface and flows into the specimen and the slider; the amount is dependent on the geometry and on the thermal, mechanical and tribological properties of both the specimen and the slider. A steady state is achieved if the heat flowing into the specimen is transmitted away by convection. Steady state temperatures measured at different locations along the heat flow direction can be used to calculate the steady state average surface temperature.

For the arrangement shown in Fig. A1, the specimen can be regarded as a fin and the heat flow as essentially one dimensional (within the specimen). This is a simplification of the more elaborate two-dimensional problem treated previously [A1]. The steady state solution to this problem is given as [A2]

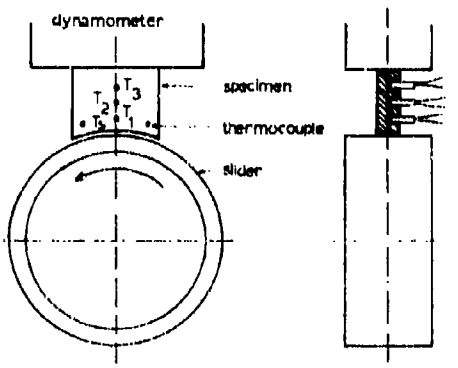

Fig. A1. Schematic arrangement of the slider, the specimen and the thermocouples.

$$\frac{T - T_a}{T_s - T_a} = \frac{\cosh (hC/kA)^{1/2}(l - \chi)}{\cosh (hC/kA)^{1/2} l} \tag{A1}$$

where T is the temperature at a distance χ from the surface, T_a is the ambient temperature, T_s the average interface temperature, h the heat transfer coefficient, C the circumference of the fin, A the cross-sectional area of the fin, k the thermal conductivity of the fin and l the length of the fin.

Generally, it is difficult to estimate the heat transfer coefficient on which the solution is dependent. Also, the length of the fin is not necessarily the length of the specimen because grips, a dynamometer etc. are attached to the specimen. Therefore, instead of calculating the surface temperature directly from eqn. (A1), it is necessary to evaluate it from experimentally measured temperatures along the direction of heat flow (perpendicular to the sliding surface) at different locations. Thus, if T_s, T_1, T_2 and T_3 are the temperatures at the surface and at distances χ_1, χ_2 and χ_3, respectively, then from eqn. (A1)

$$\begin{aligned} \frac{T_1 - T_a}{T_s - T_a} &= \frac{\cosh m(l - \chi_1)}{\cosh ml} \\ \frac{T_2 - T_a}{T_s - T_a} &= \frac{\cosh m(l - \chi_2)}{\cosh ml} \\ \frac{T_3 - T_a}{T_s - T_a} &= \frac{\cosh m(l - \chi_3)}{\cosh ml} \end{aligned} \tag{A2}$$

where $m = (hC/kA)^{1/2}$. From eqn. (A2)

$$\alpha = \frac{T_1 - T_a}{T_2 - T_a} = \frac{\cosh m(l - \chi_1)}{\cosh m(l - \chi_2)} \tag{A3}$$

$$\beta \equiv \frac{T_1 - T_a}{T_3 - T_a} = \frac{\cosh m(l - \chi_1)}{\cosh m(l - \chi_3)} \tag{A4}$$

Using the identity

$$\cosh t \equiv 1 + \frac{t^2}{2!} + \frac{t^4}{4!} + \ldots$$

and considering up to the second order terms only, then

$$\alpha (l - \chi_2)^2 - (l - \chi_1)^2 = \frac{2}{m^2}(1 - \alpha) \tag{A5}$$

$$\beta (l - \chi_3)^2 - (l - \chi_1)^2 = \frac{2}{m^2}(1 - \beta) \tag{A6}$$

Solving for l, m and T_s

$$l \approx \frac{1}{2} \frac{\chi_1^2(\beta - \alpha) - \chi_2^2\alpha(\beta - 1) + \chi_3^2\beta(\alpha - 1)}{\chi_1(\beta - \alpha) - \chi_2\alpha(\beta - 1) + \chi_3\beta(\alpha - 1)} \tag{A7}$$

$$m \approx \left(\frac{2(\beta - \alpha)}{\alpha(l - \chi_2)^2 - \beta(l - \chi_3)^2} \right)^{1/2} \tag{A8}$$

and

$$T_s \approx T_a + \frac{(T_1 - T_a) \cosh ml}{\cosh m(l - \chi_1)} \tag{A9}$$

Equation (A9) has been used in the present work to calculate the surface temperature making use of the experimentally measured temperatures T_1, T_2 and T_3 at 3, 6 and 9 mm, respectively, from the surface.

The temperatures shown in Fig. 5 should be considered as approximate average temperatures. The flash temperatures could be very high and the present technique does not allow an estimation of those values. In fact, sparks have been observed at speeds above 5 m s^{-1} during the test. Further, the temperatures along the sliding surface at distances of 3 mm from the surface at three different locations were found to differ by as much as 15%. This indicates that the heat generation rate is not the same along the surface. In the calculation of surface temperature average values of T_1 are used. However, as the agreement with the results of other investigation on similar materials, loads and speeds [A1] is reasonably good, the present method seems to be satisfactory.

References to the Appendix

A1 F. F. Ling and T. E. Simkins, Measurement of pointwise juncture condition of temperature at the interface of two bodies in sliding contact, J. Basic Eng., 85 (1963) 481 - 487.

A2 W. M. Rohsenow and H. V. Choi, Heat, Mass, and Momentum Transfer, Prentice-Hall, Englewood Cliffs, N. J., 1961, p. 106.

Wear, 44 (1977) 127 - 134

IMPLICATIONS OF THE DELAMINATION THEORY ON WEAR MINIMIZATION

NAM P. SUH, N. SAKA and S. JAHANMIR*

Massachusetts Institute of Technology, Cambridge, Mass. 02139 (U.S.A.)

(Received February 1, 1977)

Summary

Various implications of the delamination theory on wear minimization are discussed by considering various means of reducing surface tractions, microstructural changes which retard the processes necessary for wear, and precautions required in machining. Surface coating techniques are also briefly discussed.

Introduction

The Webster's New Collegiate Dictionary defines theory as "a plausible or scientifically acceptable general principle or body of principles offered to explain phenomena...". A corollary of this definition is that a theory, if it is valid, should provide insights into how problems associated with the given phenomenon can be solved. The purpose of this paper is to discuss several implications of the delamination theory of wear with regard to wear minimization.

Normally wear is prevented or minimized by using hydrodynamic or boundary lubricants, and these are by far the best means of minimizing wear if such lubrication is possible. However, there are situations where the operating conditions do not permit the use of any lubricants. Also, contingency measures for wear prevention are necessary when lubricants are depleted from critical parts (*e.g.* in the transmission casing of helicopters). In such situations, the basic wear properties of the solid materials and any modification o the surface properties that improve wear characteristics become important factors.

In the past, the wear properties of metals have been characterized in a rather cursory manner by only specifying the chemistry and the hardness of

*Present address: Mechanical Engineering Department, University of California, Berkeley, Calif. 94720, U.S.A.

metals but neglecting microstructural variables and ductility. The results presented in the preceding papers [1 - 8] clearly show that this past practice is not only less than rigorous but can lead to serious difficulties, since the wear rates of, for example, AISI 1045 steel can vary a great deal depending on its microstructure and the volume fraction of inclusions. One of the MIT group's research objectives is to establish meaningful characterization parameters which can be used by design engineers in the specification of materials for wear applications.

The microstucture of a material can be rigorously quantified in terms of the geometrical aspects of its structure: point, line, planar and volume elements. Such a characterization is made on the assumption that, no matter how a given microstructure is produced, it possesses the same properties and that it is possible to predict the properties of the aggregate from the properties of the constituents. In this paper, a simpler characterization of metals has been adopted. Here, metals are characterized as pure metals, solid solutions, two-phase alloys or composites.

Surface traction

It has been clearly pointed out in preceding papers that the wear rate is very significantly affected by the magnitude of the normal and the tangential loads. Since the normal load is controlled by the external conditions and basic nature of the materials, the only option is to control the magnitude of the tangential load. The most obvious way of reducing the wear rate is to lubricate the interface. However, only other methods of reducing wear will be discussed in this paper, since lubrication by conventional means is outside the scope of this paper.

It was shown [4] that the coefficient of friction is affected by adhesion and plowing. The plowing component of the frictional force decreases as the hardness is increased by such techniques as solid solution hardening, which in turn decreases the wear rate significantly. Therefore, it is highly desirable to make the surface as hard as possible without introducing crack nucleation sites. The low coefficient of friction exhibited by such hard materials as group IV B and group V B carbides attests to this conclusion.

The adhesional component of the frictional force has a similar effect on the wear rate. An identical or similar pair of metals has a greater tendency for adhesion than those which differ to the extent of not forming solid solutions [9]. Rabinowicz has investigated this problem extensively and has produced a compatibility chart for various combinations of pure elements, as shown in Fig. 1. It is clear that the best combination for low friction and low wear applications is two hard single-phase materials which are not chemically compatible (*i.e.* those shown by solid circles in Fig. 1).

The crystal structure of metals has a significant influence on the wear rate. Since the crystallographic orientation of metals near the surface changes so that the slip planes line up parallel to the surface, the frictional force is

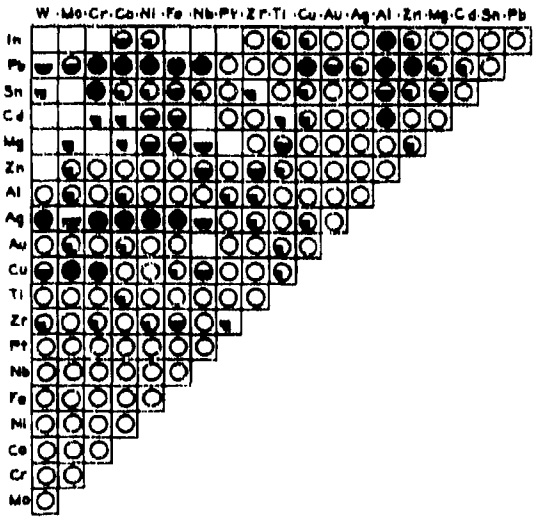

Fig. 1. Rabinowicz's compatibility chart for various metal combinations derived from binary diagrams of the respective elements (from ref. 9) in terms of preferred anti-friction surfaces: ● two liquid phases, solid solution less than 0.1% solubility (lowest adhesion); ◉ two liquid phases, solid solution greater than 0.1%, or one liquid phase, solid solution less than 0.1% solubility (next lowest adhesion); ◎ one liquid phase, solid solution between 0.1% and 1% solubility (higher adhesion); ○ one liquid phase, solid solution over 1% (higher adhesion). Blank boxes indicate insufficient information.

lowered by the easier slip (especially in the absence of plowing). Hexagonal close packed (h.c.p.) metals with their c/a ratios greater than the ideal 1.633 are generally recognized as metals with easy slip. However, even metals such as cobalt which has a c/a ratio of 1.626 can be modified through the formation of solid solutions to give good slip properties. One technique of making use of the slip properties of such h.c.p. metals is to disperse a small volume fraction of hard particles such as WC in an h.c.p. matrix such as cobalt (note that WC and Co form a solid solution). In such a system, the normal load is carried by the hard particles and the matrix provides low friction properties. Although the frictional force can be very small when sliding against such a surface, this type of surface is only good when the applied normal load is relatively low, as in instruments. Such a coating has been made by plasma spraying.

Microstructural considerations

As discussed earlier [1], the processes that lead to wear of metals are subsurface deformation, crack nucleation and crack propagation. It is clear

that wear of materials can be minimized by slowing down or suppressing these processes. Lowering the friction coefficient and raising the hardness of materials reduces the subsurface deformation and hence the crack nucleation rate. Raising the toughness decreases the crack growth rates. Therefore, for effective wear control all that is necessary is to design the microstructure of materials to reduce the friction coefficient and to raise the hardness and toughness of materials. Unfortunately, it is not possible to achieve both high hardness and toughness with a single microstructure. Normally, any manipulation of the microstructure to raise the hardness reduces the toughness of materials and therefore a careful optimization is necessary. The design of the microstructure of wear resistant materials is an exercise in such an optimization process.

The flow strength of materials should be made as high as possible without introducing any undesirable effects such as internal crack nucleation sites. It has already been noted that the coefficient of friction and the wear rates are decreased if at least one member of the sliding pair is a solid solution [4]. The improved wear resistance is due to the lowered frictional force and the decreased surface layer deformation rate, and the consequent lower rate of crack nucleation. Nitriding and carburizing of steel is certainly a desirable thing to do in this sense. However, one of the problems encountered in making solid solutions is the segregation of solutes, forming a weak two-phase material. Graphite formation in steel and the segregation of nickel in brass may be only two of many examples of solute segregation.

In many metals hardening is often accomplished by the generation or introduction of second phases, since solid solution hardening may not give an adequate increase in hardness. As soon as large second-phase particles are introduced, crack nucleation occurs quite readily and the crack propagation rate tends to become the wear rate determining process [2]. One interesting investigation would be to make two-phase materials in which the second phase is so small (according to Argon *et al.*, less than 200 Å [10]) that it only contributes to the hardness without providing crack nucleation sites. Another possibility is to increase the volume fraction of hard particles to a point where the matrix metal constitutes only a small fraction of the volume, *e.g.* cutting tools made of tungsten carbide bonded with cobalt.

One interesting means of minimizing wear is through the creation of a fiber reinforced composite with preferentially oriented fibers. It seems reasonable to speculate that if fibers are placed with their axes perpendicular to the surface, cracks parallel to the surface will not be able to propagate, since the crack tip opening displacement (and therefore the stress concentration at the crack tip) will be prevented by the stiffness of the fibers. Such an idea was tried by undergraduate students at MIT using a uniaxially oriented Kevlar organic fiber–epoxy composite [11]. Their results are shown in Fig. 2. The specimens with fibers normal to the surface had the highest coefficient of friction and yet had the lowest wear rate, whereas the reverse was true for the specimens with fibers parallel to the surface. The exact wear mechanisms of these composites are being investigated at MIT.

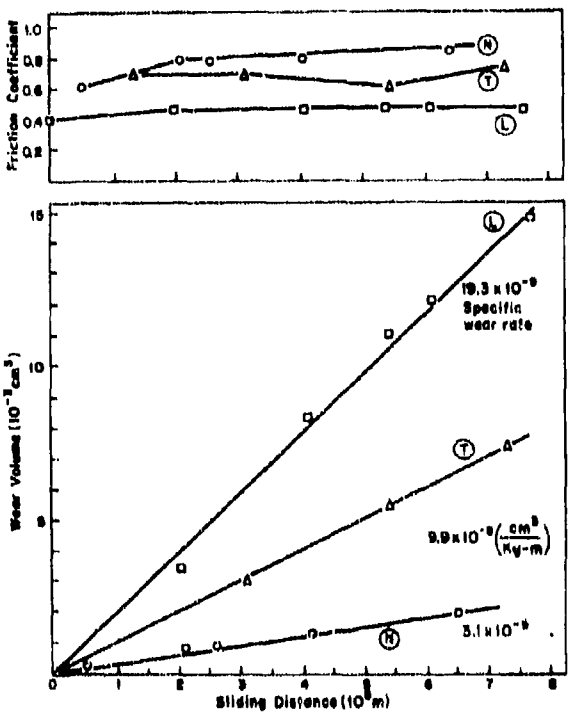

Fig. 2. Friction coefficient and wear rate of Kevlar fiber reinforced epoxy composites under a load of 1 kg and a sliding speed of 2.54 m s $^{-1}$. L and T denote the specimens with fibers oriented parallel and transverse to the sliding direction, lying in the plane of the surface; N denotes specimens with fibers oriented perpendicular to the surface (from ref. 11). The specific wear rates (cm^3 kg $^{-1}$ m $^{-1}$) were: —○— 19.3 × 10 $^{-9}$; —△— 9.9 × 10 $^{-9}$; —○— 3.1 × 10 $^{-9}$.

Coating techniques

Soft coatings

As discussed earlier in relation to the effect of surface traction on wear, it is desirable to use liquid and solid lubricants to lower the coefficient of friction. Since solid lubricant technology is outside the scope of this paper, only the implications of the delamination theory on thin soft metal layers will be discussed.

Notwithstanding the controversy concerning the dynamics of dislocations near a surface, the results obtained to date prove conclusively that a thin metal layer bonded to a hard substrate can reduce the wear rate by several orders of magnitude [12]. The critical nature of the thickness of the plate was brought out by the delamination theory [1, 12]. In general, the thickness of the soft layer must be of the order of 0.1 μm. Recent experi-

ments at MIT indicate that such a coating is effective even at high speeds and prevents seizure even in situations where seizure would occur immediately upon contact in the absence of a coating. Further research must be done on techniques to attach a well-bonded layer to various surfaces.

Hard coatings

Another way of increasing the wear resistance is to put a very hard layer on a substrate such that plastic deformation cannot take place in the substrate and in the coating. Since a plastic deformation zone has not been observed deeper than 200 μm, the thickness of the hard layer should be of this order of magnitude, although in many situations it may be much less than this value. The coating must be coherent and free of microcracks since crack propagation is possible even in the absence of plastic deformation if there are pre-existing cracks.

Good candidates for coating materials are such hard ceramics as Al_2O_3, WC, TiC and HfC. They can be applied using chemical vapor deposition (CVD) techniques or physical vapor deposition techniques. The choice of the coating technique will depend on the nature of the substrate and on the physical and chemical properties of the materials involved. There are a number of excellent references on coating techniques and their applications [13, 14].

Another interesting possibility is the generation of a surface consisting of a supersaturated solid solution using a rapid heating and cooling technique such as laser heating. Whether or not such a material will undergo a rapid precipitation when strained is not known at this time.

One of the main advantages of hard coatings over soft coatings is the abrasive wear resistance of hard coatings. In any sliding situation where abrasive wear is possible soft coatings cannot be used since they can easily be removed by abrasive wear. A major disadvantage of hard coatings in a non-abrasive environment is that if any large wear particle is generated from the coating material it can act as an abrasive particle and can damage the soft surfaces of other sliding components. This problem becomes more critical as the coating–substrate bond strength decreases.

Coating formed during sliding

The formation of a soft or a hard layer on a substrate through a chemical reaction between certain components in the lubricant and the substrate should be investigated by considering whether or not it lowers the coefficient of friction. The effect of these layers may be not only the minimization of metal-to-metal adhesion but also the reduction of the tangential component of load which in turn affect the wear behavior. A coherent and stable oxide layer which lowers the coefficient of friction can have similar beneficial results. In contrast, if these layers get removed at a faster rate than the delamination rate by the sliding action, the wear rate will be accelerated.

Surface quality

Since the initial wear rate depends so sensitively on the surface topography and the surface integrity (which define the surface quality), the effect of machining and other preparation techniques on surface quality is an important consideration in tribological applications. Even steady state wear can be affected by the initial wear rate if the initial wear particles are either entrapped or return to the sliding interface.

When the final surface is generated by machining, the tool should be sharp if a damage-free surface is to be generated. However, if the machined surface is to be lapped or run in, the surface preparation technique is not particularly critical. The surface roughness obtained through machining is not a good indication of its "wearability" since this depends on particular loading applications [6].

The effect of the surface waviness in a stiff sliding system (*i.e.* a geometrically constrained system) on wear was discussed elsewhere [15]. Since the tangential component of the surface traction can increase to a large value when there is a long range variation of the surface profile (*i.e.* waviness), the wear rate can be increased significantly owing to the waviness. However, at this time surface waviness is not specified as part of manufacturing guidelines.

Conclusions

The delamination theory provides guidelines for wear minimization through control of the metallurgical structures and chemistry of sliding surfaces, modification of the surface, and machining practices. The theory may also be used in creating composite structures for minimum wear. It is clear that the wear characteristics of metals with the same chemical composition can be substantially different depending on their microstructures and therefore a material for wear applications is not well defined until the wear characteristics have been specified in addition to the current specifications.

References

1 N. P. Suh, An overview of the delamination theory of wear, Wear, 44 (1977) 1 - 16.
2 S. Jahanmir and N. P. Suh, Mechanics of subsurface void nucleation in delamination wear, Wear, 44 (1977) 17 - 38.
3 J. R. Fleming and N. P. Suh, Mechanics of crack propagation in delamination wear, Wear, 44 (1977) 39 - 56.
4 J. J. Pamies-Teixeira, N. Saka and N. P. Suh, Wear of copper-based solid solutions, Wear, 44 (1977) 65 - 75.
5 N. Saka, J. J. Pamies-Teixeira and N. P. Suh, Wear of two-phase metals, Wear, 44 (1977) 77 - 86.
6 S. Jahanmir and N. P. Suh, Surface topography and integrity effects on sliding wear, Wear, 44 (1977) 87 - 99.

7 T. Nagao, J. J. Pamies-Teixeira and N. P. Suh, Behavior of medium carbon steel under combined fatigue and wear, Wear, 44 (1977) 101 - 108.
8 N. Saka, A. M. Eleiche and N. P. Suh, Wear of metals at high sliding speeds, Wear, 44 (1977) 109 - 125.
9 E. Rabinowicz, ASLE Trans., 14 (1971) 198 - 205.
10 A. S. Argon, J. Im and R. Safoglu, Metall. Trans., 6A (1975) 825 - 837.
11 P. Patt, R. Maresca and K. Launie, The effect of fiber orientation on friction and wear of Kevlar/epoxy composites, 2.30 Rep., Massachusetts Institute of Technology, December 1976.
12 S. Jahanmir, E. P. Abrahamson, II, and N. P. Suh, Wear, 40 (1976) 75 - 84.
13 R. W. Berry, P. M. Hall and M. T. Harris, Thin Film Technology, Van Nostrand Reinhold, New York, 1968.
14 N. P. Suh, Coated carbides, past, present and future — a keynote paper. In Advances in Hard Material Tool Technology, Carnegie Press, Pittsburgh, Pa., 1976.
15 N. P. Suh and T. Nagao, Implications of wear theories on surface quality and functional requirement, CIRP Ann. Int. Inst. Prod. Eng. Res., 25 (2) (1976) 513 - 519.

Wear, 44 (1977) 135 - 143

THE STACKING FAULT ENERGY AND DELAMINATION WEAR OF SINGLE-PHASE F.C.C. METALS

N. P. SUH and N. SAKA

Department of Mechanical Engineering, Massachusetts Institute of Technology, Cambridge, Mass. 02139 (U.S.A.)

(Received May 18, 1977)

Summary

The role of the stacking fault energy (SFE) in the delamination wear of single-phase f.c.c. metals is discussed, based on the data obtained with four different copper-based solid solutions and with aluminum, nickel and AISI 304 stainless steel. Since crystal plasticity (and thus the SFE) affects all aspects of delamination wear (*i.e.* surface traction, plastic strain accumulation, crack nucleation and crack propagation) and since the interactions between them are complex, there is no simple general relationship between the SFE and the wear rate.

Introduction

In the preceding papers [1 - 8] it was shown that the wear of metals with inclusions and hard second-phase particles is largely controlled by the crack propagation rate since cracks can nucleate readily. It was shown that crack nucleation in these metals is controlled by the location of the hard particles, the hardness of the matrix and the surface traction. For single-phase metals, however, this model for crack nucleation does not apply, although it is expected that the crack propagation phenomenon is the same for both single- and multi-phase metals. Since cracks may not nucleate readily in single-phase metals, it is still not certain whether crack nucleation or crack propagation controls the wear rate.

Suh [9] speculated on various plausible mechanisms for crack nucleation in single-phase metals, including crack nucleation at the walls of dislocation cells. However, no definitive work has been done to date. The difficulty is that changes in physical properties introduced by metallurgical means affect all aspects of delamination wear and therefore the role of each cannot be easily isolated. The purpose of this paper is to shed some light on these unresolved questions by considering the wear process in terms of stacking fault energy (SFE), especially in view of the recent publications by Hirth and Rigney [10] and Rigney and Glaeser [11].

It is well established that SFE affects such mechanical properties of metals as flow stress, work hardening behavior, crack nucleation and crack propagation through its effect on dislocation mobility and interactions. Owing to ease of cross-slip [12], the f.c.c. metals with high SFE readily form dislocation cells when plastically deformed. When the SFE is low, the deformation of f.c.c. metals tends to be more planar. Also, the crack propagation rate increases with the SFE [13], and consequently low cycle fatigue life is improved with a decrease in the SFE [12]. In view of these observations, Hirth and Rigney's argument that the walls of dislocation cells may act as crack nucleation sites and as the path for crack propagation is certainly plausible [10]. However, the role of the SFE in delamination wear cannot be assessed similarly through a simple extrapolation of the bulk behavior since the SFE also affects hardness, which in turn controls crack nucleation and propagation rates through its effect on surface traction and the resulting stress field [2, 3]. The results presented in this paper illustrate this complex interaction.

Experimental

A variety of single-phase f.c.c. metals and alloys with different hardnesses, SFEs and friction coefficients (when slid against an AISI 52100 steel slider) were chosen for study. Copper–zinc solid solutions with up to 30 wt.% zinc were added to the list of Cu–Cr, Cu–Si and Cu–Sn solid solutions studied earlier [6]. Commercially pure nickel and 1100 aluminum were chosen because their SFEs are the highest among f.c.c. metals. AISI 304 stainless steel was also chosen because its hardness is comparable with that of nickel but it has a low SFE of 20 erg cm^{-2}, like the majority of copper alloys.

Commercially pure 1100 aluminum in the form of 12.7 cm diameter rods was swaged down to 0.635 cm diameter at room temperature without any intermittent annealing. The swaged rods were then annealed in air at 300 °C for 1 h. Commercially pure nickel, which was obtained as cold-drawn rod of 0.635 cm diameter, was annealed in vacuum-sealed Vycor capsules at 800 °C for 1 h. Metallographic examination did not show any observable precipitates at 1000 ×. The AISI 304 stainless steel was tested as received. All specimens in the form of 0.635 cm diameter and 7.5 cm long rods were polished on abrasive papers of various grits and diamond lapping compound. The final polishing was done with 0.25 μm diamond lapping compound. The AISI 52100 steel slider (0.635 cm diameter) was polished similarly.

All the tests were carried out with a cylinder-on-cylinder geometry at a sliding speed of 2 m min^{-1} and a normal load of 2 kg in a dry deoxygenated argon atmosphere. The normal load and the friction coefficient were continuously monitored by a dynamometer–Sanborn recorder assembly. Except in the case of 1100 aluminum, the duration of each test was 100 min. The test duration for aluminum was 20 min because the wear rate was very high and the geometry of the wear track changed substantially after 20 min. The

specimens were weighed before and after the wear test to an accuracy of 0.01 mg and the difference was recorded as weight loss due to wear. Other details are the same as those given in an earlier paper on copper-based solid solutions [6].

Results and discussion

Figure 1 shows the wear rates of copper-based solid solutions, aluminum, nickel and AISI 304 stainless steel as a function of hardness. Table 1 also lists other physical properties of aluminum, nickel and AISI 304 stainless steel.

The experimental results with copper-based solid solutions show that except in the case of Cu–Zn alloys the wear rate decreases with increase in hardness. This is consistent with the fact that the increase in hardness decreases both incremental plastic deformation and surface traction (Fig. 2). These results are discussed in detail in a preceding paper [5].

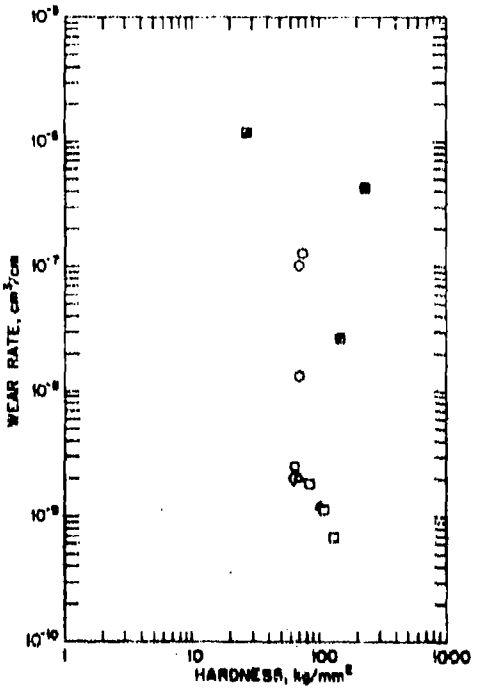

Fig. 1. The wear rate *vs.* the hardness for all the experimental materials: ○ OFHC copper, △ Cu–Si, □ Cu–Sn, ○ Cu–Zn, ◇ Cu–Cr, ■ AISI 304 stainless steel, ■ 1100 aluminum, ■ Ni; normal load 2 kg; sliding speed 2 m min^{-1}.

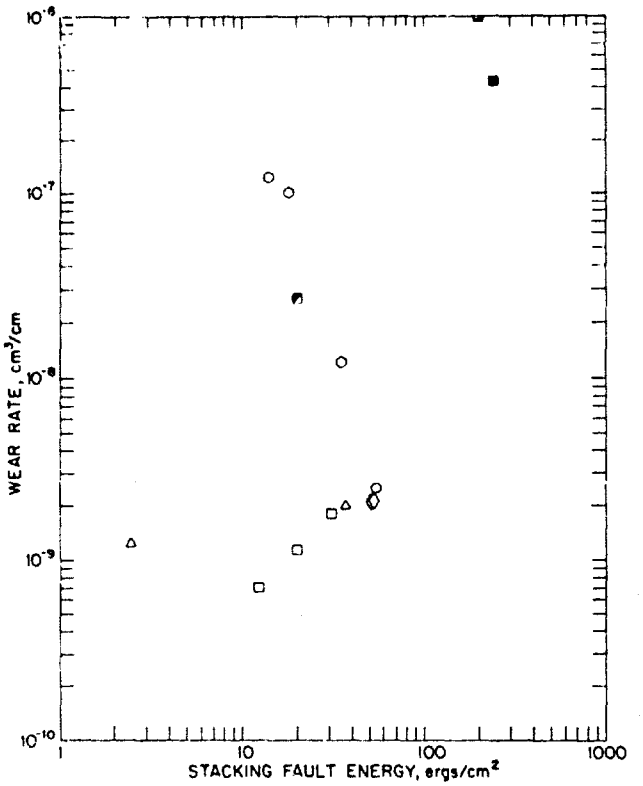

Fig. 3. The wear rate as a function of the SFE: ○ OFHC copper, △ Cu–Si, □ Cu–Sn, ○ Cu–Zn, ◇ Cu–Cr, ◩ AISI 304 stainless steel, ◪ 1100 aluminum, ■ Ni.

rates has been explained earlier in terms of hardness and surface traction. The plot also shows that most of the copper-based alloys (except the Cu–Zn alloys) have low wear rates and low SFE. However, the results of Cu–Zn alloys and stainless steel show that low SFE metals do not necessarily have low wear rates.

In order to clarify the observed wear phenomenon, the wear rates of copper and Cu–Si alloys will be used to illustrate how various factors of delamination wear affect the wear behavior. The wear rates of Cu and Cu–Si alloys are about the same, although the SFEs of these metals differ by an order of magnitude. This fact is unexpected since Ishii and Weertman [13] showed, using Cu–Al alloys, that the crack propagation rate of copper solid solutions decreases with increase in solute content and with decrease in the SFE (Fig. 5). Therefore one would expect that OFHC copper would wear much faster than Cu–Si alloys. This difference in the wear rate, however, can also be explained by considering the differences in hardness and coefficient of friction. Copper is softer than Cu–8.6 at.% Si by about 36%, while the coefficient of friction of copper is 0.98 and that of the copper–silicon alloy

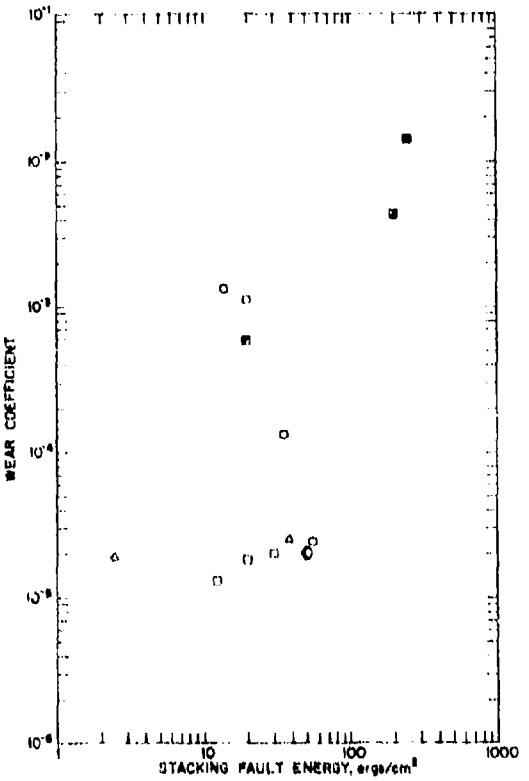

Fig. 4. The wear coefficient *vs.* the SFE: ○ OFHC copper, △ Cu–Si, □ Cu–Sn, ○ Cu–Zn, ◇ Cu–Cr, ▲ AISI 304 stainless steel, ■ 1100 aluminum, ■ Ni.

is 0.74. Therefore the higher crack nucleation and propagation rates in copper were compensated for by the higher hardness and lower coefficient of friction of the copper–silicon alloys. Similar reasoning can be applied to all copper-based solid solutions except the Cu–Zn alloys.

The behavior of the copper–zinc alloys deviates from the general pattern established by the other copper-based solid solutions. Its wear rate increases with the solute content, while that of the others decreases instead. These results, however, are consistent with the results published in the literature [14]. It is also interesting to note that the hardness of brass increases slightly with solute content up to 30% zinc. Consequently, its coefficient of friction also decreases slowly. These experimental results obtained with brass may be explained as follows. The SFE of brass approaches an asymptote when the solute content exceeds about 20% (Fig. 6). As a result the crack nucleation and propagation rates of brass may not change significantly when the solute content exceeds 20%. Furthermore, their hardness and frictional coefficient

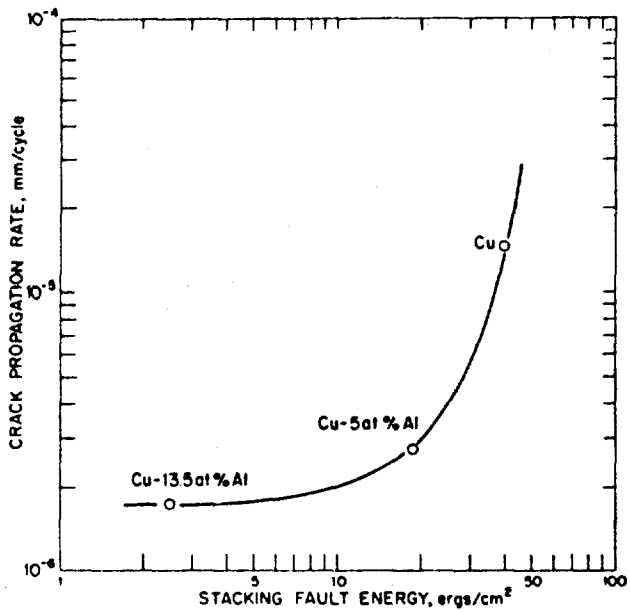

Fig. 5. The crack propagation rate as a function of the SFEs of Cu–Al alloys [10] at room temperature; $\Delta K = 9$ kg mm$^{-3/2}$.

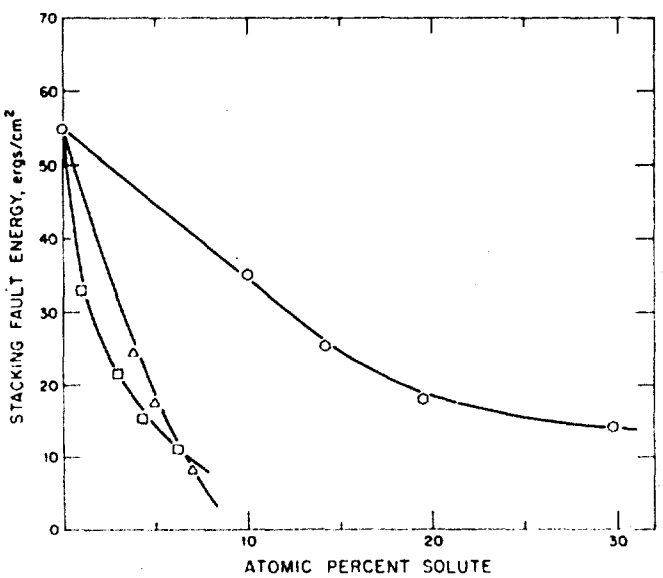

Fig. 6. The SFE as a function of the solute content of copper-based solid solutions [15]: ○ Cu, △ Cu–Si, □ Cu–Sn, ○ Cu–Zn.

do not vary significantly in this range of solute content. Therefore it is reasonable to expect similar wear rates for brass with 20% and 30% solute content. However, the higher wear rate of brass in comparison with copper and the lower wear rate of the Cu–10 at.% Zn alloy in comparison with the brass with higher zinc contents cannot be explained on this basis. It appears that the segregation of zinc at grain boundaries is the major cause for the observed anomaly [16].

Conclusions

In sliding wear all the factors involved (namely, surface traction, plastic deformation, crack nucleation and crack propagation) must be considered in evaluating the effect of metallurgical variables on the wear rate of metals. The SFE may affect the wear rate through its influence on hardness and the crack nucleation and crack propagation rates. However, the wear rate need not be a simple function of the SFE.

Acknowledgments

This work was sponsored by the Defense Advanced Research Projects Agency through the Office of Naval Research under contract no. 0001-67-A-0204-0080. The authors are grateful to Drs. Arden L. Bement, Edward van Reuth and Richard S. Miller and Lt. Commander Kirk Petrovic for their support.

References

1 N. P. Suh, Wear, An overview of the delamination theory of wear, Wear, 44 (1977) 1 - 16.
2 S. Jahanmir and N. P. Suh, Mechanics of subsurface void nucleation in delamination wear, Wear, 44 (1977) 17 - 38.
3 J. R. Fleming and N. P. Suh, Mechanics of crack propagation in delamination wear, Wear, 44 (1977) 39 - 156.
4 J. R. Fleming and N. P. Suh, The relationship between crack propagation rates and wear rates, Wear, 44 (1977) 57 - 164.
5 J. J. Pamies-Teixeira, N. Saka and N. P. Suh, Wear of copper-based solid solutions, Wear, 44 (1977) 65 - 75.
6 N. Saka, J. J. Pamies-Teixeira and N. P. Suh, Wear of two-phase metals, Wear, 44 (1977) 77 - 86.
7 S. Jahanmir, E. P. Abrahamson, II, and N. P. Suh, The effect of second-phase particles on wear, Proc. 3rd North American Metalworking Research Conf., Carnegie Press, Pittsburgh, 1975, pp. 854 - 864.
8 N. Saka, A. M. Eleiche and N. P. Suh, Wear of metals at high sliding speeds, Wear, 44 (1977) 109 - 125.
9 N. P. Suh, Microstructural effects in wear of metals, Battelle Materials Science Colloquium, September, 1975, Plenum Press, to be published.

10 J. P. Hirth and D. A. Rigney, Crystal plasticity and the delamination theory of wear, Wear, 39 (1976) 133 - 141.
11 D. A. Rigney and W. A. Glaeser, The significance of near-surface microstructure in the wear process, Proc. Int. Conf. on Wear of Materials, St. Louis, 1977, ASME, New York, 1977, pp. 41 - 46.
12 A. Saxena and S. D. Antolovich, Low cycle fatigue, fatigue crack propagation and substructures in a series of polycrystalline Cu–Al alloys, Metall. Trans., 6A (1975) 1809 - 1828.
13 H. Ishii and J. Weertman, Fatigue crack propagation in copper and Cu–Al single crystals, Metall. Trans., 2 (1971) 3441 - 3452.
14 Y. Taga and K. Nakajima, Wear, 37 (1976) 365 - 375.
15 P. C. J. Gallagher, The influence of alloying, temperature and related effects on the stacking fault energy, Metall. Trans., 1 (1970) 2429 - 2461.
16 J. F. Breedis, personal communication.

Wear, 44 (1977) 145 - 162

CHEMICAL EFFECTS IN SLIDING WEAR OF ALUMINUM*

MING-KAI TSE and NAM P. SUH

Department of Mechanical Engineering, Massachusetts Institute of Technology, Cambridge, Mass. 02139 (U.S.A.)

(Received May 18, 1977)

Summary

The mechanism of the sliding wear of metals in corrosive media was investigated. In particular, the role of chemical heterogeneities on chemical interactions between the sliding surface and its environment was studied using 2024 aluminum alloy and sodium chloride solutions of varying pH and NaCl concentration. Sliding wear tests with a cylinder-on-cylinder geometry were performed at a sliding speed of 1 m min^{-1} and a normal load of 9.8 N (1 kgf). The results show that at pH = 0 and pH = 14, the wear rate is dominated by the dissolution of aluminum into the NaCl solution. In the intermediate pH range, the wear rate is shown to be controlled by the conjoint actions of corrosion and delamination wear. Microscope examination of the worn specimens by means of a scanning electron microscope further confirms that the mode of corrosion is of a localized nature.

Introduction

The sliding wear of metals is generally controlled by material properties, loading conditions and environment. The preceding papers [1 - 10] on the delamination theory of wear have covered various theoretical and practical aspects of the first two controlling factors, *i.e.* material properties and loading conditions. The purpose of this paper is to present the work done on the effect of any chemical interaction of the sliding surfaces with the environment. The mode of wear under this condition is commonly referred to as corrosive wear.

Chemical effects on the sliding wear of metals are important in many practical situations. Examples are boundary and extreme pressure (EP) lubrication of sliding surfaces, which is often considered as a form of controlled corrosive wear, and lubrication and wear of machinery in a marine environment, in which salt water and salt-bearing air provide a corrosive

*This paper was added to this series after the paper "An overview of the delamination theory of wear" [1] was accepted for publication.

medium. The practical implications of this study can be summarized in two aspects of wear control:

(1) to provide insight into the controlling factors of effective lubrication;

(2) to understand better the mechanism of corrosive wear and its relationship to delamination wear in practical situations.

From either the lubrication or the component failure viewpoint, the conventional conception of corrosive wear is primarily the regeneration and removal of a surface film on the sliding surfaces.

In the absence of an "active" lubricant, the corrosive wear problem has always been considered in terms of oxidative wear models [11 - 13]. The basic assumption of these models is that wear of the sliding surfaces is a result of removal of the surface oxide layer, and hence the wear rate is controlled by the diffusion of oxygen atoms through the oxide layer. The validity of these models, however, is questionable when one considers the observations of plate-like wear particles and the large-scale subsurface deformation on a sliding surface. The delamination process, *i.e.* subsurface deformation, crack nucleation and crack propagation, has indeed been shown [8] to be dominant in the wear of metals even at high sliding speed, in spite of the fact that the wear track is highly oxidized owing to excessive temperature rise during sliding.

From the boundary (and EP) lubrication perspective, there seems to be a general acceptance of the view that lubrication is brought about by a chemically formed surface film at the sliding interface. However, the nature of this surface film has not been conclusively identified. Some researchers have claimed that the surface film is an organometallic compound [14 - 16], while others have suggested an inorganic film [17]. In addition to the dispute on the nature of the surface film, no one seems to know how to control the formation of such surface films on a scientific basis. The role of various controlling factors such as the environment is not well understood.

In summary, the existing theories of corrosive wear have neither depicted a clear picture of the mechanism involved nor adequately provided a scientific basis for the design or selection of lubricants. Their limitations stem from the fact that most of these theories failed to recognize several important physical phenomena on the sliding surfaces, such as the following.

(1) Chemical and mechanical actions have always been assumed to act independently. Chemical reactions may reduce the surface traction (and hence the friction coefficient) through the formation of a surface film, which in turn reduces the plastic deformation on the sliding surfaces. Concurrently, plastic deformation due to mechanical interactions leads to an accumulation of strain energy, thus enhancing chemical reactivity. Such accumulation of stored energy is most probably non-uniformly distributed on the sliding surface because of the structurally heterogeneous nature of the surface. The mechanical action may also expose nascent metals which could act as catalysts for any chemical reaction between the metal surface and its environment.

(2) Although it has been considered in very general terms, the heterogeneous nature of the metallurgy and the chemistry of the metal surfaces has always been disregarded in the study of corrosive wear. This fact hampers the applicability of most existing theories.

(3) It is generally recognized that there is a limit of operation of the surface film as an anti-wear agent. What will happen beyond this operating range or where the surface film is ruptured is still an open question.

The inherent chemical and structural heterogeneities, the induced heterogeneity due to non-uniformly distributed stored energy, and the non-uniformity in the coverage of the sliding surfaces by a surface film all lead to the following conclusion: the possibility of a localized corrosion mechanism which may significantly affect the wear rate has been overlooked in the previous studies of corrosive wear. In view of the metallurgical complexity involved in the engineering alloys in use today, the role of heterogeneities in corrosive wear can hardly be overemphasized.

Therefore the primary objective of this investigation was to explore qualitatively the feasibility and the effect of the localized corrosion mechanism in the sliding wear of metals in corrosive media. It is intended to demonstrate that the conventional homogeneous corrosive wear theory does not account for the observed wear rate, and that the overall wear rate is a complex function of localized reaction, film formation and delamination.

Materials and procedures

2024 aluminum alloy (4.5% Cu, 1.5% Mg, 0.6% Mn, Al balance) and sodium chloride solution were chosen for the study. The 2*XXX* series of aluminum alloys is known to exhibit intergranular corrosion in an aqueous medium containing chloride ions [18]. The susceptibility of 2024 aluminum alloy to intergranular corrosion can be explained in terms of preferential precipitation of an Al_2CuMg intermetallic phase along the grain boundaries [19], resulting in an anodic copper-depleted solid solution region around these precipitates. In a corrosive medium such as sodium chloride solution, the anodic copper-depleted region corrodes preferentially by an electrochemical process.

In the study, the as-received aluminum rods (6.35 mm diameter) were cut into 100 mm pieces. These specimens were then solutionized at 773 K for 60 min, water-quenched to room temperature immediately, then aged at 448 K for 120 min and finally water-quenched again to room temperature. This heat treatment cycle has been reported [19] to enhance the susceptibility to intergranular corrosion of aluminum alloy. Sliding wear tests were performed with this heat-treated aluminum alloy in aqueous sodium chloride solutions (see Fig. 1).

Two parameters were adjusted during the experiment: (1) the concentration of NaCl in solution; (2) the pH of the solution. These two parameters

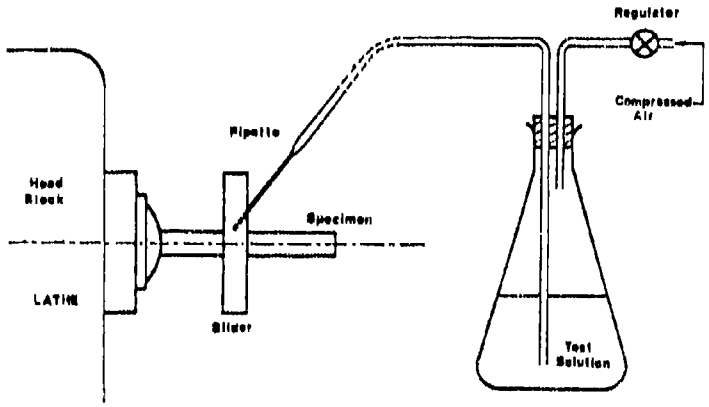

Fig. 1. Schematic diagram of the sliding wear test set-up.

were chosen because of their influences on corrosion rates as well as the mode of corrosion. After each wear test, the wear volume was measured and the wear coefficient was then determined.

To substantiate the localized corrosive wear hypothesis, the wear rate was also determined as a function of the aging time of the same 2024 aluminum alloy at room temperature. Since intergranular corrosion of this aluminum alloy is a result of preferential precipitations along the grain boundaries it was expected that the varying extent of precipitation with aging time would affect the corrosion process. The aging temperature was chosen to be room temperature (298 K) after a trial aging test at 448 K had indicated that the precipitation proceeded too rapidly at an elevated temperature (as revealed by the specimen's hardness change), making aging time impractical for use as a variable in the wear tests. The wear tests were performed during the aging process.

In all the sliding wear tests, the slider material was AISI 304 stainless steel. This material was chosen for two reasons.

(1) The hardness of this material was approximately 1.47×10^9 N m^{-2} (150 kg mm^{-2}), whereas that of the heat-treated aluminum alloy specimen was 8.8×10^8 N m^{-2} (90 kg mm^{-2}). The higher hardness of the slider minimized complications due to deformation of the slider during the tests.

(2) The corrosion current density in the 2024 aluminum–AISI 304 stainless steel galvanic cell was measured to be 12.8 μA cm^{-2} in a 3.5% NaCl solution at 298 K [20]. This low corrosion rate does not modify the corrosion rate of the aluminum specimen very substantially through a galvanic coupling effect.

The sodium chloride solutions were prepared by dissolving laboratory grade granular NaCl in freshly prepared distilled water. The pH of the distilled water and NaCl solutions was varied by addition of HCl or NaOH to cover the pH range 0 - 14. In most laboratory corrosion tests on aluminum alloys,

hydrogen peroxide is added to the test solution to speed up cathodically controlled reactions [19]. In these tests 15 g l^{-1} of 3% H_2O_2 was added to all solutions.

Before the wear tests, the heat-treated specimens were abraded with silicon carbide papers to remove the surface oxide layer. They were then fine polished with 1 μm then 0.25 μm polishing compounds, cleaned with soap and water, rinsed with alcohol and dried with an air blower.

For all wear tests the normal load was 9.8 N (1 kgf) and the sliding speed was maintained at 1 m min^{-1}. The duration of each wear test was 50 min, allowing sufficient time for the wear process to reach a steady state. The pH of the test solution was monitored at the beginning and at the end of each test. The friction coefficient was also monitored and the steady state value recorded. After each wear test the specimen was rinsed carefully with water and any surface reaction products were brushed away lightly using a cotton swab. The specimen was then blow dried.

The transverse profile of the wear groove was traced by a Talysurf profilometer; the product of the measured cross-sectional area of the groove and the circumference of the specimen (20 mm) gave the wear volume.

Selected specimens were cut, polished, etched with Keller's reagent and then observed in a scanning electron microscope (SEM).

Most of the tests were repeated three to five times to check the reproducibility.

Results

Figure 2 shows the corrosion characteristics of 2024 aluminum alloy in NaCl at pH 6 under the same conditions as the wear tests, except that there was no normal load applied. These corrosion tests showed that in a neutral aqueous solution containing Cl^-, the aluminum alloy exhibits intergranular corrosion and pitting characteristics.

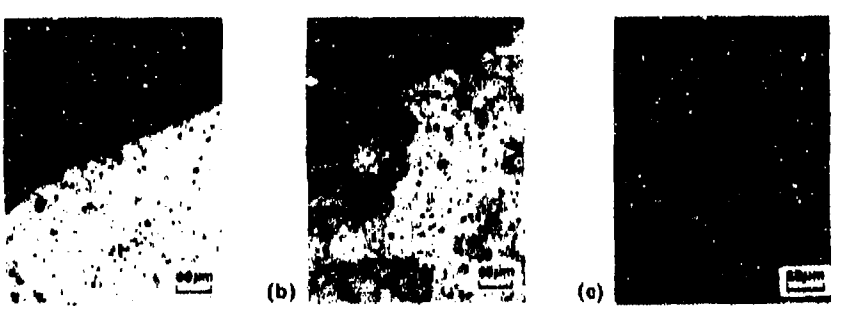

Fig. 2. Intergranular corrosion of 2024 aluminum alloy in sodium chloride solutions containing 15 g l^{-1} H_2O_2: [NaCl] = (a) 0.001 M, (b) 0.1 M, (c) 1 M. Corrosion tests lasted 300 min at 298 K. The pH of all three solutions was measured as 6.

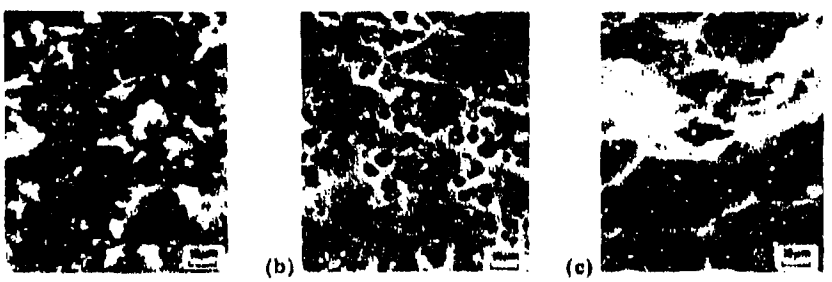

Fig. 3. The surface topography of corroded 2024 aluminum specimens in 0.001 M NaCl at (a) pH = 0, (b) pH = 6, and (c) pH = 14.

Figure 3 is a scanning electron micrograph of the surface topographies of similar corrosion test specimens at three pH levels (0, 6 and 14). At pH 6 the figure shows pitting and intergranular corrosion, whereas at pH 0 or 14 the specimen indicates corrosion through uniform dissolution of the aluminum matrix.

After the intergranular corrosion and pitting behavior of 2024 aluminum alloy in NaCl had been established, the effect of such localized corrosion on sliding wear was investigated. The results are shown in Figs. 4 - 7.

Figure 4(a) shows the variation of the wear coefficient with NaCl concentration in the test solution at pH 6. The figure shows that the wear coefficient is not a monotonic function of NaCl concentration. During the wear tests, it was observed that the wear tracks appeared shiny until the concentration was increased to 0.006 M, above which a black gelatinous deposit was formed. The quantity of the deposit seemed to increase with NaCl concentration.

The dependence of friction coefficient on NaCl concentration is shown in Fig. 4(b). At all concentrations the friction coefficient is higher than that obtained with distilled water alone. The figure also shows that there is a decrease in friction in the high NaCl concentration range (above 0.01 M). This decrease in friction seems to be related to the formation of the gelatinous reaction products.

Figure 4(c) shows the variation of the pH of the solution collected from the zone of sliding contact as a function of NaCl concentration. The pH of all solutions before the wear test was about 6. Above 0.001 M the pH of the solutions after a wear test increased with concentration, indicating an increase in hydroxyl ion concentration.

The above observations show that the presence of chloride ions in the test solution leads to a higher wear coefficient than that obtained with distilled water only. These results, coupled with the observations in the corrosion tests, suggest that a localized corrosion mechanism provides a plausible explanation for the increase of the wear coefficient with NaCl concentration. However, the decrease in wear coefficient in the high NaCl concentration range (associated with the formation of a gelatinous deposit) indicates that

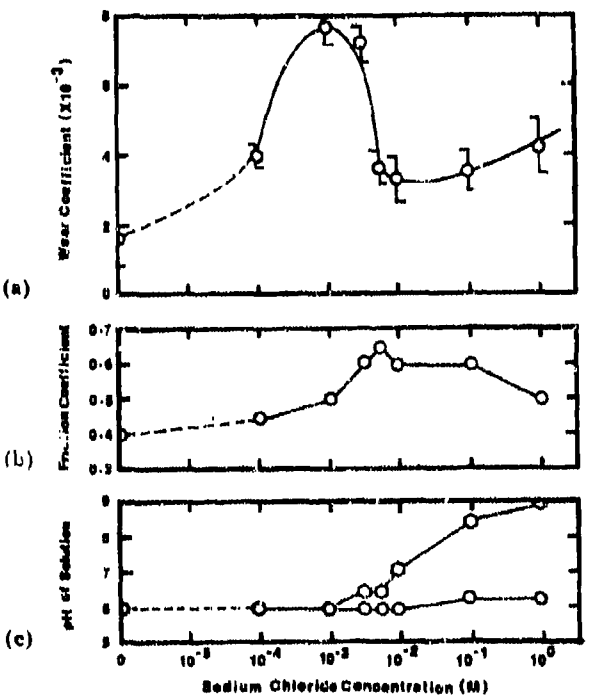

Fig. 4. (a) Wear coefficient, (b) friction coefficient and (c) pH of solution after wear test as a function of sodium chloride concentration in molars: ○ before test, ○ after test.

the overall wear rate is also affected by the formation of a surface film. The corrosion product appears to lower the friction coefficient and hence the wear coefficient.

Figures 5 - 7(a) show the dependence of the wear coefficient on pH at three NaCl concentrations (0 M, 0.001 M and 1.0 M respectively). Figure 4(a) has indicated that the wear behaviors are different at these three concentrations.

With distilled water only (Fig. 5) the wear coefficient is relatively constant within the pH range 3 - 11. At both the low pH (below 3) and high pH (above 11) ends the wear coefficient increases very rapidly to 10^{-3}. This value is extraordinarily high compared with the wear coefficient experienced in most wear modes, which is typically less than 10^{-4}. Such a high value of the wear coefficient suggests that most of the material loss is probably due to severe corrosion (dissolution). This argument is indeed supported by the measured depth of material loss due to corrosion alone, as shown in Fig. 5(c); this figure shows the depth of uniform corrosion on the sides of the wear track, which were covered by a film of the test solution during the wear test. Visual examination of the wear specimens during the wear tests showed

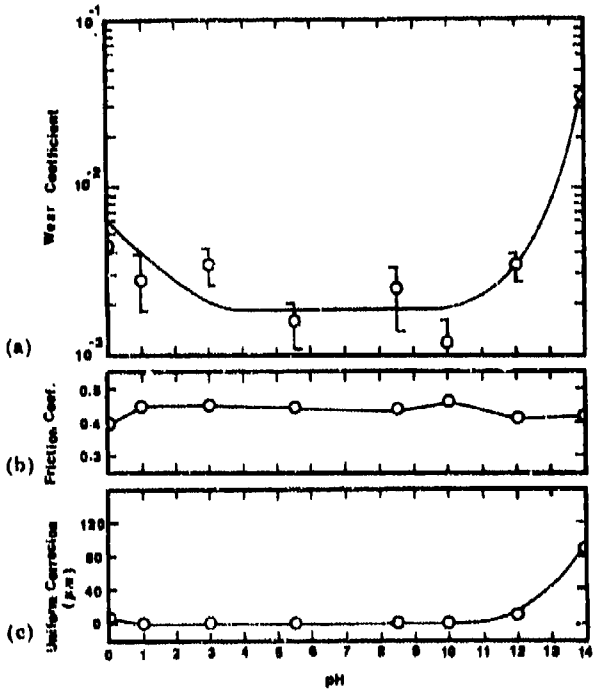

Fig. 5. (a) Wear coefficient, (b) friction coefficient and (c) uniform corrosion as a function of pH of distilled water.

that a black gelatinous deposit was formed as the pH was increased to 10 and above. The friction coefficient is shown in Fig. 5(b) to be relatively constant over the pH range 0 - 14.

At an NaCl concentration of 0.001 M the variation of the wear coefficient with pH (Fig. 6(a)) at the high and low pH range (pH less than 1 and pH above 12) is similar to that shown in Fig. 5(a). The uniform corrosion characteristics are also similar in these pH ranges (Figs. 5(c) and 6(c)). In the intermediate pH range (2 - 12) the wear coefficient varies parabolically with pH, whereas in the case with water only the wear coefficient is independent of pH. This result shows the detrimental effect of Cl ion on the sliding wear of 2024 aluminum alloy in an aqueous environment. At pH = 0 - 1 and pH = 10 - 12 a black deposit was again noticed on the wear track. Figure 6(b) shows that the friction coefficient is roughly constant (about 0.5) between pH 2 and pH 6, but that it decreases gradually to about 0.4 as the pH increases to 14. However, there is a relatively sharp decrease in friction coefficient to about 0.3 at the low pH end (pH = 0 and 1). Once again, these observations suggest that the overall wear rate is a complex function of localized corrosion, surface film formation and mechanical action.

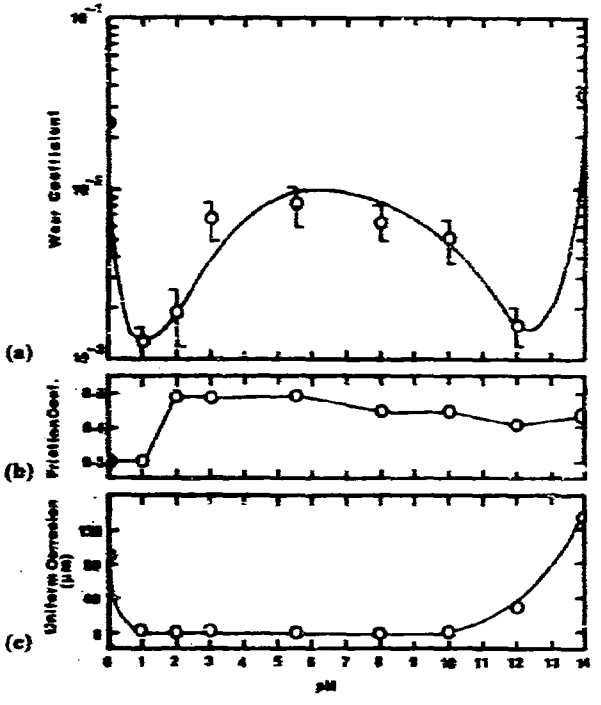

Fig. 6. (a) Wear coefficient, (b) friction coefficient and (c) uniform corrosion as a function of pH of a 0.001 M NaCl solution.

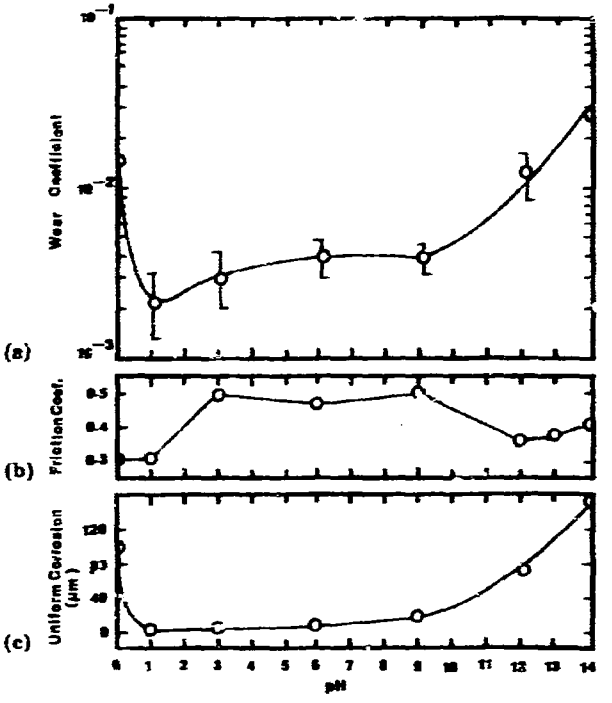

Fig. 7. (a) Wear coefficient, (b) friction coefficient and (c) uniform corrosion as a function of pH of a 1.0 M NaCl solution.

At an NaCl concentration of 1.0 M, the wear coefficient–pH relationship (Fig. 7(a)) is similar to that obtained with distilled water alone, except that in the intermediate pH range the wear coefficient is about 3.5×10^{-3} compared with 1.7×10^{-3} in the latter liquid. The friction coefficient (Fig. 7(b)) follows a trend similar to that obtained at an NaCl concentration of 0.001 M, *i.e.* low values at both the high and low pH ends. Inspection of the wear tracks showed the formation of a black gelatinous deposit throughout the whole pH range (0 - 14). The uniform dissolution characteristics (Fig. 7(c)) are similar for all three NaCl concentrations considered.

To strengthen further the localized corrosion hypothesis, sliding wear tests in NaCl solution were performed as a function of the aging time of the 2024 aluminum specimen at room temperature (298 K). The wear tests were performed with both distilled water and 0.001 M NaCl. The progress of the precipitation hardening process is shown in Fig. 8. The figure shows that the hardness reaches its maximum value of approximately 9.2×10^{8} N m $^{-2}$ in

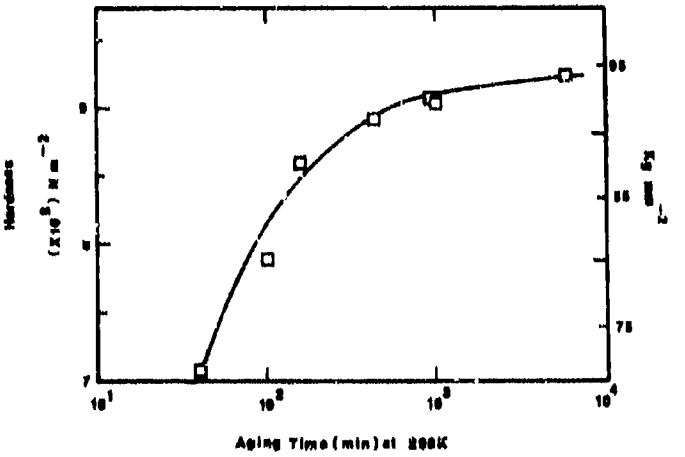

Fig. 8. The hardness of 2024 aluminum alloy as a function of aging time at 298 K. The specimens were solutionized at 773 K for 1 h, water-quenched and then aged.

about 1000 min. The wear tests results are shown in Fig. 9; the figure shows that for the 0.001 M solution the wear coefficient increases as aging time increases. The wear coefficient for the tests with distilled water, however, shows only a marginal increase for the same aging time. This result with distilled water shows that the increase in wear coefficient with aging time in the 0.001 M NaCl solution is not a consequence of the hardness change but is due to the presence of the chloride ions.

An interesting observation from this test result is that the wear coefficient increases as the hardness of the material increases with aging time. This observation is inconsistent with the postulate of the adhesion theory of wear

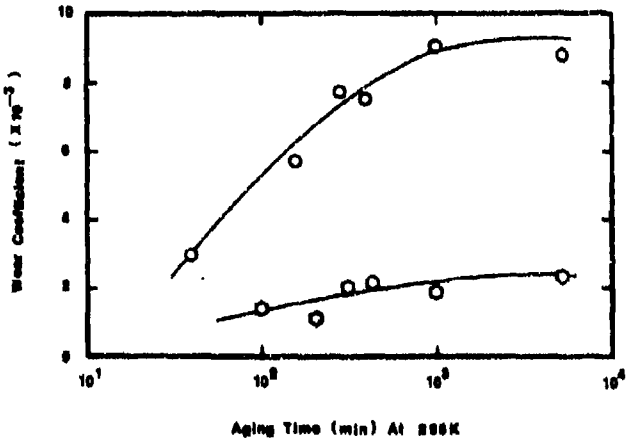

Fig. 9. The wear coefficient as a function of aging time for 2024 aluminum alloy at 298 K: ○ with 0.001 M NaCl, ● with distilled water only.

which suggests that the wear coefficient is inversely proportional to the hardness of a material. However, this observation has been explained in terms of the delamination theory of wear [5].

Microscope examination of the worn specimens revealed the dominant mechanism of wear particle formation in the intermediate pH range, namely conjoint actions of delamination and localized corrosion.

Figures 10 - 12 provide evidence supporting the delamination theory of wear. These figures illustrate the delamination processes of subsurface deformation, subsurface crack initiation and propagation, and eventual detachment of sheet-like particles from the sliding surface, respectively.

Fig. 10. Subsurface deformation in a sliding wear specimen. The specimen material is 2024 aluminum alloy. The wear test was in distilled water at pH 6.

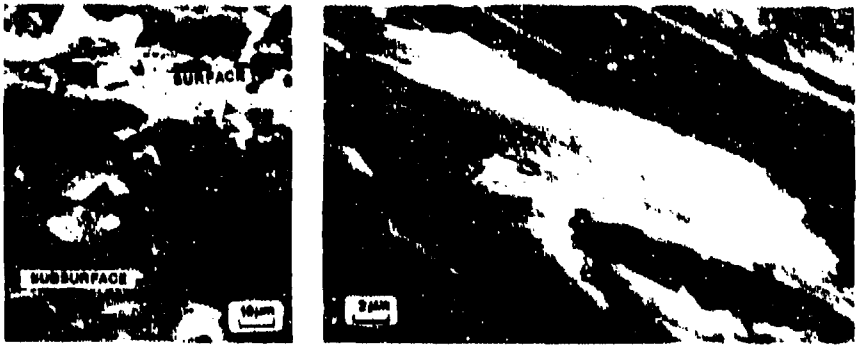

Fig. 11. A subsurface crack propagating parallel to the surface on a sliding wear specimen. The specimen material is 2024 aluminum alloy. The test solution was 0.001 M NaCl at pH 6.

Fig. 12. A typical delaminated wear particle. The specimen material is 2024 aluminum alloy. The test solution was 0.001 M NaCl at pH 6.

Figure 13 shows the initiation of a surface crack along a grain boundary as a result of preferential chemical reaction. Sheet-like particles are detached from the surface as a result of the simultaneous development of surface (chemically initiated) and subsurface (mechanically induced) cracks. Such a sheet-like particle is also observed in Fig. 13. Figure 14 is another typical example of pits initiated on the surface, complementing the propagating subsurface cracks in the formation of a wear particle. The figure also shows that the corrodant probably passed through the surface pits and chemically attacked the subsurface crack.

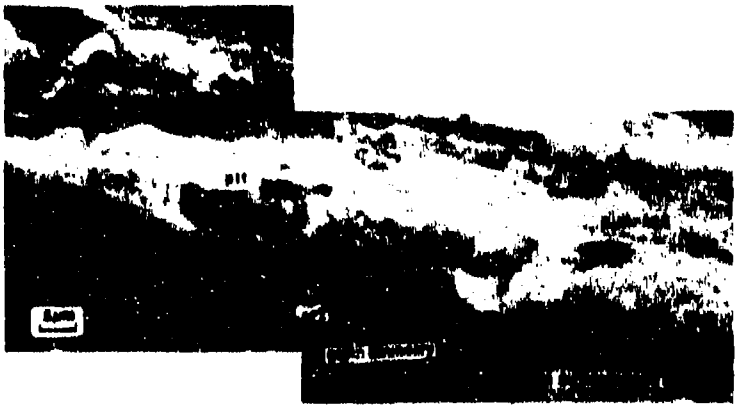

Fig. 13. Chemically initiated pit along a grain boundary of a 2024 aluminum specimen. The wear test was in 0.001 M NaCl at pH 6.

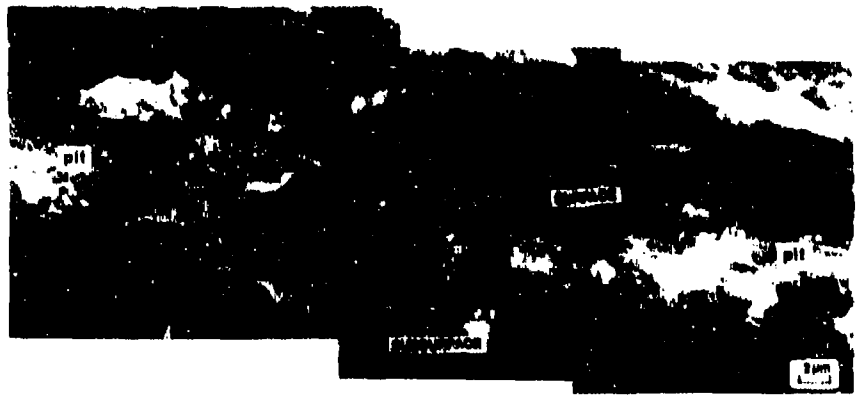

Fig. 14. Wear particle formation by conjoint actions of surface pits and subsurface cracks. The wear test was in 0.001 M NaCl at pH 6.

Figure 15 differentiates the surface appearances of the wear specimens in 0.001 M and 1.0 M NaCl solutions at pH 6. With the former solution no surface film was observed during the wear tests, while in the latter a residual surface film was observed.

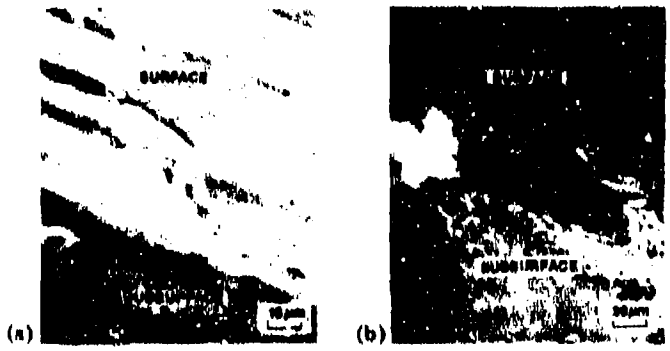

Fig. 15. Comparison of the wear track characteristics. Test (a) was in 0.001 M NaCl at pH 6. Test (b) was in 1.0 M NaCl at pH 6. Note the surface film on specimen (b).

Figure 16 shows the subsurface of a specimen tested in a 0.001 M NaCl solution at pH 1. It has been reported that a surface film was observed during the wear test (Figs. 6(a) and 6(b)). Hence this figure shows that intergranular corrosion occurs even in the presence of a surface film (note the difference in the etched appearances of two adjacent grains).

Fig. 16. Intergranular corrosion of 2024 aluminum specimen during wear test in 0.001 M NaCl at pH 1.

Discussion

In the previous studies on the delamination wear of materials [1 - 10], the test conditions were so chosen that the environment effect was negligible. In this study the role of chemical interactions between the environment and the sliding surfaces was emphasized. The results indicate that chemical interactions exhibit two major effects on the wear rate.

(1) They modify the friction coefficient through the formation of a surface film of reaction products.

(2) They promote the wear rate through localized chemical interactions which initiate surface cracks.

From a lubrication standpoint the results in this study agree with the recognized lubricating capability of some corrosion products. This conclusion is based on the observation that the friction coefficient as well as the wear coefficient were lowered wherever the wear tests conditions were such that a gelatinous surface film was visually present.

Surface traction, together with other factors such as normal load and hardness, determines the rate of the delamination processes of subsurface deformation, crack initiation and propagation. Hence the presence of a surface film diminishes the contribution of delamination wear through a reduction of the surface traction. Extrapolating this argument to a situation where the friction coefficient is very low, one could conclude that the wear rate would then be predominantly determined by chemical interactions. In practice, an extremely low friction coefficient can only be achieved in a thick film lubrication regime, *i.e.* hydrodynamic lubrication. In this regime, however, it is well known that the effectiveness of a lubricant is controlled by its physical properties such as viscosity rather than its chemical properties. In contrast, the friction coefficient in the boundary (and EP) lubrication regime, where the external load is high and/or the sliding speed is low, is typically of the order of 0.1 - 0.3. Under these circumstances, the role of delamination in determining wear rate is again significant. In this study, the

friction coefficient was about 0.4 - 0.5 for most tests and the formation of wear particles by delamination is evident from the micrographs (Figs. 10 - 12).

As a consequence of the preceding discussion, one of the major drawbacks of the conventional theories of corrosive wear becomes apparent, *i.e.* the importance of surface traction has not been considered. In these theories, material loss is solely attributed to the mechanical removal of surface reaction products, which may hold true only in a situation with extremely low friction coefficient.

Nonetheless the overall wear rate in a chemically reactive environment is determined by neither removal of surface film nor delamination alone. The micrographs shown in Figs. 13 and 14 demonstrate that wear particles formed as a result of conjoint actions of chemically initiated surface cracks (pits) and mechanically induced delamination.

Based on both thermodynamic and kinetics arguments, the chemically and structurally heterogeneous sliding surfaces favor preferential chemical reactions at localized sites. The chemically different constituents on an engineering alloy surface would involve different amounts of Gibbs free energy changes when reacting chemically with the environment. Moreover, the kinetics for reactions involving different phases on a multiphase material surface could be very different. Hence the assumption of a homogeneous surface in the realm of conventional theories of corrosive wear is inevitably questionable. Indeed, the experimental results in this study show that in the intermediate pH range (Fig. 6(a)) the wear rate of 2024 aluminum alloy was increased substantially by the presence of chloride ions, and the results of the tests with aging time at room temperature as a variable validate the hypothesis that this increase in wear rate is a consequence of preferential corrosion at localized sites. Coupled with the microscope observations of the worn specimens, these experimental results therefore lead to the conclusion that the overall wear rate is a complicated function of delamination, localized corrosion, and regeneration and removal of surface film. This observation is incompatible with the concept of a homogeneous material surface in the conventional theories; consequently, the major contribution of this study is that the picture of a heterogeneous surface is rejuvenated.

This study has also raised another question on the assumption of a complete coverage of the sliding surface by a surface film in most existing models of corrosive wear. The micrograph shown in Fig. 16 indicates that, under the wear test conditions in which a surface film is formed, localized corrosion still takes place, resulting in a network of intergranular cracks. Such cracks could be detrimental to the life of a mechanical component by acting as stress intensified sites. In fact the question of what would happen to the sliding surface where the surface film is ruptured has never been looked into systematically.

In summary, this investigation has illustrated the significance of localized corrosion (as a consequence of surface heterogeneities) in the study of corrosive wear, which has been astonishingly disregarded in most existing corrosive wear theories.

Up to this point, the electrochemistry in the wear tests has not been discussed. A brief discussion is thus attempted here to explain some of the experimental observations:

(1) dissolution of aluminum at high and low pH (Fig. 3);

(2) formation of the black gelatinous product (Fig. 15);

(3) increase in pH at high chloride ion concentration (Fig. 4(c)).

It is well known that the corrosion behavior of aluminum in aqueous solution is strongly influenced by a protective film of oxide (*e.g.* see the Pourbaix diagram for the Al--water system at 25 °C [21]).

In a highly acidic medium the protective oxide film is thermodynamically unstable, resulting in dissolution and loss of protective action of this oxide layer. Consequently, dissolution of aluminum occurs according to the following reaction:

$$Al \rightarrow Al^{3+} + 3e^{-}$$

Dissolution of the oxide layer also takes place at highly alkaline pH levels. Corrosion (dissolution) of aluminum again takes place owing to complex ion formation:

$$Al + OH^{-} + H_2O \rightarrow AlO_2^{-} + \frac{3}{2}H_2$$

In the intermediate pH range, the passivating oxide film is thermodynamically stable. However, this protective behavior is known to be greatly modified when certain anions such as Cl^{-} are present. Hoar [22] has shown that a process of ion exchange probably takes place between adsorbed anions on the outside of the film and the oxygen ions of the oxide lattice. Under the action of the electric field induced by polarizable adsorbed anions, metal cations are pulled outwards through the film, whereupon they dissolve as anion complexes. In this manner, an adsorption–exchange process enhances the corrosion (dissolution) of aluminum. It has also been shown [23] that the electric field induced increases as the anion concentration increases, thus enhancing the rate of the dissolution process. With this background, explanations for the formation of the black deposit and the increase in pH at high chloride concentration seem plausible.

The presence of Cl^{-} enhances the dissolution of aluminum in anodic sites, and the dissolved cationic aluminum subsequently hydrolyses:

$$Al^{3+} + 3H_2O \rightarrow Al(OH)_3 + 3H^{+}$$

This reaction shows that $Al(OH)_3$ may precipitate, forming a deposit on the sliding interface; the reaction is pH dependent. The pH dependence suggests that the deposit observed in the highly acidic solution (Fig. 4) could be a blend of $AlCl_3$ (which normally is highly soluble in water) and $Al(OH)_3$ since then the reverse reaction is favored.

So far we have ignored the possible reaction(s) at the cathodic site. It is known that in a near-neutral aqueous solution with dissolved oxygen the dominant cathodic reaction is

$$O_2 + 2H_2O + 4e^{-} \rightarrow 4OH^{-}$$

This reaction shows that the alkalinity at the cathodic sites increases. However, the above discussion on the effect of Cl^- on the corrosion behavior of aluminum suggests that this cathodic reaction is enhanced by the increasing concentration of Cl^- (since anodic and cathodic reactions are simultaneous equal rate processes). Thus it seems reasonable to speculate that this is the reason for the observed pH increase shown in Fig. 4(c).

Apart from the initiation of surface cracks by the chemically reactive environment, many other possible factors that may affect the wear rate have been neglected in the above discussion. For example, the role of the residual strain energy produced by plastic deformation in the subsurface is not clearly identified. Figure 14 shows that NaCl solution has probably passed through the surface pits and chemically attacked the subsurface crack; the exact nature of such influence of the corroding medium on subsurface crack propagation has not been pursued in detail. Furthermore, it has been assumed in this study that growth of the surface crack is a result of chemical processes, and we have neglected the possible influence of a tensile zone behind an asperity on these surface cracks [3]. All these possibilities may only have minor influences on wear rate and await further clarification in the future.

Conclusions

The chemical effects of a chloride-containing environment on the sliding wear of 2024 aluminum alloy have been studied. The results of this study lead to the following conclusions.

(1) The formation of a corrosion product reduces the friction coefficient and the wear coefficient. This observation agrees with the conventional view on the lubricating capability of a surface film formed in boundary (or EP) lubrication.

(2) The surface film does not provide complete passivation of the surface. Preferential reactions leading to localized corrosion are still possible.

(3) Preferential chemical reaction at localized sites as a result of chemical and structural heterogeneities can accelerate the wear process (*i.e.* increase the wear rate) by initiating surface cracks.

(4) A complete picture of the corrosive wear process should include both the formation of a surface film and the localized reactions. The latter have been disregarded by the classical theories of corrosive wear.

(5) The overall wear rate is a complex function of both mechanical and chemical interactions. Microscope examination of the wear tracks and the subsurfaces of the worn specimens indicated that the wear is due to the delamination wear mechanisms (*i.e.* subsurface deformation, crack nucleation and propagation) as well as the corrosive effect of the environment which generates surface cracks by heterogeneous chemical interactions.

Acknowledgments

The work presented in this paper would not have been possible without the support of the Defense Advanced Research Projects Agency under con-

tract no. N 00014-67-A-0204-0080, through the Office of Naval Research. The authors are particularly grateful to Dr. Edward C. van Reuth and Dr. Richard G. Miller for their personal support (D.P.O.) of the work. The MIT staff is also grateful to Dr. Arden Bement and Lt. Commander Kirk Petrovic for their continuing support.

References

1 N. P. Suh, An overview of the delamination theory of wear, Wear, 44 (1977) 1 - 15.
2 S. Jahanmir and N. P. Suh, Mechanics of subsurface void nucleation in delamination wear, Wear, 44 (1977) 17 - 38.
3 J. R. Fleming and N. P. Suh, Mechanics of crack propagation in delamination wear, Wear, 44 (1977) 39 - 56.
4 J. J. Pamies-Teixeira, N. Saka and N. P. Suh, Wear of copper-based solid solutions, Wear, 44 (1977) 65 - 75.
5 N. Saka, J. J. Pamies-Teixeira and N. P. Suh, Wear of two-phase metals, Wear, 44 (1977) 77 - 86.
6 S. Jahanmir and N. P. Suh, Surface topography and integrity effects on sliding wear, Wear, 44 (1977) 87 - 99.
7 T. Nagao, J. J. Pamies-Teixeira and N. P. Suh, Behavior of medium carbon steel under combined fatigue and wear, Wear, 44 (1977) 101 - 108.
8 N. Saka, A. M. Eleiche and N. P. Suh, Wear of metals at high sliding speeds, Wear, 44 (1977) 109 - 125.
9 J. R. Fleming and N. P. Suh, The relationship between crack propagation rates and wear rates, Wear, 44 (1977) 57 - 64.
10 N. P. Suh, N. Saka and S. Jahanmir, Implications of the delamination theory on wear minimization, Wear, 44 (1977) 127 - 134.
11 E. Rabinowicz, Lubrication of metal surfaces by oxide films, ASLE Trans., 10 (1967) 400 - 407.
12 T. F. J. Quinn, Oxidational wear, Wear, 18 (1971) 413 - 419.
13 F. F. Tao, A study of oxidation phenomena in corrosive wear, ASLE Trans., 12 (1969) 97 - 105.
14 R. S. Fein and K. L. Kreuz, Chemistry of boundary lubrication of steel by hydrocarbons, ASLE Trans., 8 (1965) 29 - 38.
15 F. G. Rounds, ASLE Trans., 9 (1966) 88 - 100.
16 J. K. Appeldoorn and F. F. Tao, Lubricity characteristics of heavy aromatics, ACS Div. of Petrol. Chem. preprints 13/2, 1960, B15-B25.
17 D. Godfrey, Chemical changes in steel surfaces during extreme pressure lubrication, ASLE Trans., 5 (1962) 57 - 66.
18 D. O. Sprowls and R. H. Brown, Stress corrosion mechanisms for aluminum alloys, Proc. of Conf. on Fundamental Aspects of Stress Corrosion Cracking, 1967, National Association of Corrosion Engineers, 1969, pp. 466 - 512.
19 R. B. Mears, R. H. Brown and E. H. Dix, Jr., A generalized theory of stress corrosion of alloys, Symp. on Stress Corrosion Cracking of Metals, 1944, ASTM and AIME, p. 329.
20 F. Mansfield, D. H. Hengstenberg and J. V. Kenkel, Galvanic corrosion of Al alloys: 1, effect of dissimilar metal, Corrosion — NACE, 30 (10) (1974) 343 - 353
21 M. Pourbaix, Atlas of Electrochemical Equilibrium in Aqueous Solutions, translated from French by J. A. Franklin, Pergamon Press, Oxford, 1966.
22 T. P. Hoar, D. C. Mears and G. P. Rothwell, Corros. Sci., 5 (1965) 279.
23 M. Pourbaix, On the effect of chlorides on the behavior of metals and alloys in the presence of aqueous solutions, Symp. on the Coupling of Basic and Applied Corrosion Research, March 21 - 23, 1966, National Association of Corrosion Engineers, pp. 67 - 74.

THE DELAMINATION THEORY OF WEAR - III

Third Progress Report

to

Defense Advanced Research Projects Agency, DoD
Contract Number: N00014-67-A-0204-0080
NR 229-011

N.P. Suh
N. Saka
S. Jahanmir
J.R. Fleming
J.J. Pamies-Teixeira
M-K. Tse
T. Nagao
A.M. Eleiche

Dept. of Mechanical Engineering

Laboratory for Manufacturing and Productivity
School of Engineering
Massachusetts Institute of Technology
Cambridge, Massachusetts 02139

December 1977

UNCLASSIFIED
SECURITY CLASSIFICATION OF THIS PAGE (When Data Entered)

REPORT DOCUMENTATION PAGE

READ INSTRUCTIONS BEFORE COMPLETING FORM

1. REPORT NUMBER: ----	2. GOVT ACCESSION NO.: ----
3. RECIPIENT'S CATALOG NUMBER: ----	
4. TITLE (and Subtitle): The Delamination Theory of Wear - III. ~~Third Progress Report.~~	5. TYPE OF REPORT & PERIOD COVERED: Progress rept. no. 3 Jul[illegible]75-Dec[illegible]76
	6. PERFORMING ORG. REPORT NUMBER: ----
7. AUTHOR(s): ~~[illegible]~~ Suh, N. Saka, S. Jahanmir, J.R. Fleming, J.J. Pamies-Teixeira, ~~M-K. Tse, T. Nagao, [illegible]~~ Eletcha	8. CONTRACT OR GRANT NUMBER(s): N00014-67-A-0284-0089 NR 229-011
9. PERFORMING ORGANIZATION NAME AND ADDRESS: Laboratory for Manufactering and Productivity, School of Engineering, M.I.T., Cambridge, Ma.	10. PROGRAM ELEMENT, PROJECT, TASK AREA & WORK UNIT NUMBERS: 000000#4D10
11. CONTROLLING OFFICE NAME AND ADDRESS: Department of the Navy, Office of Naval Research, Arlington, Virginia 22217 N00014	12. REPORT DATE: December [illegible]977
	13. NUMBER OF PAGES: 52 78 P.
14. MONITORING AGENCY NAME & ADDRESS (if different from Controlling Office): Office of Naval Research M.I.T. Resident Representative Room E19-628 Cambridge, Massachusetts 02139 (N66017)	15. SECURITY CLASS. (of this report): Unclassified
	15a. DECLASSIFICATION/DOWNGRADING SCHEDULE: ----

16. DISTRIBUTION STATEMENT (of this Report)

The distribution of this document is unlimited.

17. DISTRIBUTION STATEMENT (of the abstract entered in Block 20, if different from Report)

18. SUPPLEMENTARY NOTES

19. KEY WORDS (Continue on reverse side if necessary and identify by block number)

delamination, sliding wear, subsurface deformation, void formation, crack propagation, soft metallic coating, surface roughness, surface integrity, wear reduction mechanics of delamination, high speed sliding, chemical effects, combined fatigue and wear, solid solutions, two-phase metals, stacking faults

20. ABSTRACT (Continue on reverse side if necessary and identify by block number)

This third progress report describes the work done by the MIT - Wear Research Group on fundamentals of wear by delamination. Such topics as the mechanics of subsurface deformation, crack nucleation, crack propagation, sliding velocity, combined fatigue and wear, the effect of microstructure, the effect of surface roughness and integrity and chemical effects on wear are examined.

DD FORM 1 JAN 73 1473 EDITION OF 1 NOV 65 IS OBSOLETE
S/N 0102-014-6601

UNCLASSIFIED
SECURITY CLASSIFICATION OF THIS PAGE (When Data Entered)

220 022 - JUR

Distribution List

	No. of Copies
W.J. Anderson NASA-Lewis Research Center 2100 Brookpark Road Cleveland, Ohio 44135	1
Prof. George S. Ansell Department of Materials Science Rensselaer Polytechnic Institute Troy, New York 12181	1
Prof. Ali S. Argon Dept. of Mechanical Engineering Massachusetts Institute of Tech. Room 1-306 Cambridge, Massachusetts 02139	1
Mr. A. Beerbower Esso Research and Engineering Co. P.O. Box 51 Linden, New Jersey 07036	1
Dr. Arden Bement, Director Defense Advanced Research Projects Agency 1400 Wilson Boulevard Arlington, Virginia 22209	1
Mr. R.C. Bowers Code 6050 Naval Research Laboratory Washington, D.C. 20375	1
Mr. F. Brooks Air Force Materials Laboratory Wright-Patterson Air Force Base Dayton, Ohio 45433	1
Dr. D.H. Buckley NASA-Lewis Research Center 2100 Brookpark Road Cleveland, Ohio 44135	1
Prof. Bernard Budiansky Div. of Eng. and Applied Physics Harvard University 313 Pierce Hall Cambridge, Massachusetts 02138	1
Prof. R.A. Burton Dept. of Mechanical and Engineering and Astronautical Sciences Northwestern University Evanston, Illinois 60201	1
Prof. Morris Cohen Materials Science and Engineering Massachusetts Institute of Tech. Room 13-5046 Cambridge, Massachusetts 02139	1
Mr. W. Campbell Wear Sciences Inc. 32 Sutherland Drive Scotia, New York 12302	1
Prof. H.S. Cheng Dept. of Mechanical Engineering and Astronautical Sciencas Northwestern University Evanston, Illinois 60201	1
Prof. N.H. Cook Dept. of Mechanical Engineering Massachusetts Institute of Tech. Room 35-132 Cambridge, Massachusetts 02139	1
Mr. M.J. Devine Aero Material Department Naval Air Development Center Warminster, Pennsylvania 18974	1
Mr. Edwin Ditto Manufacturing Development General Motors Technical Center General Motors Corporation Warren, Michigan 48090	1
Mr. S. Dordoff Office of Naval Research Arlington, Virginia 22217	1
Dean D. Drucker College of Engineering University of Illinois Urbana, Illinois	1

**Please notify Ms. Rosalie M. Allen 617-253-2234 if your address is incorrect: Massachusetts Institute of Technology, Room 35-136, Cambridge, Massachusetts 02139.

	No. of Copies
Prof. N.S. Eiss, Jr. Virginia Polytechnic Institute Blacksburg, Virginia 24060	1
Dr. R. Fein Fundamental Research Section Texaco Research Center Beacon, New York 12508	1
Dr. Michael Field Metcut Research Associates, Inc. 3980 Rosslyn Drive Cincinnati, Ohio 45209	1
Prof. I. Finnie Dept. of Mechanical Engineering University of California Berkeley, California 94720	1
Prof. M. Furey Mechanical Engineering Department Virginia Polytechnic and State U. Blacksburg, Virginia 25061	1
Dr. Frank S. Gardner Office of Naval Research Scientific Department 495 Summer Street Boston, Massachusetts 02210	1
Prof. Peter Gielisse University of Rhode Island Kingston, Rhode Island 02881	1
Dr. D. Godfrey Chevron Research Company 576 Standard Avenue Richmond, California 94800	1
Mr. D.F. Hayes Mechanical Development Department Research Laboratory General Motors Corporation Warren, Michigan 48090	1
Prof. John P. Hirth Dept. of Metallurgical Engineering The Ohio State University 116 West 19th Avenue Columbus, Ohio 43210	1
Commander M. Hoobchack Naval Sea Systems Commands Code Sea 04321H Washington, D.C. 20362	1
Mr. C. Hudson AFAPL/SFL Air Force Aero Propulsion Laboratory Wright-Patterson Air Force Base Dayton, Ohio 45433	1
Dr. L. Jarvis, Director Code 6170 Technical Information Division Naval Research Laboratory Washington, D.C. 20375	6
Dr. Thomas F. Jones, Jr. Vice President for Research Massachusetts Institute of Tech. Room 3-305 Cambridge, Massachusetts 02139	1
Prof. C.H. Kahng Department of Mechanical Engineering Michigan Technological University Houghton, Michigan 49931	1
Prof. D.F. Kettlebourgh Mechanical Engineering Department Texas A&M University College Station, Texas 77843	1
Prof. E.E. Klaus Department of Chemical Engineering Pennsylvania State University University Park, Pennsylvania 16802	1
Dr. Ranga Komanduri Corporate Research and Development General Electric Company Building K-1, Room 4837 P.O. Box 8 Schnectady, New York 12301	1
Dr. P.M. Ku, Director Dept. of Aerospace Properties Research Southwest Research Institute 8500 Culebra Road San Antonio, Texas 78206	1

	No. of Copies
Prof. Jorn Larsen-Basse Dept. of Mechanical Engineering University of Hawaii 2540 Dole Street Honolulu, Hawaii 96822	1
Mr. D. Lauver Code 411 Office of Naval Research Arlington, Virginia 22217	1
Prof. F.F. Ling Department of Mechanics Rensselaer Polytechnic Institute Troy, New York 12181	1
Mr. W.E. Littmann Timken Company 1835 Dueber Avenue, S.W. Canton, Ohio 44706	1
Prof. K. Ludema Dept. of Mechanical Engineering University of Michigan Ann Arbor, Michigan 48105	1
Prof. C.J. Maday Dept. of Engineering Mechanics North Carolina State University Raleigh, North Carolina 27607	1
Prof. Frank A. McClintock Massachusetts Institute of Technology Department of Mechanical Engineering Room 1-304C Cambridge, Massachusetts 02139	1
Prof. Charles J. McMahon, Jr. Dept. of Metallurgy & Materials Science University of Pennsylvania Philadelphia, Pennsylvania 19174	1
Mr. J. Meyer Ford Motor Company Research Laboratory Dearborn, Michigan 48120	1
Dr. R.S. Miller Code 473 Office of Naval Research Arlington, Virginia 22217	6
Dr. D.V. Minuti Materials Engineer, Code 30-73 ARP/SLP Project Office Air Vehicle Technology Dept. Naval Air Development Center Warminister, Pennsylvania 18974	1
Mr. M.S. Ojalvo National Science Foundation Engineering Mechanics Division 1800 G Street Washington, D.C. 20050	1
Prof. Walter S. Owen Dept. of Metallurgy & Materials Science Massachusetts Institute of Technology Cambridge, Massachusetts 02139	1
Mr. R. Parker NASA - Lewis Research Center 2100 Brookpark Road Cleveland, Ohio 44135	1
Dr. E. Passaglia National Bureau of Standards Department of Commerce Washington, D.C. 20234	1
Dr. H.W. Paxton Vice President - Research U.S. Steel Corporation 600 Grant Street, Room 56-06 Pittsburgh, Pennsylvania 15230	1
Lt. Commander, W.K. Petrovic Code 221 Office of Naval Research 800 North Quincy Street Arlington, Virginia 22217	1
Mr. B. Poppert Code 349E Naval Air Systems Command Washington, D.C.20360	1
Prof. Ernest Rabinowicz Dept. of Mechanical Engineering Massachusetts Institute of Technology Room 35-010 Cambridge, Massachusetts 02139	1

	No. of Copies
Dr. Robert J. Reynick National Science Foundation Washington, D.C. 20550	1
Prof. J. Rice Division of Engineering Brown University Providence, Rhode Island 02912	1
Dr. O. Richman U.S. Steel Corporation Research Laboratory 125 Jamison Lane Monroeville, Pennsylvania 15146	1
Prof. David A. Rigney Dept. of Metallurgical Engineering The Ohio State University 116 West 19th Avenue Columbus, Ohio 43210	1
Mr. C.N. Rowe Mobil Research & Development Corporation P.O. Box 1025 Princeton, New Jersey 08540	1
Dr. E. Rudy Oregon Graduate Center 19600 N.W. Walker Road Beaverton, Oregon 97005	1
Dr. W. Ruff National Bureau of Standards Department of Commerce Washington, D.C. 20234	1
Prof. J.A. Schey Dept. of Materials Engineering University of Illinois P.O. Box 4348 Chicago, Illinois 60680	1
Prof. A. Seireg University of Wisconsin 1513 University Avenue Madison, Wisconsin 53706	1
Mr. P. Senholze Code SE-624 Naval Air Engineering Center Group Support, Equipment Division Philadelphia, Pennsylvania 19112	1
Dr. William J. Shack Materials Science Division Argonne National Laboratory 9700 South Cass Avenue Argonne, Illinois 60439	1
Prof. Milton C. Shaw Arizona State University Engineering Science Department Room ECG 247 Tempe, Arizona 85281	1
Prof. Oleg D. Sherby Dept. of Materials Science and Eng. Stanford University Stanford, California 94305	1
Mr. J.J. Sherlock Maic Division Pure Carbon Company, Inc. St. Marys, Pennsylvania 15357	1
Prof. Paul G. Shewmon Chairman, Dept. of Metallurgical Eng. The Ohio State University 116 West 19th Avenue Columbus, Ohio 43210	1
Mr. W. Smith Code 2832 Naval Ship Research and Development Annopolis, Maryland 21401	1
Dr. A. Thiruvengadam Institute of Ocean Science and Eng. The Catholic University of America Washington, D.C. 20017	1
Dr. A.P.L. Turner Argonne National Laboratory 9700 South Cass Avenue Argonne, Illinois 60439	1
Dr. Edward van Reuth ARPA 1400 Wilson Boulevard Arlington, Virginia 22209	1
Mr. Vernon C. Westcott Foxboro/Trans-Sonics, Inc. P.O. Box 435 Burlington, Massachusetts 01803	1

No. of Copies

Dr. B.A. Wilcox 1
Division of Materials Research
National Science Foundation
1800 G Street
Washington, D.C. 20550

Dr. Russel Young 1
National Bureau of Standards
Mechanics Division
Institute of Basic Standards
Washington, D.C. 20234

Prof. Victor F. Zackay 1
Dept. of Materials Science and Eng.
University of California
Hearst Mining Building
Berkeley, California 94720

Defense Documentation Center 12
Building 5
Cameron Station
Alexandria, Virginia 22314

Assistant Chief for Technology 1
Office of Naval Research
Code 200
Arlington, Virginia 22217

FOREIGN MAILING

Prof. M.F. Ashby 1
University Engineering Department
Cambridge University
Trumpington Street
Cambridge CB2 1PZ, England

Prof. F.T. Barwell 1
University College of Swansea
Singleton Park
Swansea, SA2 8PP Wales

Dr. B.J. Briscoe 1
University of Cambridge
Physics and Chemistry of Solids
Cavendish Laboratory
Madingley Road
Cambridge CB2 OHE, England

Prof. Alistair Cameron 1
Imperial College of Science and Tech.
Department of Mechanical Engineering
Exhibition Road
London, SW7 England

No. of Copies

Prof. J.D. Campbell 1
Department of Engineering Science
University of Oxford
Parks Road
Oxford OX1 3PJ, England

Dr. V.N. Constantinescu 1
Institute of Fluid Mechanics
Academy of the Socialist Republic Rumania
Bucharest, Rumania

Dr. J.H. Dautzenberg 1
Mechanical Engineering Materials Lab.
University of Technology
Eindhoven, Netherlands

Prof. E. Hornbogen 1
Ruhr-Universitat Bochum
Institut fur Werkstoffe
463 Bochum-Querenburg
Postfach 2148
Bochum, Germany

Dr. A. Palmgren 1
AB-Svenska Kullagerfabriken
Group Headquarters
S41550
Gothenberg, Sweden

Dr. L.E. Samuels 1
Defense Standards Laboratory
P.O. Box 50
Ascot Value 3032, Australia

Mr. D. Scott 1
National Engineering Laboratory
East Kilbride, Glasgow
Scotland

Dr. Markus O. Speidel 1
Brown, Boveri & Company, Inc.
Research Centre
5401, Baden, Switzerland

Prof. D. Tabor 1
University of Cambridge
Cavendish Laboratory
Madingley Road
Cambridge CB3 OHE, England

Dr. R.B. Waterhouse 1
University of Nottingham
Department of Metallurgy and Materials
University Park, Nottingham NG7 2RD
Great Britain